UNIVERSIDADE DE LISBOA
FACULDADE DE CIÊNCIAS
DEPARTAMENTO DE ENGENHARIA GEOGRÁFICA, GEOFÍSICA E ENERGIA

Analysis of new indicators for Fault detection in grid connected PV systems for BIPV applications

Mário Filipe Aires da Silva

Dissertação

Mestrado Integrado em Engenharia da Energia e do Ambiente

2014

UNIVERSIDADE DE LISBOA
FACULDADE DE CIÊNCIAS
DEPARTAMENTO DE ENGENHARIA GEOGRÁFICA, GEOFÍSICA E ENERGIA

Analysis of new indicators for Fault detection in grid connected PV systems for BIPV applications

Mário Filipe Aires da Silva

Dissertação de Mestrado Integrado em Engenharia da Energia e do Ambiente

Trabalho realizado sob a supervisão de:

Dr. Santiago Silvestre Berges (UPC)

Dr. Miguel Centeno Brito (FCUL)

2014

Acknowledgements

I would like to thank to everyone who contributed in one way or another to the successful accomplishment of this thesis, but in particular I would like to thank to:

Supervisor Professor Miguel Centeno Brito for his availability and collaboration before and during this work;

Co-supervisor Professor Santiago Silvestre Berges for his good orientation and help during this work. I am also grateful the good way he received me in Polytechnic University of Catalunya (UPC).

Doctor Daniel Guasch Murillo for his availability and help with the understanding of his MatLab models.

Carolina Pires for her important support during the execution of this thesis.

My friend Engineer Arturo Marban for his help with MatLab when I most needed.

Finally, I am grateful to my parents, Mário and Paula, my brother Bruno and my grand-parents, Horácio and Clotilde, for their support and the strength they gave me during my academic path and my staying in Barcelona.

Abstract

In this work we present a new procedure for automatic fault detection in grid connected photovoltaic (PV) systems. Most diagnostic methods for fault detection of PV systems already known are time consuming and need expensive hardware. In order to completely avoid the use of modeling and simulation of the PV system in the fault detection procedure we defined two new current and voltage indicators, NRc and NRv respectively, in the DC side of the inverter of the PV system. This method is based on the evaluation of these indicators. Thresholds for these indicators are defined taking into account the PV system configuration: Number of PV modules included in series and parallel interconnection to form the PV array. The definition of these thresholds for the voltage and current indicators must be adapted to the specific PV system to supervise and a training period is recommended to ensure a correct diagnosis and reduce the probability of false faults detected. A simulation study was carried using MatLab and the data used was monitored by the inverter, pyranometers, thermocouples and reference cells installed in a grid connected PV system located in the Centre de Développement des Energies Renouvelables (CDER), Algeria. The proposed method is simple but effective detecting the main faults of a PV system and was experimentally validated and has demonstrated its effectiveness in the detection of main faults present in grid connected applications.

Key word: Photovoltaic Energy, PV systems, Fault Detection, Diagnosis of Faults, New Indicators.

Resumo

Neste trabalho apresentamos um novo procedimento para deteção automática de falhas em sistemas fotovoltaicos (PV) ligados à rede. A maioria dos métodos de diagnóstico para deteção de falhas em sistemas PV já conhecidos são consumidores de tempo e precisam de equipamento caro. De forma a evitar completamente o uso de modelação e simulação do sistema PV no processo de deteção de falhas, nós definimos dois novos indicadores de corrente e voltagem, NRc e NRv, respetivamente, no lado DC do inversor do sistema PV. Este método é baseado na avaliação desses novos indicadores. Foram definidos limites para esses indicadores de forma a ter em conta a configuração do sistema PV: número de módulos PV incluídos em série e em paralelo que formam o PV array. A definição desses limites para os indicadores de voltagem e corrente têm que ser adaptados ao sistema PV específico a supervisionar e um período de treino é recomendado de forma a garantir um diagnóstico correto e reduzir assim a probabilidade de falsas falhas detetadas. Um estudo de simulações foi feito em MatLab e usando informação monitorizada pelo inversor, piranómetros, termopares e células de referência instaladas no sistema PV conectado à rede localizado no Centro de Desenvolvimento das Energias Renováveis (CDER), Algéria. O método proposto é simples mas eficaz na deteção das falhas principais de um sistema PV e foi experimentalmente validado e demonstrou a sua eficácia na deteção de falhas presentes em aplicações conectadas à rede.

Palavras-chave: Energia Fotovoltaica, Sistemas PV, Deteção de Falhas, Diagnóstico de Falhas, Novos indicadores.

Table of Contents

1. Introduction 1
   1.1 Motivations 1
   1.2 Outline of the thesis 2
   1.3 Solar cell & PV module 3
   1.4 The I-V curves 5
      1.4.1 Scaling I-V curve 5
      1.4.2 Impacts of Temperature and Irradiance on the I-V curve 6
   1.5 Power curves & MPP 8
   1.6 Photovoltaic systems configurations 11
      1.6.1 Stand-alone PV systems 11
      1.6.2 Grid connected PV systems 11
   1.7 Components of grid connected photovoltaic systems 12
   1.8 Common faults and degradation factors 15
   1.9 O&M practice 17
2. State of the art 19
   2.1 Monitoring systems 19
   2.2 Fault detection & diagnosis 20
   2.3 Review of Chouder's procedure 21
      2.3.1 Description of the PV system installed at CDER and the monitoring system 21
      2.3.2 PV module Parameters extraction 23
      2.3.3 Fault Diagnosis based on energy yields, current and voltage indicators 24
      2.3.4 Power loss factors in PV systems 24
      2.3.5 Indicators for failure detection 29
3. New Indicators for Fault Detection and Diagnosis of PV Systems 31
   3.1 Soft environment & MatLab 31
   3.2 New I&V indicators 32
      3.2.1 New Indicators, NRc and NRv 32
      3.2.2 Calculation of I_{scm} and V_{ocm} (PV Module) 32
      3.2.3 Calculation of I_{mm} and V_{mm} (PV Module) 35
      3.2.4 Calculation of I_{sc} and V_{oc} (Array) 37
      3.2.5 Indicators in Fault-Free operation 37
   3.3 Faults on PV systems 38
      3.3.1 Fault detection 38
      3.3.2 Analysis of the thresholds for indicators of voltage and current 39
   3.4 Simulation Study using the new indicators and thresholds 43

3.4.1 Introduction 43
3.4.2 Simulated systems 43
3.4.3 Indicators values for the simulations of all systems 45
3.4.4 Obtaining α and β by using both procedures 45
3.5 Impacts of string faults and short-circuited modules 47
3.5.1 Impacts of faulty strings 47
3.5.2 Impacts of short-circuited PV modules 50
3.5.3 Impacts on the output Power 52
4. Experimental Validation 56
4.1 System Behavior 56
4.1.1 Case of study 1: Free Fault 57
4.1.2 Case of study 2: String Fault 59
4.1.3 Case of study 3: Short-circuited PV modules 62
4.2 Detection and diagnose of changing energy loss type of failures 64
4.2.1 Partial Shadowing 64
4.2.2 Grid Fault 68
5. Conclusions 73
6. Annex 74
7. References 85

Nomenclature

PV	Photovoltaic
NRc	New Ratio of Current
NRv	New Ratio of Voltage
CDER	Centre de Développement des Energies Renouvelables
η	Efficiency
G	Irradiance
I-V	Current-Voltage curve
Ns	Number of cells/modules connected in series
Np	Number of cells/modules connected in parallel
STC	Standard Test Conditions
MPP	Maximum Power Point
MPPT	Maximum Power Point Tracker
FF	Fill Factor
Si	Silicon
DC	Direct Current
AC	Alternate Current
O&M	Operating & Maintenance
IEA	International Energy Agency
Yr	Reference Yield
Ya	Array Yield
Yf	Final Yield
PR	Performance Ratio
V_m	Voltage at Maximum Power Point
I_m	Current at Maximum Power Point
NRvbm	New Ratio of Voltage with short-circuited module
NRcfs	New Ratio of Current with faulty string
TNRcfs	Threshold of faulty string fault
TNRvbm	Threshold of short-circuited module fault
δ and σ	Standard deviation

List of Figures

Fig. 1.1- Typical silicon solar cell 3
Fig. 1.2- Schematic of a solar cell connected to a load 3
Fig. 1.3- Typical Silicon PV module 4
Fig. 1.4- Cells connected in series with bypassed diodes 4
Fig. 1.5- Simulated I-V curve for one solar cell of the PV module Isofoton 106/12, at STC 5
Fig. 1.6- Scaling the I-V curve from a solar cell to a PV array 6
Fig. 1.7- Simulated I-V curve for the PV module Isofoton 106/12, at STC 6
Fig. 1.8- Effect of Diverging R_s & R_{sh} from Ideality 7
Fig. 1.9- Effect of the Irradiance (G) on the I-V curve at 25°C 7
Fig. 1.10- Effect of the Cell Temperature (Tcell) on the I-V curve at 1000 W/m^2 8
Fig. 1.11- Typical I-V curve including P-V curve for a random PV module 9
Fig. 1.12- Effect of the Irradiance (G) on the Power curve and MPP, at 25°C 10
Fig. 1.13- Effect of Tcell on the Power curve and MPP, at 1000 W/m^2 10
Fig. 1.14- Standard configuration of a Stand-alone PV system 11
Fig. 1.15- Standard configuration of a Grid connected PV system 12
Fig. 1.16- Common PV Inverter - Sunny Boy 2500HF 13
Fig. 1.17- Junction box 14
Fig. 1.18- Pyranometers on the tilted and horizontal planes 14
Fig. 1.19- Cleaning the soiling in a PV array 16
Fig. 1.20- Snow covering PV modules 17
Fig. 1.21- Partial shading 17
Fig. 2.1- General Scheme of the PV system installed in CDER 22
Fig. 2.2- Monitoring system installed at CDER 22
Fig. 2.3- PV system output Power, DC side – measured and simulated 23
Fig. 2.4- Loss mechanisms in PV systems 26
Fig. 2.5- Capture losses evolution on free fault operation of the PV system 28
Fig. 2.6- Capture losses evolution on faulty string operation of the PV system 29
Fig. 2.7- Most probable faults present in the PV system 30
Fig. 3.1- I-V curves with G=1000 W/m^2, BP 5160S 34
Fig. 3.2- I-V curves with G=1000 W/m^2, Helios 1500 34
Fig. 3.3- Power curve - BP BP5160S 36
Fig. 3.4- Power curve – Helios 1500 36
Fig. 3.5- Model for detection of both faults: short-circuited modules and faulty strings 42
Fig. 3.6- Common scheme of a grid connected PV system 44
Fig. 3.7- α parameter values as a function of Np 46
Fig. 3.8- β parameter values as a function of Ns 47
Fig. 3.9- Output Current profile with different number of faulty strings 48
Fig. 3.10- NRc: Current ratio profiles 48
Fig. 3.11- Power profile with different number of faulty strings 49
Fig. 3.12 Voltage profile with different number of short-circuited modules 50
Fig. 3.13- NRv: Voltage ratio profile 51
Fig. 3.14- Power profile with different number short-circuited modules 52
Fig. 3.15- NRv progression – PV system number 3 53
Fig. 3.16- NRv progression – PV system number 8 53
Fig. 3.17- NRc progression – PV system number 3 54
Fig. 4.1- Irradiance profile - Free fault day 57

Fig. 4.2- Cell Temperature profile - Free fault day 57
Fig. 4.3- Ratios and threshold for output current – Free fault 58
Fig. 4.4- Ratios and threshold for output voltage – Free fault 58
Fig. 4.5- Irradiance profile – string fault day 59
Fig. 4.6- Cell Temperature profile – String fault day 60
Fig. 4.7- Ratios and threshold for output current – String fault 60
Fig. 4.8- Ratios and threshold for output voltage – String fault 61
Fig. 4.9- Irradiance profile – Short-circuited module day 62
Fig. 4.10- Cell Temperature profile – Short-circuited module day 62
Fig. 4.11- Ratios and threshold for output Voltage – Short-circuited PV module 63
Fig. 4.12- Ratios and threshold for output Current – Short-circuited PV module 63
Fig. 4.13- Irradiance profile with Shading 65
Fig. 4.14- Cell Temperature profile with Shading 65
Fig. 4.15- Current profile at DC side of the PV system with Shading 66
Fig. 4.16- Voltage profile at DC side of the PV system with Shading 66
Fig. 4.17- Power profile at the DC side with Shading 67
Fig. 4.18- NRc profile with Shading 67
Fig. 4.19- NRv profile with Shading 68
Fig. 4.20- Irradiance profile with Shading 69
Fig. 4.21- Cell Temperature profile with Shading 69
Fig. 4.22- Current profile at DC side of the PV system with Shading and Grid faults 70
Fig. 4.23- Voltage profile at DC side of the PV system with Shading and Grid Faults 70
Fig. 4.24- Power profile at DC side of the PV system with Shading and Grid Faults 71
Fig. 4.25- NRc profile with Shading and Grid Faults 71
Fig. 4.26- NRv profile with Shading and Grid Faults 72

List of Tables

Table 2.1- Typical monitoring inputs in a common PV system [23] 19
Table 3.1- Commercial PV modules used on this work 33
Table 3.2- I_{sc} and V_{oc} results from manufacturer and simulated data 35
Table 3.3- V_{mpp}, I_{mpp} and P_{mpp} results from manufacturer and simulated data 37
Table 3.4- Constant Energy Loss Faults in a PV system based on the new indicators 39
Table 3.5- Systems of study configuration 44
Table 3.6- Results from all the system simulations 45
Table 3.7- Values obtained for α and β 46
Table 4.1- Ratios and thresholds values – free fault 59
Table 4.2- Ratios and thresholds values – String fault 61
Table 4.3- Ratios and thresholds values – one Short-circuited PV module 64

1. Introduction

1.1 Motivations

Due to technology developments and to a considerable demographic grown, it has been verified from decade to decade an increased consumption of energy all over the world. If there are no changes or set new laws that may affect energy markets, the consumption of energy will keep increasing. A large piece of this increase is due to fossil fuels. Unfortunately, fossil fuels are considered finite and limited resources and are the main sources of air pollution and green house effect.

Renewable energy seems to be the best alternative to fossil fuels. This kind of energy has many benefits like helping to keep the air clean, reduce the dependence on fossil fuels, reduce the production of carbon dioxide, create new jobs and create sustainable development of the countries. Wind energy, hydroelectric generation, biomass, geothermal, photovoltaic, solar thermal energy are all examples of renewable energies.

In the last few years, there was a huge grown of the number of photovoltaic systems installed all over the world. This happens thanks to the reduction of the PV modules fabrication cost and the policies adopted by most of the countries in the world that give some benefits and new fees to whom have those systems installed at home. However, this growth has not been accompanied by important improvements in the field of PV system diagnosis, supervision and fault detection [3] because it is a common belief that PV systems are maintenance free and monitoring PV systems represent an extra cost. Even if a PV panel shows a really low failure rate, it is important to keep in mind that PV systems are composed by other elements that may also have failures. Also, faults in PV systems do not only affect the performance of the system but may also lead to damage the equipment. Moreover, although PV systems generally operate without problems, when there are faults on the system they are hard to be observed by the operating personnel. In order to prevent faults and failures that lead to a decrease of the lifetime of a PV system, and to improve the system efficiency, monitoring and fault detection have to be practiced.

The fault detection procedure presented in this thesis work is based on previous works that evaluate the power losses present in the PV system for fault detection [4-6,30]. In this approach the computational analysis has been reduced avoiding the use of electrical models for simulation of the PV system behavior and the number of monitoring sensors minimized.

Nowadays most inverters designed for grid connected PV applications have a wide range of interfaces, in particular sensor inputs and communication interfaces. These sensor inputs can be used to connect irradiance sensors as pyranometers, reference cells and PV module temperature sensors. So, these inverters include monitoring capabilities for irradiance and temperature as well as for maximum power point tracking (MPPT) evolution. The proposed method uses as input variables from the inverter just the DC currents and voltages extracted from the MPPT incorporated in the inverter, the measured irradiance and cell temperature.

Therefore, this thesis work aims to develop a method of fault detection that can be integrated into the inverter without using simulation software or additional external hardware. The focus of this work is the losses and malfunction of the DC side. Two new indicators of current and voltage are used as benchmarks and both relationships can be calculated by the inverter himself.

1.2 Outline of the thesis

This thesis consists in six chapters, with the first chapter giving a little introduction to the theme of solar energy. Afterwards an overview on how the solar energy production works explaining the solar cell and PV modules concept. Then the I-V curve, Power curve and maximum power point (MPP) are introduced with the impacts of various factors that may change these indicators. Following this, the photovoltaic (PV) system itself is introduced distinguishing characteristics of the two main types of PV systems, stand-alone and grid connected PV systems. Ending this chapter we have an overview of the components of a grid connected PV system, the common faults and degradations factors, and finally the O&M.

Chapter 2 will start with the state of the art of monitoring systems used on PV systems and methods of detection and diagnosis of faults recently developed. Afterwards, will be given a review of the Chouder's work we based our new method. In this review we have a detailed explanation of the actual grid connected PV system located in the Centre de Développement des Energies Renouvelables (CDER) in Algeria, simulated and measured and an overview of the method used for the parameter extraction (R_{sh}, R_s, n, I_0, I_{PH}). Then we introduce the energy yields and the capture losses because this is the basis of the previous work of fault detection and diagnosis in PV systems. In the end of this chapter there are some results in order to better understand this method and most importantly the previous indicators reported in the literature that were the basis of the work developed in this thesis.

In chapter 3 will start with the software used in this thesis. After will be introduced the new indicators of current and voltage, NRc and NRv respectively. Afterwards, we will explain and define the variables that are related to the new indicators and then we will define the NRco and NRvo that are always the expected values in free fault operation of a PV system. Then will be described the different faults and the thresholds related to them and we are going to define the variables α and β used in the definition of the thresholds. After that we have simulations and results based in the new indicators and on the MatLab models. Ending this chapter, there is a study on the impacts of the short-circuited modules and string faults in the output power of a common PV system.

Chapter 4 is dedicated to the system validation where we simulate a sub-array of the actual PV system installed at CDER with actual monitored data and where are presented the results of fault detection and fault diagnosis with the new indicators, NRc and NRv.

Finally, chapter 5 presents the final conclusions after analyzing all the work done.

1.3 Solar cell & PV module

Fig. 1.1- Typical silicon solar cell

In order to better understand how a PV module works we have to start by the solar cell. A solar cell can be described as an electronic device able to capture the energy of the photons and directly convert it to electricity. Here the process is briefly described considering a crystal silicon cell, the cells used on this thesis. Figure 1.2 shows a simple circuit of a silicon solar cell with an external load:

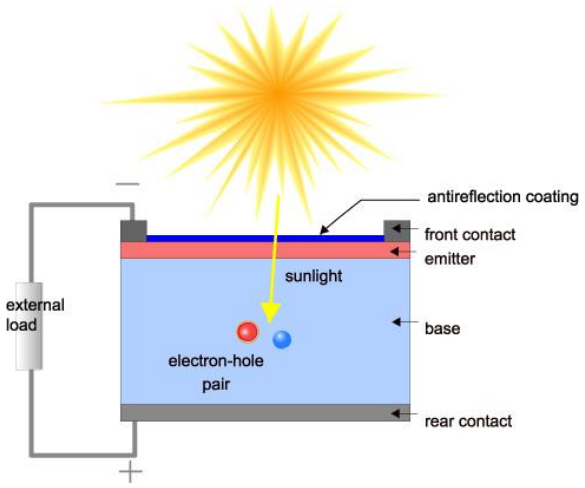

Fig. 1.2- Schematic of a solar cell connected to a load

The generation of current in a solar cell is known as the "light-generated current". When a photon is absorbed by the cell, if its energy is greater than the band gap, an electron is able to jump out in the crystal structure creating a hole-electron pair, which normally disappears as the electron recombines with the hole. In order to avoid the recombination a barrier is created by doping the silicon, on one side with small amount of a group III element (for ex. Boron) to form p-silicon and on the other side with a small amount of a group V element (for ex. Phosphorus) to form the n-silicon. The presence of the barrier does not allow the recombination, creating an excess of electrons in the n-silicon and a lack of them in the p-silicon. If an external electrical circuit is built the electrons are free to move from the n-silicon to the p-silicon passing by the electrical circuit, thus producing electricity. This is the basic principle behind the solar cell. Depending on the environmental conditions, mainly the irradiation and the temperature, the cell is able to produce a certain voltage and a certain current [7]. This process is just briefly described because this is not the main focus of this thesis is the PV system.

Fig. 1.3- Typical Silicon PV module

Therefore, a PV module is an aggregate of solar cells connected and grouped. Usually, the solar cells are connected only in series in order to increase the overall output voltage of the PV module but sometimes they also have one connection in parallel in order to increase the overall output current and when that happens the PV module has 2 internal strings of connected solar cells. The same current flows in every cell of the modules and the overall voltage generated is the sum of the voltage of every cell. Due to the fact that the cells are connected in series, the damage of one of them could affect the performance of the entire panel because the current flowing in the cells is the same and its values will adjust to the worst cell in the panel. Furthermore, if one cell of the panel is shaded, it is going to behave as a resistance, i.e. dissipating the electrical energy as heat. This effect is called hot spot. Hot spot is the increase in temperature due to the heat that will damage the solar cell in time. In order to avoid this effect, it is a common practice to introduce in the module by-pass diodes that give to the current an alternative path [8].

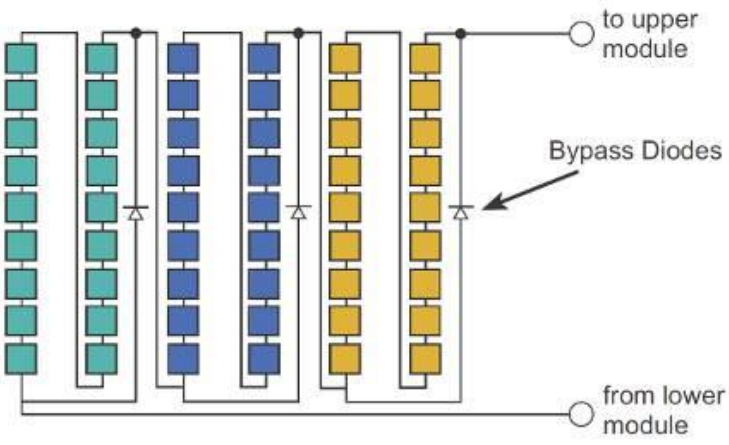

Fig. 1.4- Cells connected in series with bypassed diodes

The efficiency of the PV module is expressed as the ratio between the incident power of the solar radiation by the power produced by the module. Thus, the efficiency takes into account all the losses of the system:

$$\eta = \frac{Vmp*Imp}{G*A} \quad (1.1)$$

Where G is the incident irradiance [W/m^2]; A is the area of the module [m^2]; V_{mp} is the maximum power point voltage [V]; I_{mp} is the maximum power point current [A]. The losses will be explained in the section 1.8.

1.4 The I-V curves

The current-voltage relationship characteristic of a solar cell is typically analyzed with the I-V curve. Figure 1.5 shows us a solar cell I-V curve under predefined environmental conditions:

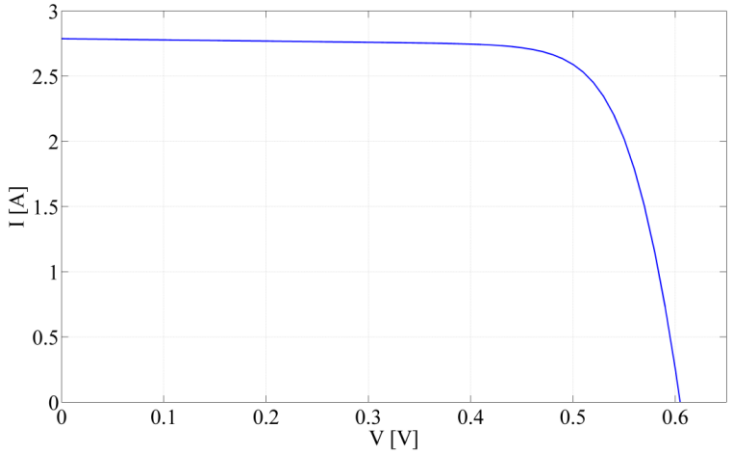

Fig. 1.5- Simulated I-V curve for one solar cell of the PV module Isofoton 106/12, at STC

The typical I-V curve of an illuminated PV cell has the shape shown in Figure 1.5. The voltage is always represented on the x-axis and current on the y-axis. The short circuit current (I_{sc}) is shown by the point in which the curve meets the y-axis, this means that in case of short circuit current the voltage is equal to zero. In the other hand, the similar happens with the open circuit voltage (V_{oc}), in this case the current is equal to zero.

1.4.1 Scaling I-V curve

The I-V curve of a PV array is a scale-up of the I-V curve of a single cell as shown in Figure 1.6. For example, if a PV module has 36 series-connected cells and a PV string has 10 of these modules in series, then the string's V_{oc} (voltage in open circuit) and also the array's V_{oc} is 360 times the voltage of that single solar cell. Similar logic applies to the I_{sc} (short circuit current), which scales with the number of cells in parallel. Therefore, the maximum power point (MPP) scales too. MPP will be explained in the section 1.5.

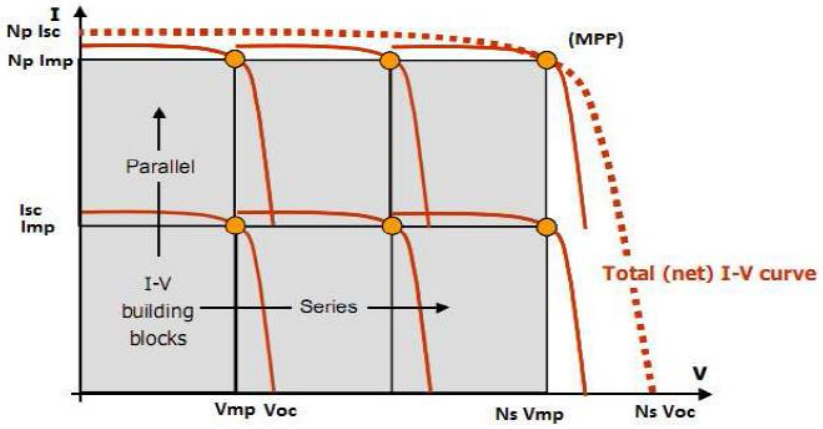

Fig. 1.6- Scaling the I-V curve from a solar cell to a PV array

Thus, from now on, the following graphs and explanations will be related to PV modules. Figure 1.7 shows the I-V curve of the PV module Isofoton 106/12 that has Ns=36 cells and Np=2 cells, totaling 72 solar cells.

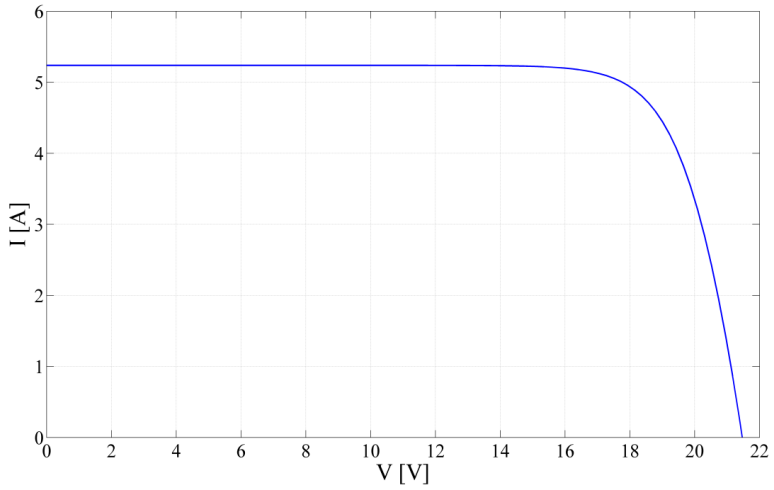

Fig. 1.7- Simulated I-V curve for the PV module Isofoton 106/12, at STC

1.4.2 Impacts of Temperature and Irradiance on the I-V curve

The I-V curve shown in Figure 1.7 is related to standard test conditions (STC: T=25ºC, G=1000W/m^2). Sometimes I-V curves may change. Those changes might occur when the following 4 parameters change: shunt resistances (R_{sh}), series resistances (R_s), irradiance (G), temperature of the solar cell (Tcell). The first two parameters are related to the solar cells/PV modules characteristics and the last two are external parameters. Usually the changes related to the resistances are not that great but as we can see in the Figure 1.8 the variations of R_s and R_{sh} may affect the I-V curve and then affect the maximum power point (MPP) of the PV module.

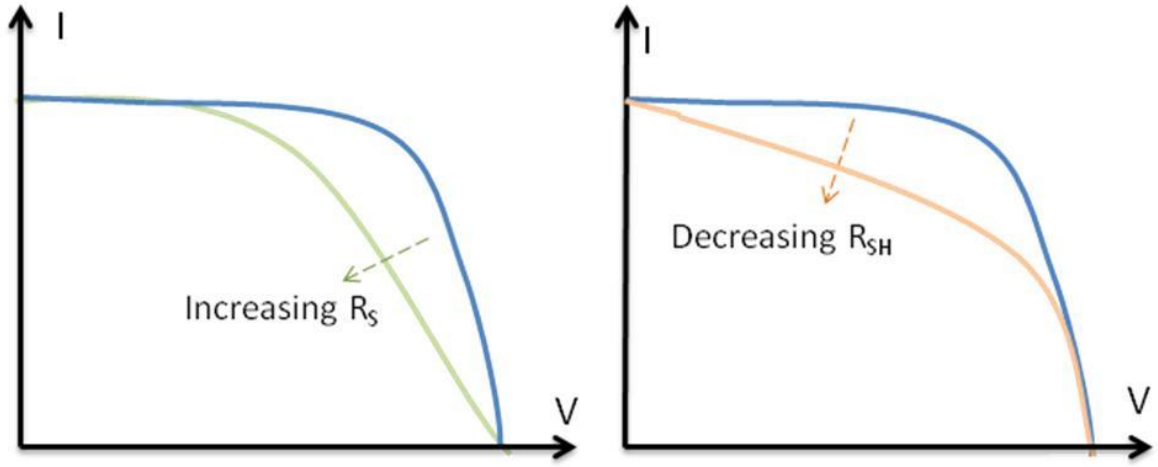

Fig. 1.8- Effect of Diverging R_s & R_{sh} from Ideality

The variations on the two external parameters, G and Tcell, change the I-V curve, in a slightly different way, but with a more important impact of the I-V curve. Figures 1.9 and 1.10 shows the impact of variations of G and Tcell, respectively, on the I-V curve of a PV module:

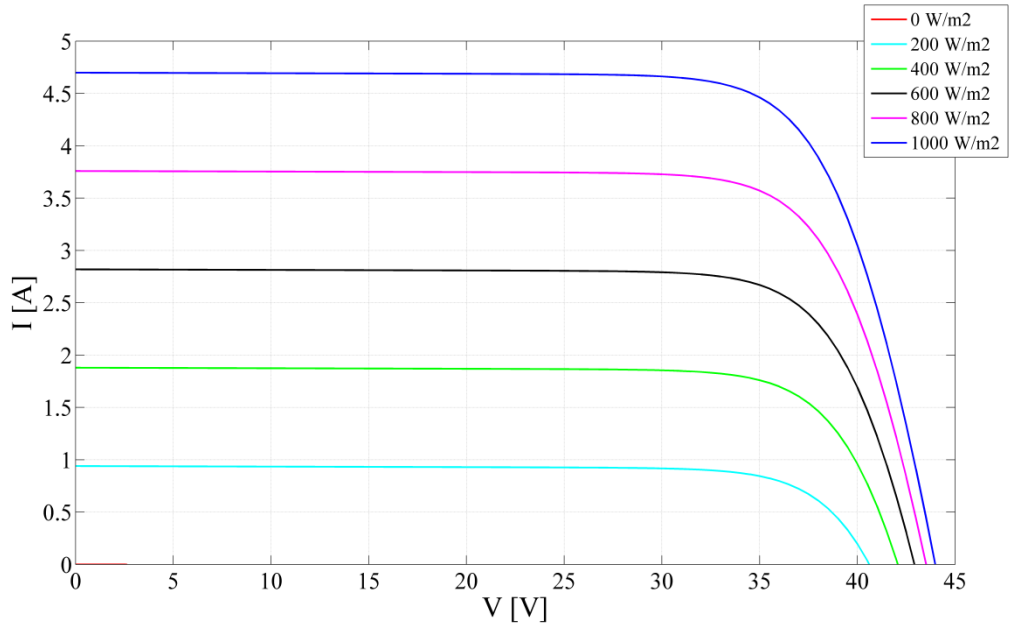

Fig. 1.9- Effect of the Irradiance (G) on the I-V curve at 25°C

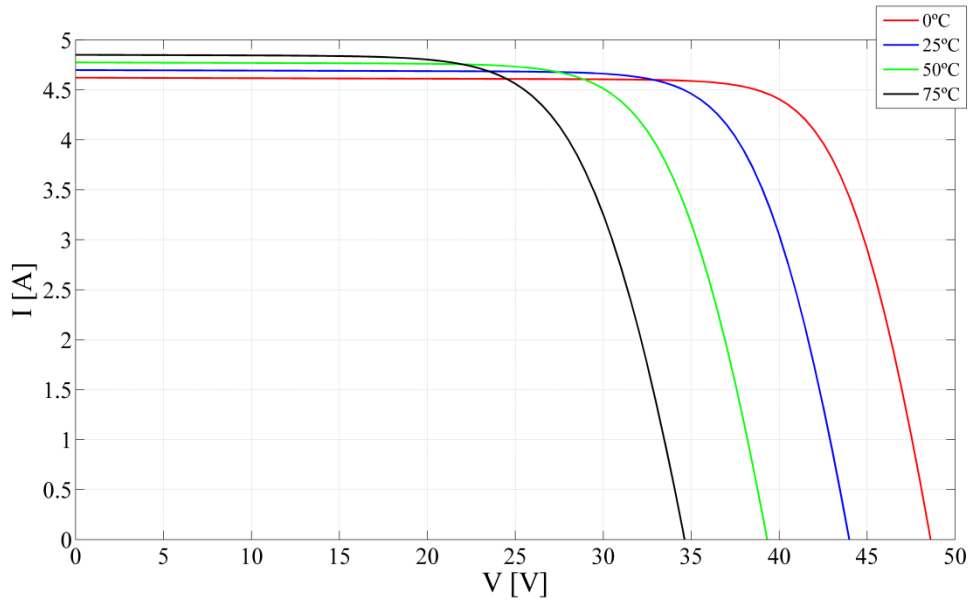

Fig. 1.10- Effect of the Cell Temperature (Tcell) on the I-V curve at 1000 W/m^2

With Figure 1.9 and 1.10 we can have some conclusions about how these external factors change the I-V curve. When the irradiance is lower, the variations are more notorious on the output current of the PV module but still there are some decreases on voltage output too when lowering the irradiance. Analyzing the temperature effects, we can see that the variations are more notorious on the output voltage of the module and there are almost no changes on the output current. Therefore, with lower temperatures of the solar cells we might have a bigger MPP thus increasing the output power from the PV module. Comparing the impacts of R_s, R_{sh}, G and Tcell on the I-V curve, can be concluded that low values of irradiance have the biggest impact on the I-V curve comparing with the other three model parameters.

1.5 Power curves & MPP

In order to maximize the energy generation of the PV module it is essential that the solar panel works at the maximum power point (MPP) and that's why the need of using a maximum power point tracker (MPPT). This device will be described in detail in the section 1.7.

The output power of a PV module is the product of the output current delivered to the electric load and the voltage across the module. The value of the power at the I_{sc} point is zero, because the voltage is zero, and also the power is zero at the V_{oc} point where the current is zero. The maximum output power of the PV module is somewhere in between. This happens at a point called the maximum power point (MPP) with the coordinates $V = V_m$ and $I = I_m$ [9].

As the output power of the PV module is the product between the current and the voltage, it is then possible to draw also the power curve as it can be seen from Figure 1.11:

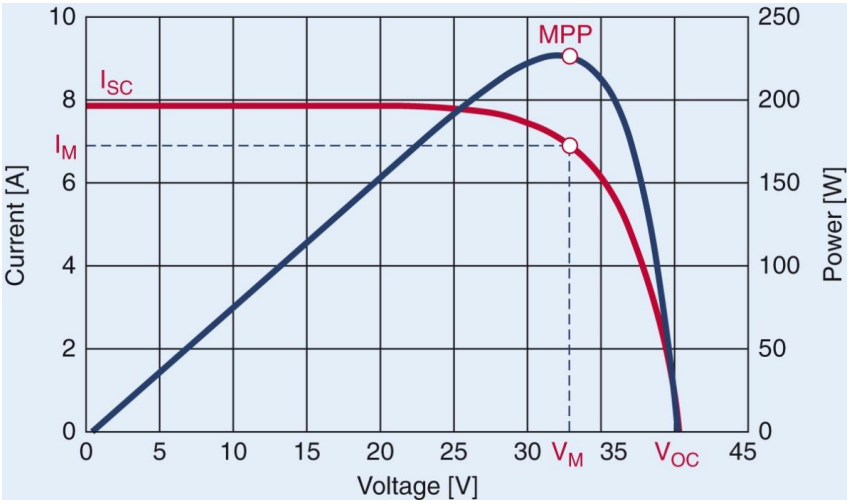

Fig. 1.11- Typical I-V curve including P-V curve for a random PV module

Another important parameter of PV modules is the fill factor, which is used for the evaluation of the PV module performance:

$$FF = \frac{Vmp*Imp}{Voc*Isc} \tag{1.2}$$

Where V_{oc} is the open circuit voltage [V] and I_{sc} is the short-circuit current [A].

The fill factor is a parameter which, in conjunction with V_{oc} and I_{sc}, determines the maximum power from a solar cell/module. Graphically, the FF is a measure of the "squareness" [10] of the solar cell and is also the area of the largest rectangle which will fit in the IV curve, as can be seen in Figure 1.11. Therefore, a higher FF means a higher module performance.

The external parameters, G and Tcell, impact the Power curve. Figure 1.12 shows the impact of different irradiances on the Power curve of a PV module:

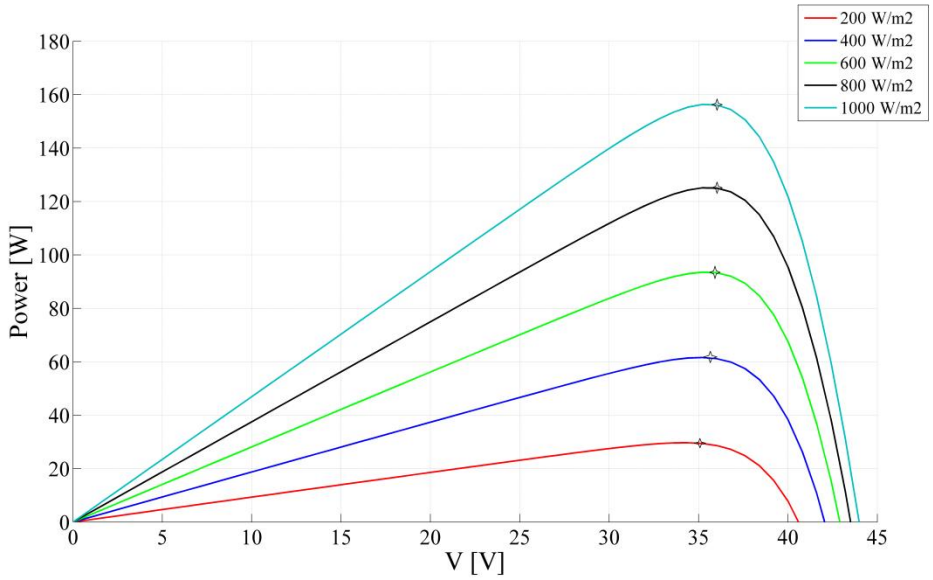

Fig. 1.12- Effect of the Irradiance (G) on the Power curve and MPP, at 25°C

Figure 1.13 shows the impact of the cell temperature (Tcell) on the Power curve of a PV module:

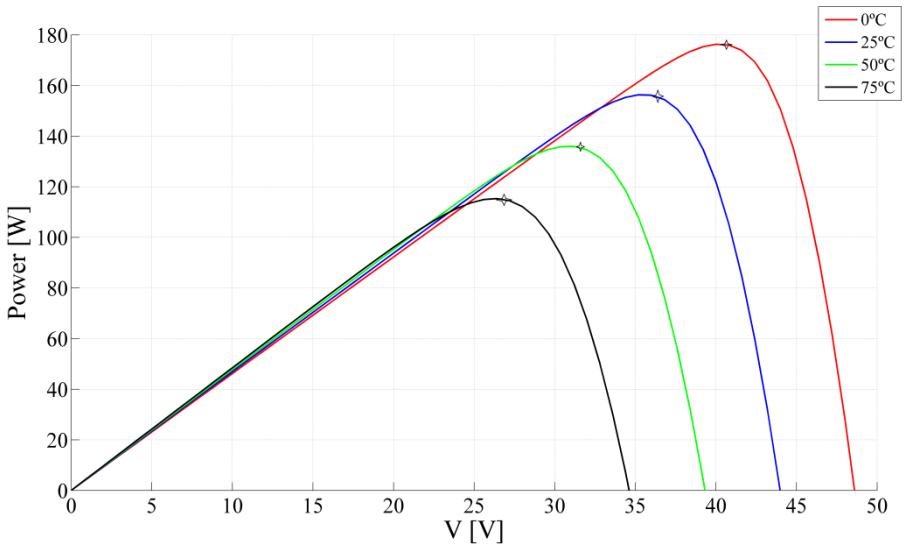

Fig. 1.13- Effect of Tcell on the Power curve and MPP, at 1000 W/m^2

With figure 1.12 and 1.13 we can have some conclusions about how these external factors may change the Power curve. The impact of G and Tcell on the Power curve is very similar to the impact on the I-V curve, already explained before. What we now realize with these Power curves is that the Tcell has a bigger impact on the output Power than we realized before, after analyzing the I-V curves. Therefore, with lower temperatures of the solar cells and with high irradiance we have a bigger MPP, thus increasing the generated energy from the PV module.

1.6 Photovoltaic systems configurations

Photovoltaic (PV) systems are mainly defined based on if the energy generated by the system is stored or it is directly connected to the grid. Thus, there are stand-alone PV systems and grid connected PV systems [11,12].

1.6.1 Stand-alone PV systems

Stand-alone PV systems are the most popular system used worldwide despite the more recent interest of the market in grid connected PV systems. A stand-alone PV system should provide enough energy to a totally main-isolated application. The standard configuration of this system is shown in Figure 1.14. In some specific cases, such as water pumping, the generator can be connected directly to the motor [13].The range of applications is constantly growing. Mini-applications such as pocket calculators, clocks are well known examples of stand-alone systems. Other typical applications for stand-alone systems are mobile systems on cars, village electrification in developing countries, solar pump systems for drinking water and irrigation, etc [11,12].

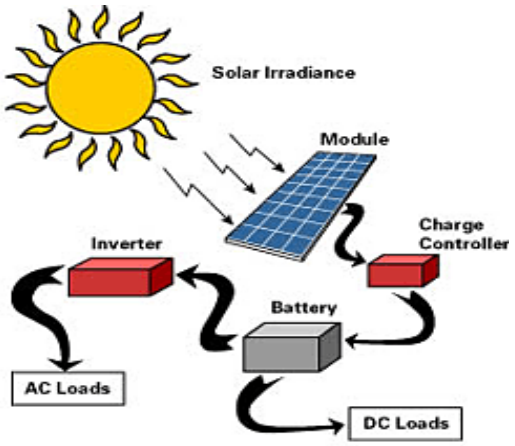

Fig. 1.14- Standard configuration of a Stand-alone PV system

Rechargeable batteries are used to store the electricity. In order to protect them, to achieve a higher availability and to have a longer lifetime it is essential the use of a charge controller. The charge controller prevents overcharging and may prevent against overvoltage of the battery.

1.6.2 Grid connected PV systems

In the last few years an important growth of grid-connected PV systems has been observed, especially in industrialized countries. Several reasons lie behind this fact apart from traditional advantages of photovoltaic electricity [14]:

- Utility grid-interactive PV systems are becoming more economically viable as the cost of PV components has been significantly decreasing in recent years, in particular the average cost of PV modules and inverters.
- Technical issues associated with inverters and interconnections of PV systems to the grid have been addressed by manufacturers and today's generation of inverters has enhanced reliability and reduced size.

- Utility benefits. The fact that solar electricity is produced in central hours of the day can add value to the electricity. This power peak demand can be partially supplied by dispersed grid-connected PV systems that are able to generate power at the same place where this power is used, reducing the heavy load supported by the transmission systems and achieving benefits in distribution and line support.

This market is becoming more and more important in photovoltaic applications. Therefore, PV power generation systems are likely to become, although small compared with other power generation sources, important sources of distributed generation, interconnected with utility grids [14].

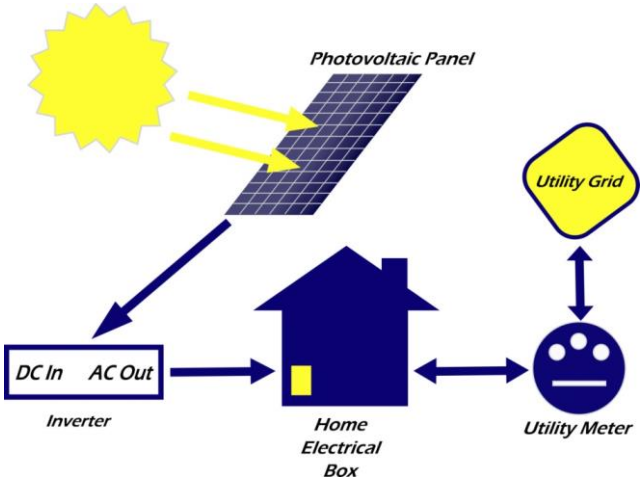

Fig. 1.15- Standard configuration of a Grid connected PV system

1.7 Components of grid connected photovoltaic systems

A PV system is more than a mere solar panel. These systems need a lot more components in order to be complete and working. Some of those components are optional and used only for certain occasions. As this new method is based in a grid connected PV system, we are not explaining certain components that are used only in stand-alone systems because they are irrelevant for our present work. Thus, this section aims to give an overview of the different components of a grid connected PV system, which are the following:

- PV modules;
- Junction box;
- Fuses box;
- Wiring;
- Inverter;
- MPPT;
- Temperature sensor (optional);
- Reference solar cell (optional);
- Pyranometer (optional);
- Device for data acquisition (optional);
- Utility meter (or bidirectional meters);
- Transformer (or isolation transformer).

The main component of a PV system is the photovoltaic module. A PV system is composed by PV modules that can be connected in series or in parallel. The solar cells that compose that PV module can be connected in series or in parallel too. The difference between a connection in series or in

parallel for both, cells or modules, is that the connection in series will increase the overall voltage output, while the connection in parallel will increase the overall current output. More about how the PV modules works is in a previous section. There are PV modules based in multijunction cells, single-juntion GaAs, Cystaline Si (silicon) cells, thin-film technologies (usually cadmium telluride - CdTe) and some emerging technologies like organic cells and more. Actually, the most common cells used in PV modules are crystalline Si cells because it's a mature technology that allows the best relation between production costs and energy generated. In this thesis, the simulations and all the work done is based in PV systems with silicon based PV modules.

The planning of a grid-connected PV system begins with the choice of an inverter. This determinates the system voltage at the DC side, and then the solar generator can be configured according to the input characteristics of the solar inverter. The inverter is the second most important component in a grid-connected PV system, after the solar generator. Its task is to convert the direct current generated by the solar cells to a 50 Hz AC current required by the grid [15].

Fig. 1.16- Common PV Inverter - Sunny Boy 2500HF

Usually, the inverter also includes components that are responsible for the daily operation mode. During the day, the optimum working point on the I-V characteristic curve shifts according to the fluctuations in solar radiation and module temperature. Intelligent inverter control includes maximum power point (MPP) tracking and continuous readjustment to the most favorable working point. As previously described, it is important that all the modules work at the maximum power point. This point is not fixed in real time because of the variations of external environmental conditions as for example the most common: temperature and irradiation. That is why it is important to track the maximum power point in real time, as explained in a previous section. In order to track this point a maximum power point tracking (MPPT) element is required to vary the output voltage of the string by maximizing the generated power in any real operating conditions [16]. Actually MPPT capabilities are usually included in the inverters used in grid connected PV systems. However, if inverters without MPPT are used, the MPPT algorithm can be separately incorporated into the system by means of DC-DC converters between the output of the PV array and the inverter input. The ideal PV system would have an individual MPPT on every PV module and that's why there are micro inverters. The presence of more than one MPPT permits better performance of the entire PV system but the costs would rise too much. Therefore, nowadays is not common to see MPPT on every module of a PV system.

Fig. 1.17- Junction box

It is common to use junction boxes, as can be seen in Fig.1.17, on every PV module in order to connect them all together, which contains also bypass diodes. However, nowadays the modules already have bypass diodes incorporated hence the junction box is usually used only to connect them. One damaged module can greatly affect the output power and then the overall energy generation of the entire system. Usually, this happens when hot-spot heating occurs. If the operating current of the overall series string approaches the short-circuit current of the "bad" cell, the overall current becomes limited by the bad cell. The extra current produced by the good cells then forward biases the good solar cells. If the series string is short circuited, then the forward bias across all of these cells reverse biases the shaded cell. Hot-spot heating occurs when a large number of series connected cells cause a large reverse bias across the shaded cell, leading to large dissipation of power in the shaded cell. Essentially the entire generating capacity of all the good cells is dissipated in the shaded cell. The enormous power dissipation occurring in a small area results in local overheating, or "hot-spots", which in turn leads to destructive effects, such as cell or glass cracking, melting of solder or degradation of the solar cell [10]. Therefore, a bypass diode is connected in parallel, but with opposite polarity. The presence of the bypass diode allows the current to follow another path bypassing the damaged solar cell or PV module. In practice, one bypass diode per solar cell is too expensive so bypass diodes are usually placed across groups of solar cells in order to decrease the final costs of the module.

Fig. 1.18- Pyranometers on the tilted and horizontal planes

Another component of a PV system is the temperature sensor, the reference solar cell and the pyranometer. The first one is used to measure the temperature of the air near the PV plant and the temperature at the cell level. Then we have the reference solar cell that enables a high level of measurement precision and is usually used to measure the irradiance that reaches the PV modules at the horizontal plane. Then the pyranometer is also used to measure the irradiance. This device can measure irradiance in both, tilted plane and in the horizontal plane. These three components are optional but they were used on the PV plant in study in order to get the data we needed for our simulations.

Usually, bi-directional meters are needed in grid connected PV systems in order to get the return credits from the energy companies because of the energy fees. Thus, a bi-directional meter records and measure the electricity flowing two ways, i.e. both the electricity drawn from the grid and the excess electricity the PV system feeds back into the grid [17].

Isolation transformers can be optionally placed at the inverter output depending on the type of inverter used in the PV system. Some inverters already include transformers of this type incorporated inside while others do not. An isolation transformer is preferably installed on the AC side of the PV inverter to eliminate the possibility of PV system injecting direct current into the power grid [18]. Some national regulations require an isolation transformer for connection to grids of medium, high or very high voltage. In most countries this is not required for low voltage connection [14].

Finally, in order to monitor all the data given by the sensors present in the system we need a monitoring device. In the PV plant in study, an Agilent 34970A was used for the data acquisition and then the data is sent to a PC via GPIB.

1.8 Common faults and degradation factors

While PV systems have no moving parts (compared to wind and micro-hydro systems) and can be extremely reliable, it does not mean they do not have potential performance problems [19]. Field surveys and inspections, like the survey of residential PV systems in Australia [20] and in Japan [3], show that a significant percentage of PV systems experience faults. For this analysis it is convenient to divide a PV system in three different parts: AC side, DC side and the inverter.

If a failure is registered on the AC side, the possible cause might be grid instability or a problem on the connections between inverter, load and grid. The grid failure is highly related and dependent to the location considered. The probability of grid fault is higher in rural areas while it has lower probability of happening in urban and more industrialized countries with a more stable grid.

Internal errors of the inverter are a common fault in PV systems and they increase with the aging of the component. They can be related with the components of the inverter itself such as switches, the MPPT, the fan or the varistors. However, the inverter has been improved considerably in the last few years in order to increase his reliability.

The DC side usually represents the lower amount of faults but this is the part of the system that raises more difficulties for fault detection and diagnosis of faults [12].

Based on several scientific papers [21], it was possible then to identify the most common faults in a PV system, displayed here from the one with higher probability to the one with the lower:

- **Internal error of the inverter:** Internal errors can be generated for different reasons and the fault detection system of the own inverter is normally able to identify them and send an error code. The probability of faults related to the inverter is decreasing significantly because they have been improved a lot in the last few years.
- **Failures of the data acquisition system:** Happens due to problems with the wires and wireless connection, damage of measurement components like the reference cell or the pyranometer.
- **Grid instability:** This kind of fault is dependent on the grid quality of the location where the PV system is installed. This fault has higher probability of happening in rural areas. This fault might cause unintentional Islanding that causes a continued energizing of the load after the disconnection from the grid and might be dangerous for the O&M technicians.
- **Short circuit with the Ground:** This happens when there is a short circuit evolving the system and the ground.
- **Broken cells:** This might occurs due to the accidental impact of objects on PV modules or due to hot spot.

- **Aging of PV modules:** PV modules are the most durable components in a PV system but they get older as every other component. The average annual degradation of a crystalline silicon module is approximately 0.2% per year, having an impact on the I_{sc} and then on the output power [3].
- **Shading:** Periodic shading cannot be considered a fault but is a cause of the decrease of generated energy. Modules affected by shadows get further deterioration due the hot spots as explained before.

Therefore, we can divide failures by their effect in terms of energy loss:

- **Constant energy loss type of failure:**
    - Degradation of the cell;
    - Short-circuited PV module;
    - Module defect;
    - Soiling.

Fig. 1.19- Cleaning the soiling in a PV array

- **Changing energy loss type of failure:**
    - Shading;
    - Grid failure;
    - MPPT errors;
    - Snow cover;
    - Data acquisition.

Fig. 1.20- Snow covering PV modules

Fig. 1.21- Partial shading

1.9 O&M practice

Usually, PV companies offer a monitoring system but none is able to provide a fault detection system. Therefore, O&M practices are mainly based on the professional experience of the operator and the installer companies. The location of the PV system strongly affects the O&M because of the weather conditions and the cost of the maintenance.

The O&M practices can be divided mainly in 3 categories [22]:

- Preventive maintenance;
- Corrective maintenance;
- Condition-based maintenance.

The preventive maintenance is based on preventive intervention in order to check the PV system and clean the power plant. However, in certain weather conditions the cleaning operations is not cost-effective, i.e. it is cheaper to lose a small percentage of the energy generated than to pay for the cleaning service.

The preventive maintenance should perform the following operations:

- Panel cleaning;
- Vegetation management;

- Wildlife prevention (variable);
- Check switches, fuses and wiring;
- Calibration of sensors (reference cell and pyranometer);
- Inverter (check the presence of dust which could damage the ventilation);
- MPPT checks for errors.

Corrective maintenance is mainly the reactive repairing of some problem of the PV system after it is detected. Finally, a condition-based maintenance relies on monitoring and fault detection of the PV system. This kind of maintenance allows the recognizing the presence of a fault that might cause a decrease of the final energy production of the system. The practice of this check varies accordingly to the software used for fault detection, but usually is around every 15 days or 1 month.

2. State of the art

2.1 Monitoring systems

System monitoring is very important in order to know how the PV system is performing under determinate conditions. Monitoring is basically the comparing of the actual and simulated power generation.

Most PV inverter manufacturers offer hardware and software to create a monitoring system to display the functioning of a system. Remote displays are easier to site, and may be provided with data from the inverter itself. A significant cost to the installing is the routing of the cabling to the display, but there already are instruments on the market that avoid this by utilizing short-range radio transmission [23].

The data acquisition uses data-loggers or computers to gather the data. Usually, the loggers are already incorporated in the inverters and used when the data is to be viewed in real time. On the other hand, the computers may be slower to gather the data but have more custom settings and the cost may be lower. For the data acquisition itself, is common to use sensors as inputs in the PV systems. Table 2.1 shows the typical monitoring variables:

Table 2.1- Typical monitoring inputs in a common PV system [23]

Parameter	Sensor	Accuracy
Solar radiation	Reference cell	3%
	Pyranometer	2%
DC current	Usually the Inverter	1%
AC current	Usually the Inverter	1%
Energy	Meter	1%
Ambient Temperature	Thermocouple	1ºC
	PRT	0.2ºC
	Thermistor	1ºC
Module Temperature	Thermocouple	1ºC
	PRT	0.2ºC
	Thermistor	1ºC
Power	AC meter	1%

2.2 Fault detection & diagnosis

The monitoring and regular performance supervision on the functioning of grid-connected photovoltaic (PV) systems is necessary to ensure an optimal energy harvesting and reliable power production. The development of diagnostic methods for fault detection in the PV systems behavior is particularly important nowadays due to the expansion degree of grid connected PV systems and the need to optimize their reliability and performance. Based on the results of precise diagnoses, a fault detection system can offer quick and proper maintenance advice that greatly simplifies the servicing and maintenance of PV systems [24].

Several researches [25-27] have been carried out, using climate data from satellites observation to generate the necessary climate data at the desired location. This is a cost-effective approach, since no climate sensors are needed on the plant, although it provides low accuracy in estimation of expected energy yield in some specific climatic conditions [27].

Other studies used meteorological data measured by local sensors on the plants to estimate energy production, together with soft computing techniques. An example can be found in Chao, Hob and Wang work [28], where a method based on the extended correlation function and the matter-element model is proposed to identify faults in a small PV plant. Furthermore, in another Chao work [29] the matter-element model is combined with a neural network to build an intelligent fault diagnosis system. Both proposals use a PV system simulator to collect power generation data of photovoltaic modules during normal and faulty operations.

Another interesting technique is proposed by the works of Silvestre, Chouder and Karapete [4-6] and Chine, Mellit, Pavan and Kalogirou [30] where authors proposed an automatic monitoring and fault detection system based on power losses analysis. The fault detection procedure presented in this thesis is based on those previous works that evaluate the power losses presented in PV systems and it will be explained in the next section. Furthermore, some works have been carried out using artificial intelligent techniques [31-33] and statistical data analysis for supervision of PV systems [34], but these techniques have not been yet optimized for fault detection analysis and clear identification of the kind of fault present in the system. For example, Vergura proposed a methodology [35] that allows detecting fault conditions in a PV system, by comparing output energy of six sub-systems that form the plant. To this aim, descriptive and inferential statistics are exploited and two steps are performed: an offline supervision, in order to set performance benchmarks of the considered PV plant, and a real-time monitoring, in order to check if the PV plant operation complies with the benchmarks. In a proposed method by Mellit [36] an Adaptive Neuro-Fuzzy Inference System (ANFIS) is used to model a stand-alone PV system. The ANFIS model is trained by using different signals recorded from a data acquisition system, in order to control the output current and voltage delivered from the overall PV system to the load. In some cases new techniques have been introduced, to detect the presence of faults in PV systems without the necessity of using climate data [3].

2.3 Review of Chouder's procedure

The important growth of installed PV systems has not been accompanied by important improvements in the field of PV system diagnosis, supervision and fault detection. Most PV systems, in use nowadays, are working without any supervision mechanism, especially PV systems with output power levels below 25 kWp. Maybe the reason has been that monitoring systems have only been implemented in big PV generators, where it represents a small cost increment respect to the whole system cost. Without the help of a minimal monitoring system it is not possible to develop any effective supervision, diagnosis or control of the PV system.

In this review we will focus only in the part of Chouder's work – "Analysis, Diagnosis and Fault Detection in Photovoltaic Systems" [2] – related to supervision and fault detection of PV systems. This work presents the supervision and fault detection procedure for grid connected PV systems based on power losses analysis. The procedure analyses the output power losses in the DC side of the PV generator. Processing certain power losses indicators such as Thermal capture losses and Miscellaneous capture losses allow the supervision procedure to generate a faulty signal as indicator of fault detection in the PV system. The procedure has been successfully tested experimentally and was carried out on Centre de Développement des Energies Renouvelables (CDER), Algeria.

The work proposed in the current thesis was based on the current and voltage indicators previous proposed on Chouder's work and it has the objective to be an improvement of that work.

2.3.1 Description of the PV system installed at CDER and the monitoring system

The procedure of fault detection in grid connected PV systems based on the current and voltage indicators described in this review was tested in a grid connected PV system located in the Centre de Développement des Energies Renouvelables (CDER), Algeria. This PV system of 9.6 kWp is divided in three sub-arrays of 3.2 kWp each one, which are connected to 2.5 kW (IG30 Fronius) single phase inverters. Each sub-array is formed by 30 PV modules (Isofoton 106W-12V) in a configuration of two parallel strings, Np=2, of 15 PV modules in series, Ns=15.

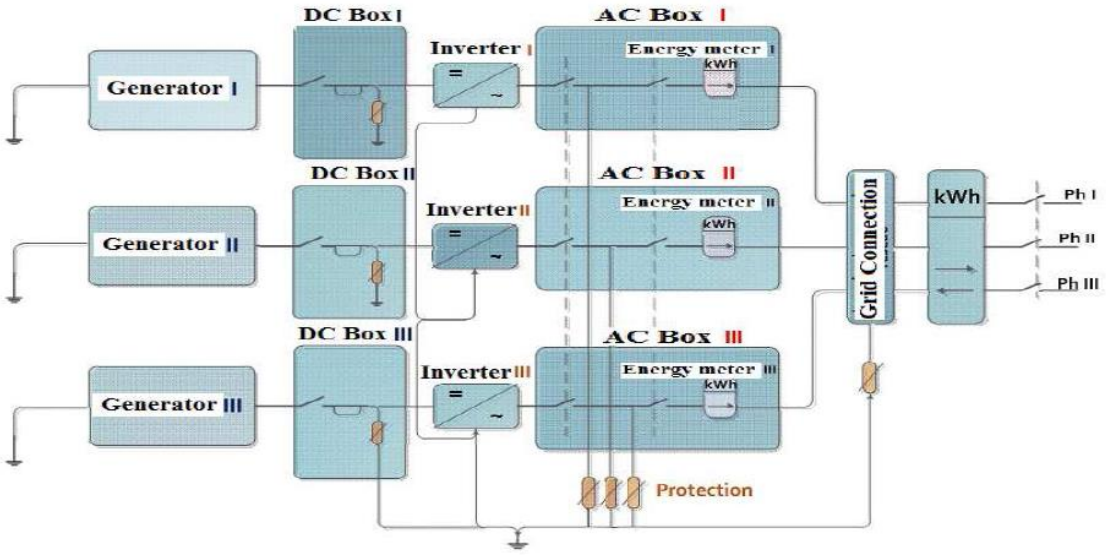

Fig. 2.1- General Scheme of the PV system installed in CDER

This PV system includes a monitoring system using an Agilent 34970A for the data acquisition as well as two pyranometers (Kipp & Zonen CM 11 type) and a reference solar cell to measure irradiance at different planes. One of the pyranometers and the reference cell are installed at two different places of the PV plant to measure irradiance in the tilted plane. A second pyranometer measures the irradiance in the horizontal plane. On our work in this thesis we use the measurement from the second pyranometer correspondent to the horizontal irradiance. For the measurement of the temperatures the monitoring system includes k type thermocouples.

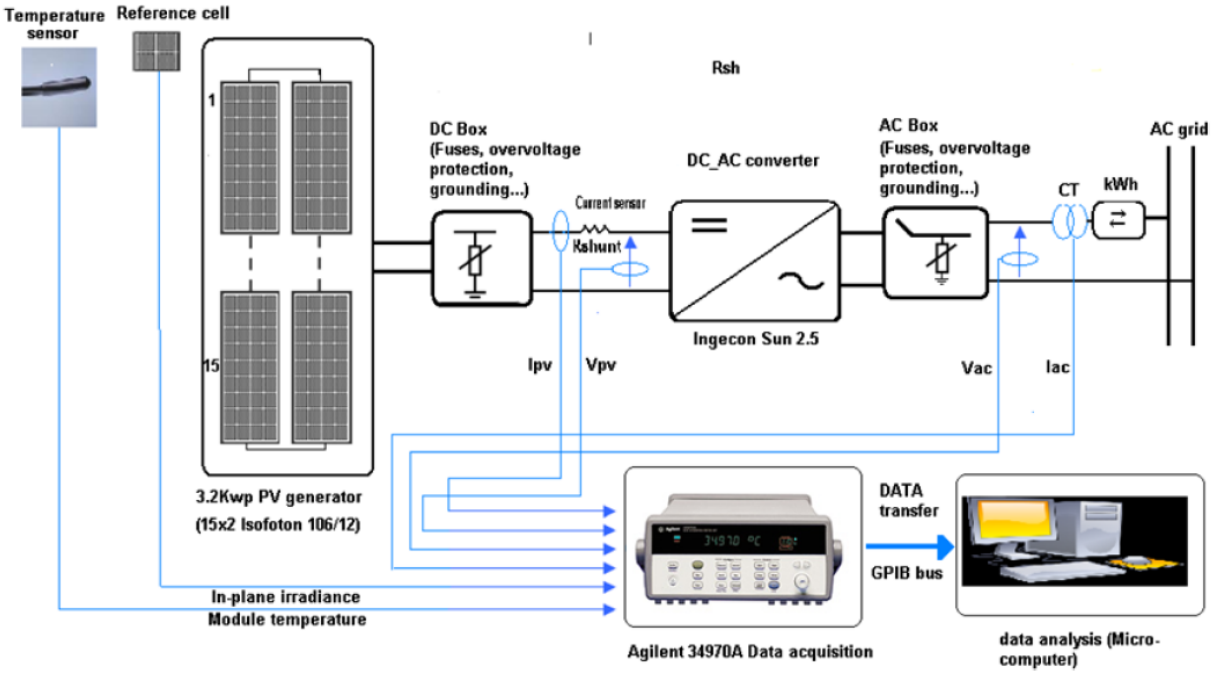

Fig. 2.2- Monitoring system installed at CDER

2.3.2 PV module Parameters extraction

In order to find the main five parameters of the PV module, Isofoton 106/12, the well know "Five parameter" model was used. In this method, the relationship between output current and voltage is given by the following nonlinear implicit equation:

$$I = I_{PH} - I_0 \left[\exp\left(\frac{V+R_S I}{nV_t}\right) - 1\right] - \left(\frac{V+R_s.I}{R_{sh}}\right) \quad (2.1)$$

Where the five parameters are: cell photocurrent (I_{PH}); diode reverse saturation current (I_0); ideality factor (n); series resistance (R_s) and shunt resistance (R_{sh}). I and V are the output PV cell current and voltage, V_t is the thermal voltage. The effect of temperature in output voltage and current are also incorporated into the model. A nonlinear regression algorithm has been applied to both data sets; measured I-V data from the PV system and data generated by the previous model, in order to minimize the following quadratic function [37-39]:

$$S(\theta) = \sum_{i=1}^{N} [I_i - I(V_i, \theta)]^2 \quad (2.2)$$

where: $\theta = (I_{PH}, I_0, n, R_{s,} R_{sh})$

This model has been tested using the operational data from the grid connected branch of 3.2 kWp of the CDER PV system. For the simulation of the branch, the environmental conditions of irradiance and cell temperature had to be linked to the simulation model. Figure 2.3 compares the measured and simulated power at DC side, of this branch (Array of the main PV system) with the real data between 8:33 and 17:47 of that day.

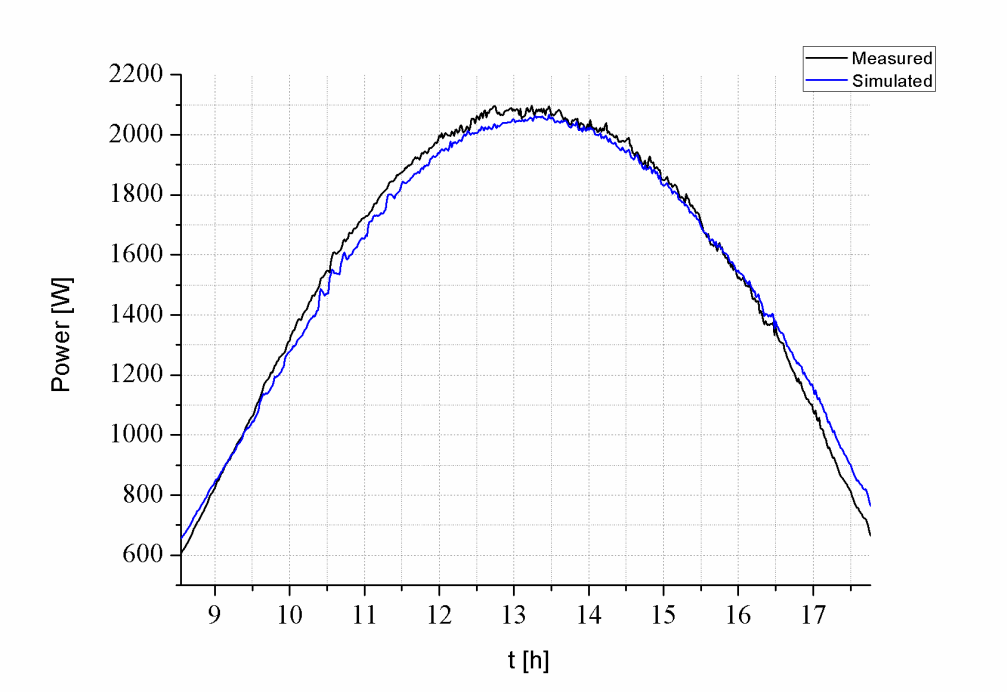

Fig. 2.3- PV system output Power, DC side – measured and simulated

As can be seen, there is a good agreement between simulation results and monitored data for the time evolution of the main PV system parameters.

2.3.3 Fault Diagnosis based on energy yields, current and voltage indicators

This approach is based mainly on the observation of the measured performance ratio (PR). Although this parameter gives a global idea of the system behavior, its practical use for the identification of malfunctioning components is limited. The PR for a particular system during certain period is not suitable quantity to indicate in which way the PV system can be improved due to the following reasons:

- Performance ratio gives no intuition in different component losses;
- There is no way to identify improperly functioning components;
- The numerical simulation must be based on reliable simulation tools and models validated experimentally.

2.3.4 Power loss factors in PV systems

2.3.4.1 Quantifying power losses

International Energy Agency (IEA) Photovoltaic Power System Program established four performance parameters that define the overall system performance with respect to the energy production, solar resources, rated power and overall effect of system losses. These performance parameters are the reference yield (Y_r), array yield (Y_a), final yield (Y_f) and the performance ratio (PR) which is defined as a ratio of the measured system efficiency and the nominal efficiency of the PV modules. A detailed explanation of each one of the parameters will be explained in detail:

- **Reference yield (Y_r)**

The reference yield is the total in-plane irradiance (H_i) divided by the reference irradiance (G_{ref}). It represents the equivalent amount of hours necessary for the array to receive the reference irradiance. This reference yield defines the solar radiation resource for the PV system. The value of the reference yield (Y_r) is calculated in Equation 2.3:

$$Y_r = \frac{H_i}{G_{ref}} \tag{2.3}$$

where:

H_i= Total in-plane irradiance [Wh/m^2]

G_{ref}= reference irradiation at STC (1000 W/m^2)

Y_r [Hours]

- **Array Yield (Y_a)**

The array yield is the energy generated by the PV array (Wh) divided by the rated output power of the PV array (Wp). It gives the number of hours where the installed PV system produces its rated output DC power. The value of the array yield (Y_a) is calculated in Equation 2.4:

$$Y_a = \frac{E_{dc}}{P_{ref}} \tag{2.4}$$

where:

E_{dc}= energy generated by the PV array [Wh]

P_{ref}= maximum power output of the PV array [Wp]

Y_a [Hours]

- **Final Yield (Y_f)**

The final yield is the AC energy output (consumed energy) divided by the rated DC power (P_{ref}) of the installed PV array. It represents the number of hours that the PV array operates at its rated power to produce that amount of AC energy. The value of the final yield (Y_f) is calculated by Equation 2.5:

$$Y_f = \frac{E_{ac}}{P_{ref}} \tag{2.5}$$

where:

E_{ac}= consumed PV energy [Wh]

P_{ref}= System rated power [Wp]

Y_f [Hours]

- **Performance Ratio (PR)**

The performance ratio (PR) quantifies the overall effect of losses on the rated DC output due to inverter efficiency, wiring mismatch and other losses when converting from DC to AC power; PV module temperature; incomplete use of irradiance by reflection from the module front surface; soiling or snow; system down-time; and component failures [2]. The value of the performance ratio (PR) is calculated by Equation 2.6:

$$PR = \frac{Y_f}{Y_A} \tag{2.6}$$

Therefore, the performance ratio gives a global idea of the system behavior and the overall system performance but it is not a good indicator for the identification of improperly functions of the PV system.

2.3.4.2 Power loss factors

This topic was already described in more detail in a previous section but in order to better understand this review, here is a quick overview of the loss factors in a PV system. Overall losses in PV systems happen in both DC and AC sides and are influenced by a number of factors. Figure 2.4 shows the main factors of power losses in PV systems:

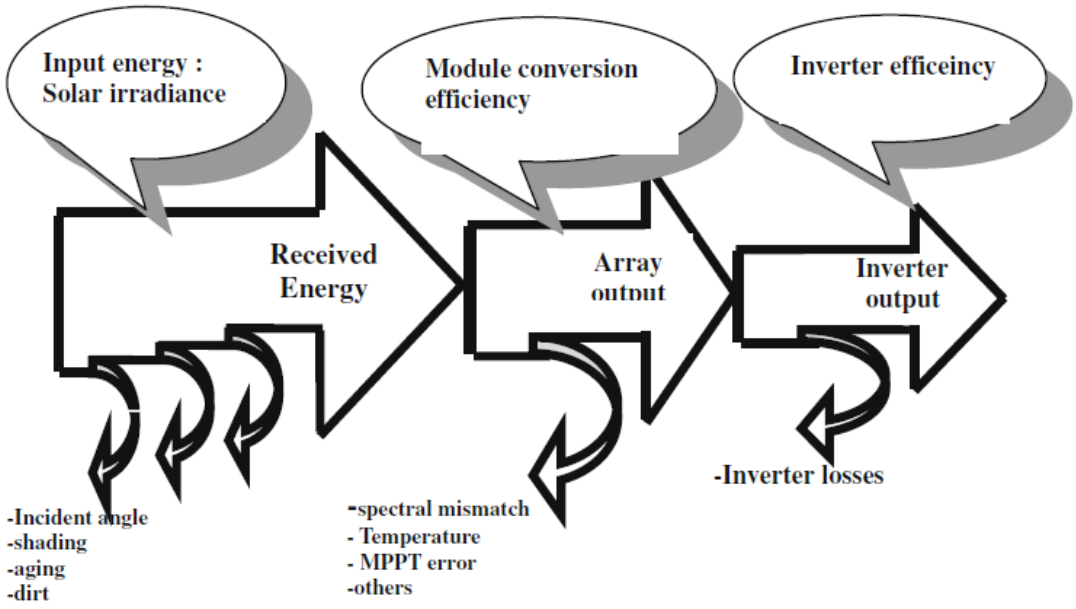

Fig. 2.4- Loss mechanisms in PV systems

The main loss factors are the following [40]:

- **Capture losses**

This kind of losses occur mainly at the DC side of the PV system and they are attributed to operating temperature, PV efficiency temperature dependency, dependency on solar irradiance level, shading and losses when sunlight is at a high angle of incidence (AOI).

- **System Losses**

They are mainly referred to the power conditioning units, which in our case are the DC-DC converter (MPPT) responsible to extract the maximum available power from the PV plant and the DC-AC converter. These two parts are usually presented by their efficiencies due to the ohmic power losses in the static switches forming part of both converters. In this previous work, the investigation was focused on the losses and malfunctions at DC side because until then and now there is no common way to prevent excessive losses or components breakdown at this part of the PV system contrary to the AC side where the inverters are well protected against improperly functions.

2.3.4.3 The capture losses – AC side

The capture losses can be divided into two kinds of losses [41]:

- **Thermal capture losses (Lct)**

The crystalline PV modules have a temperature coefficient for the maximum power point of -0.0044/°K. Also, the module efficiency at standard test conditions (STC) is defined at 25°C. Depending on the wind speed and the type of mounting of the PV modules, free-standing or roof integrated, there is a temperature rise of the modules with respect to the ambient of 20°C to 40°C at 1000 W/m^2. The corrected temperature at real working irradiance and a standard temperature of 25°C can be obtained by the simulation model where the input are the monitored irradiance and a fixed temperature of 25°C. The normalized capture losses can be determined by the following Equation:

$$Lct_{sim} = Ya_{sim}(G, 25℃) - Ya_{sim}(G, Tc) \tag{2.7}$$

where:

Lct_{sim} are the simulated thermal losses, Ya_{sim}(G,25°C) is the normalized energy yield at real working irradiance and 25°C of temperature, and Ya_{sim}(G,Tc) is the array yield at real working irradiance and real module temperature, Tc. Normalized thermal losses can give us the amount of power losses due the rise of temperature above 25°C. For temperatures below 25°C the Lct_{sim} will be negative representing a gain on the final performance of the system.

- **Miscellaneous capture losses (Lcm)**

In this kind of losses we gather all the other losses such as wiring, low irradiance, dirt accumulation, MPPT errors, and losses caused by faulty operation at the DC side such as faulty strings, faulty modules, partial shadowing, short circuit of modules, etc.

In this previous work the inputs of the simulations of the PV plant were the effective irradiance and the module temperature. Therefore, the simulated capture losses can be calculated with the following Equation:

$$Lc_{sim} = Yr(G, Tc) - Ya_{sim}(G, Tc) \tag{2.8}$$

where Lc_{sim} are the capture losses and Y_r(G,Tc) is the measured reference yield. Then the simulated reference miscellaneous capture losses are given by:

$$Lcm_{sim} = Lc_{sim} - Lct_{sim} \tag{2.9}$$

A daily comparison between measured capture losses and simulated capture losses was performed by the system diagnosis and failure detection procedure. The main idea of this method of system diagnosis and fault detection on the DC side of a PV system was based on the continuous check of the measured capture losses. For this purpose, were established theoretical boundaries in which the measured capture losses do not exceed any of them, otherwise the system is considered in faulty operation. The upper and lower boundaries of the inherent capture losses are evaluated by the

introduction of clear sky in-plane irradiance data to the simulation model [42]. Thus, the upper and lower boundaries are calculated by means of statistical approach and in case of PV system under normal operation. The measured capture losses remain the theoretical boundaries as given by the following equation:

$$Lc_{sim} - 2\delta < Lc_{mes} < Lc_{sim} + 2\delta \tag{2.10}$$

where δ is the standard deviation, calculated in daily basis of simulated capture losses given in case of clear sky conditions.

An example of how these boundaries work is presented on the following figures:

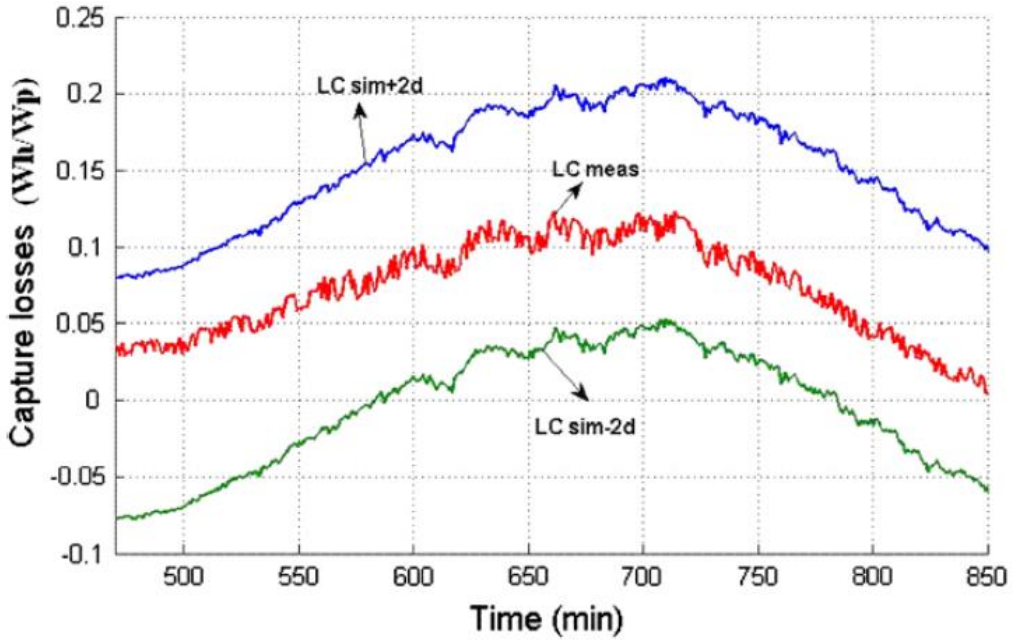

Fig. 2.5- Capture losses evolution on free fault operation of the PV system

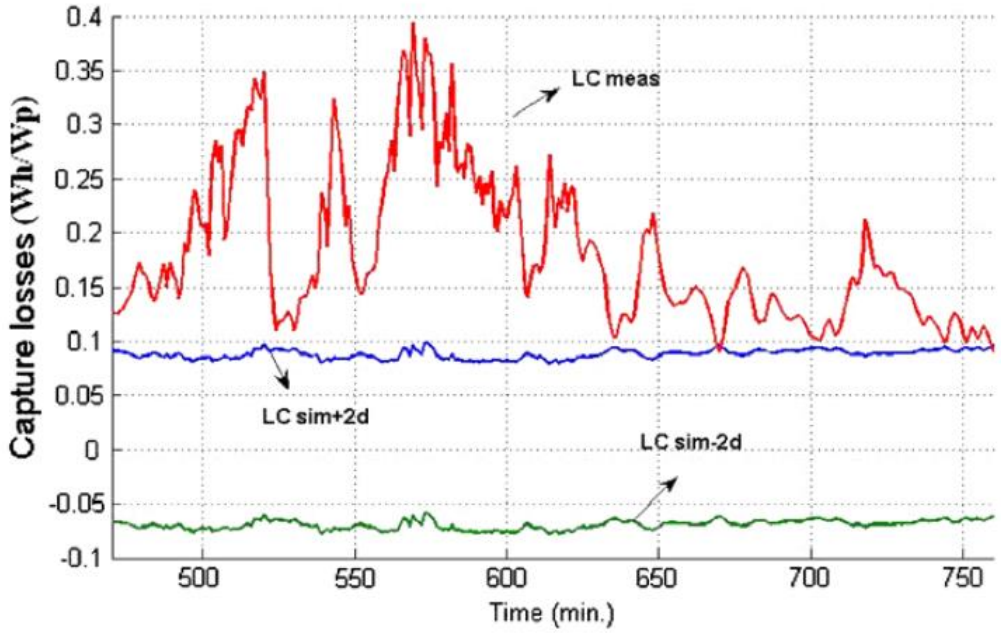

Fig. 2.6- Capture losses evolution on faulty string operation of the PV system

These capture losses indicators at AC side, were used in this previous work in order to simulate and predict capture losses based on the energy yields [2]. With the simulations of the capture losses indicators based on energy yields it was possible to define and predict the system performance with respect to the energy production, solar resources, rated power and overall effect of system losses. In order to know the effect of the system losses on the PV system we compared the DC output power measured in real time with the simulated DC output power.

2.3.5 Indicators for failure detection

The diagnosis procedure described above allows determining whether the actual capture losses are inside or outside the predetermined boundaries. In order to isolate the improperly function detected and determining the failure type, were defined two indicators of the deviation of the DC variables respect to the simulated ones. These indicators are the current and voltage ratios given by the following expressions [2]:

$$Rc = \frac{I_{PV\_sim}}{I_{PV\_meas}} \tag{2.11}$$

$$Rv = \frac{V_{PV\_sim}}{V_{PV\_meas}} \tag{2.12}$$

where I_{PV_meas} and V_{PV_meas} are the current and voltage measured at the DC output of the PV array respectively, and I_{PV_sim} , V_{PV_sim} are the results obtained for those parameters in the simulation of the PV system behaviour by using real irradiance and temperature monitored profiles.

Analysing the ratios, the most probable failure or malfunction is found following the flowchart at Figure 2.7 bellow:

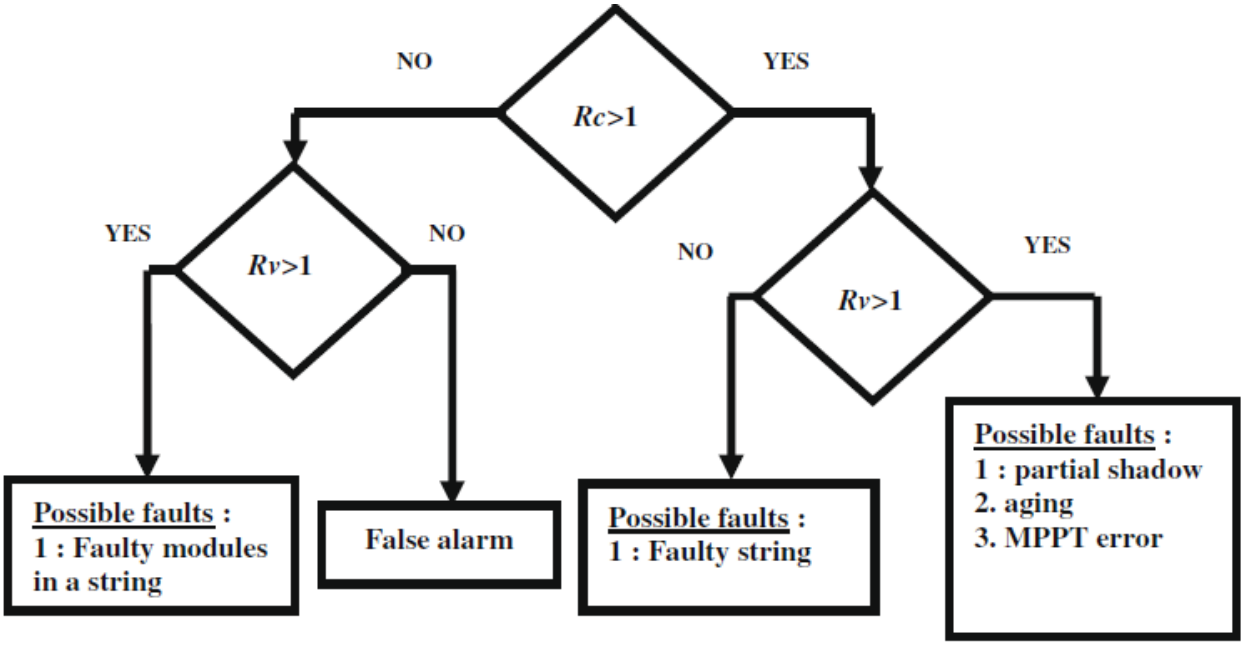

Fig. 2.7- Most probable faults present in the PV system

3. New Indicators for Fault Detection and Diagnosis of PV Systems

It is true that in the last 20 years photovoltaic panels show really low failure rates but it is important to keep always in mind that a PV panel it is fragile. Therefore when a PV module has a failure it compromises and has a big impact in the output power of the PV array. Moreover, although photovoltaic systems generally operate without problems, when faults or breakdowns do occur, these may not be detected for several months if no effective operation and monitoring system is in place. Therefore, this thesis work proposes a new method for detection and diagnosis of faults.

This section represents the core of this thesis. It starts describing the software used in this thesis. Afterwards, the new indicators, NRc and NRv, proposed for fault detection and diagnosis of PV systems are defined, and also the equations used to get these indicators and the validation of these same equations, comparing our results with manufacturer's PV modules data, in order to prove their validity. After this we present the simulations and results which prove their functionality. Then we show how the new parameters α and β can be very useful and the both ways to calculate them. Afterwards we have the impacts of faults on the behaviour of a PV system showing different results. Finally there is a study on how short-circuited PV modules and string faults may impact the output power of a PV system.

3.1 Soft environment & MatLab

The rapid growth of the PV industry over the years has expanded interest and the need for education and training worldwide at all levels of photovoltaic, but especially at the system level where more people are involved. This growth needed solutions and that's why engineers and technicians started to look for software that helps them with PV design, sizing and analysis. Today's engineers, professionals working in the field and students know how to use computers and are familiar with running specialized software. This section explains the software used for our simulations and work in this thesis.

PVSOL is an advanced design tool for sizing of grid-connected PV systems. This software is the choice for most of the installers and engineers who want performance prediction with improved detail and optimal grid-connected battery storage. We have used PVSOL to design different PV systems for our simulations. These PV systems had the objective of having different Power installed, PV modules, inverters, and systems configuration (Ns and Np). Therefore, with this software we were able to compare and size different PV systems and obtain detailed information about the different PV modules used in our simulations.

Photovoltaic engineering is a multidisciplinary specialty deeply rooted in semiconductor physics for solar cell theory and technology, and heavily relying on electrical and electronic engineering. Therefore, PSpice is a good choice of simulator for PV modeling because of its worldwide use in electric and electronic circuit simulation and its widespread availability [9]. It can be used to learn about photovoltaic systems or to solve technical problems of design, sizing and analysis.

Then we have MatLab that is a high-level and interactive environment for numerical computation, visualization and programming. MatLab can be used for a range of applications, including signal processing and communication, image and video processing, control systems, test and measurement, computational finance, and computational biology.

For our simulations we had to choose between PSpice and MatLab. Finally we chose MatLab because this software is very good for built-in graphs for visualizing data and tools for creating custom plots and also because the MatLab simulations were carried out by using models of PV modules based on

the five parameters models developed by Daniel Guasch [1] that have been adapted to the work developed in this thesis in order to achieve a proper detection of main faults present in grid connected PV system applications. In annex are some examples of the MatLab scripts used for the simulations done in this work.

3.2 New I&V indicators

Most diagnostic methods for fault detection of PV systems already known are time consuming and need expensive hardware. Therefore we propose a new method of fault detection, based in the previous work reviewed in the section 2.3 that evaluates the power losses present in the PV system for fault detection. This new method is based on new current and voltage indicators of the DC side of the inverter.

3.2.1 New Indicators, NRc and NRv

Chouder presented a diagnosis method for PV systems based in the evaluation of the power losses present in the PV system. In this previous work the fault detection procedure is also based in the current and voltage ratios as can be seen in Equation 2.11 and 2.12, respectively. The same parameters of Isofoton 106/12 were used on the method proposed by the present thesis work. In our work we did not used the energy yields method.

This method was successfully experimentally evaluated and allows identifying main faults in grid connected PV systems. However, this method requires the use of simulation tools that imply important computational effort to evaluate the losses in the PV system and also to calculate the current and voltage ratios. In order to completely avoid the use of modeling and simulation of the PV system in the fault detection procedure we defined two new current, NRc, and voltage, NRv, ratio indicators as follow:

$$NRc = \frac{I_m}{I_{sc}} \tag{3.1}$$

$$NRv = \frac{V_m}{V_{oc}} \tag{3.2}$$

where V_m and I_m are the voltage and current of the maximum power point (MPP) at the PV array DC output respectively, I_{sc} is the short circuit current of the PV array and V_{oc} the open circuit voltage of the PV array. On the later simulations using the Equations 3.1 and 3.2, the values of I_{sc} and V_{oc} are always referred to the free fault operation of the PV system while V_m and I_m may vary accordingly to the operation conditions of the system. The operation of the system may be fault free or a faulty operation.

3.2.2 Calculation of I_{scm} and V_{ocm} (PV Module)

For an arbitrary value of the irradiance and temperature, the short circuit current of a PV module, I_{scm}, is given by Equation 3.3 [9]:

$$Iscm = \frac{Iscmr}{1000} G + \left(\frac{dIscm}{dT} \right) (Tcell - Tr) \tag{3.3}$$

where I_{scmr} and Tr are the short circuit current of the PV module and the temperature at for standard test conditions (STC: G = 1000 W/m^2 and T = 25 °C) respectively, G is the actual irradiance on the PV module and Tcell is the real operating cell temperature. The open circuit voltage of the PV module, V_{ocm}, can be written as [9]:

$$Vocm = Vocmr + \left(\frac{dVocm}{dT}\right)(Tcell - Tr) + V_T \ln\left(\frac{Iscm}{Iscmr}\right) \quad (3.4)$$

where V_{ocmr} is the open circuit voltage of the PV module at STC and V_T the thermal voltage. The values of I_{scm} and V_{ocm} can be easily estimated for any condition of temperature and irradiance, by using Equations 3.3 and 3.4 taking into account the PV module parameters given by manufacturers at STC. Thus, we do not need to monitor these values because we can simulate them with high accuracy.

Afterwards, we will use the equations 3.3 and 3.4 to estimate both parameters, I_{scm} and V_{ocm}, for a set of commercial PV modules and then a comparison was made with values given by the manufacturers. Table 3.1 describes the commercial PV modules considered as well as main PV module parameters. The parameters of the Isofoton are resulting from the five parameter extraction model and the parameters of the other three PV models, BP, Helios and Siemens are from literature [50].

Table 3.1- Commercial PV modules used on this work

Model **Parameter**	**Isofoton 106W-12**	**BP 5160S**	**Helios 1500**	**Siemens SP150**
n	1.14	1.12	1.2	1.13
I_o (A)	3×10^{-10}	1.56×10^{-09}	2.83×10^{-8}	2.6×10^{-09}
R_s (Ω)	0.33	0.587	0.182	0.932
R_{sh} (Ω)	199	1946	39.21	348.2
I_{sc} (A)	6.54	4.7	7.88	4.8
Solar cells (Ns x Np)	36 x 2	72 x 1	36 x 1	72 x 1
V_{oc} (V)	21.6	44	21	43.4
P (W)	106	150	120	150
V coeff. (mV/K)	-144.7	-160	-90	-77
I coeff. (mA/K)	2.5	3.05	0.2	2.06

In order to test if the estimations of V_{ocm} and I_{scm}, using Equations 3.3 and 3.4 agreed with the data presented in the PV module manufacturer sheets, we traced the I-V curve for two of the PV modules used and then we compared our I-V curves with the curves provided by the manufacturers. On the next figures are shown the respective I-V curves simulated:

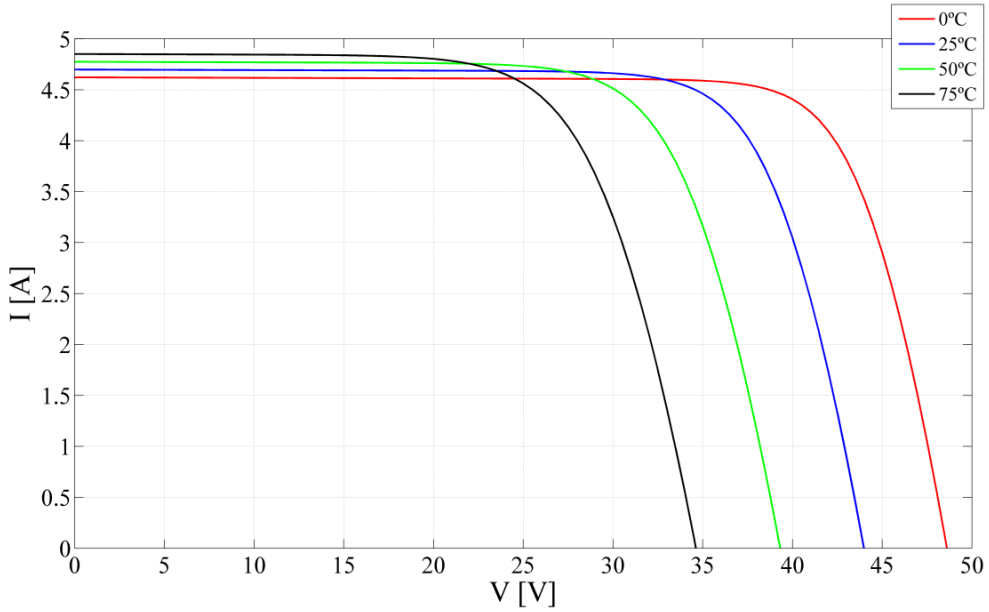

Fig. 3.1- I-V curves with G=1000 W/m^2, BP 5160S

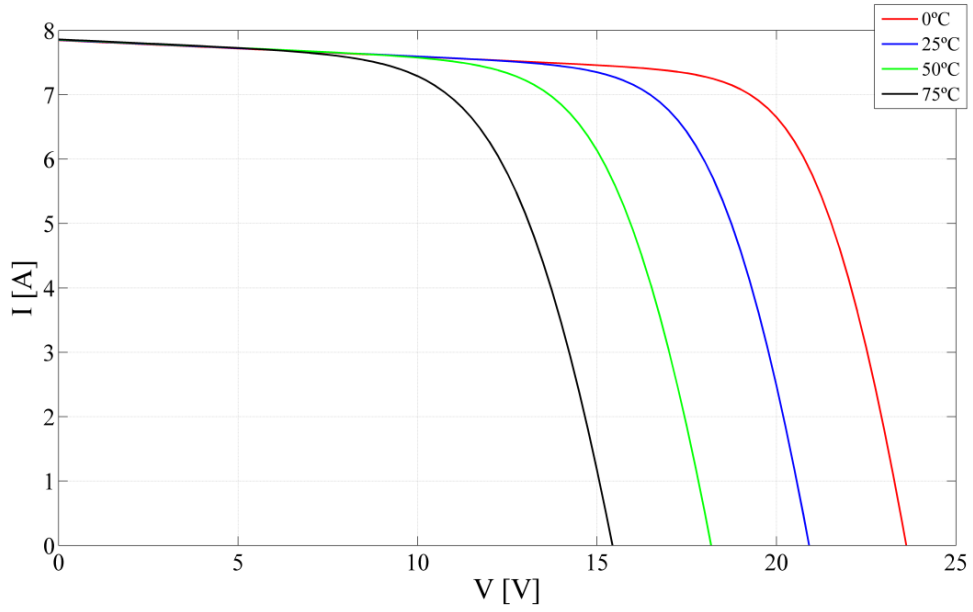

Fig. 3.2- I-V curves with G=1000 W/m^2, Helios 1500

After analyzing these I-V curves we gathered the results in the Table 3.2 that show us the estimation of the I_{sc} and V_{oc} respectively, on STC, for the commercial PV modules in comparison with values given by its manufacturers:

Table 3.2- I_{sc} and V_{oc} results from manufacturer and simulated data

	BP5160S		Helios 1500	
STC	Manufacturer	Simulated	Manufacturer	Simulated
I_{sc} [A]	4.70	4.70	7.88	7.85
V_{oc} [V]	44.00	43.92	21.00	20.88

As can be seen, the values given by the PV module manufacturers agree with our estimations obtained by using Equations 3.3 and 3.4. The simulations of Table 3.2 have an error of about 3% as the simulations already done in previous works using the same simulation models [37,48]. Furthermore, we can compare the I-V curves with the manufacturer sheets shown in the annex section.

3.2.3 Calculation of I_{mm} and V_{mm} (PV Module)

The coordinates of the MPP for the PV array, I_m and V_m, are available at the inverter input, considering that the inverter includes maximum power point tracking (MPPT), which is the case of most inverters used in grid connected applications. This is also the case of the inverter used in our actual PV system in study, the grid connected PV system located in the Centre de Développement des Energies Renouvelables (CDER), Algeria. Therefore, for the applications in real systems we will have actual values of I_m and V_m available at the DC input of the inverter.

After we dealt with the actual system we had to simulate more systems we did not had real data of I_m and V_m from the inverters, even though they include a MPPT. The solution was to simulate the current and voltage at MPP for the PV modules, where I_{mm} is given by Equation 3.5 and V_{mm} is given by Equation 3.6 [9]:

$$\mathrm{Im}\,m = \left(\frac{\mathrm{Im}\,mr}{1000} G + \left(\frac{dIscm}{dT} \right) (Tcell - Tr) \right) \tag{3.5}$$

$$Vmm = \left(N_{sc} V_T \ \ln\left(1 + \frac{Iscm - \mathrm{Im}\,m}{Iscm} \left(e^{\frac{Vocm}{N_{sc} V_T}} - 1 \right) \right) - \mathrm{Im}\,m \ Rsm \right) \tag{3.6}$$

Afterwards, I_{mm} and V_{mm}, are going to be used to calculate I_m and V_m for the whole array of the different PV systems simulated. The configurations of these systems are described on a later section of this thesis.

In order to test the estimations of V_{mm} and I_{mm} with the data presented in the PV module manufacturer sheets, we analyzed the evolution of I_{mm} and V_{mm} at STC, using Equations 3.5 and 3.6. For two of the PV modules used on our simulated systems, we traced the Power curve as can be seen in the following figures:

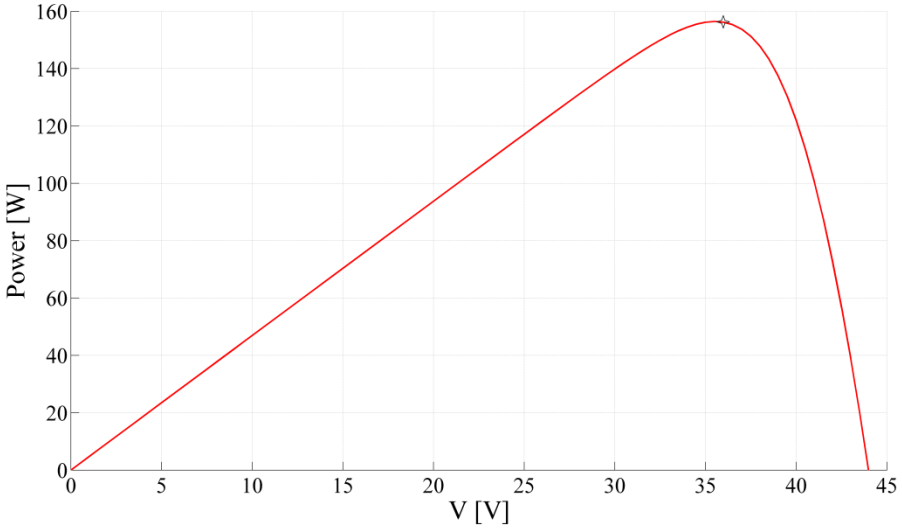

Fig. 3.3- Power curve - BP BP5160S

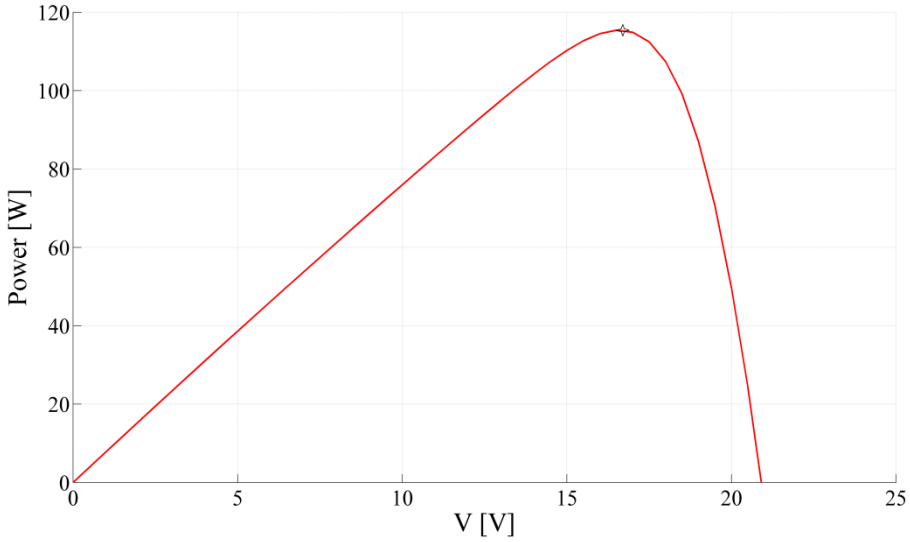

Fig. 3.4- Power curve – Helios 1500

After analyzing these Power curves we were able to calculate the Power at the maximum power point (P_{mpp}), I_{mm} and the V_{mm}. The maximum power point (MPP) is marked in the Figures 3.3 and 3.4 for each PV module. Therefore, we gathered the results in the Table 3.3 that show us the estimation of the P_{mpp}, V_{mm} and I_{mm}, respectively at STC, for the commercial PV modules in comparison with values given by its manufacturers:

Table 3.3- V_{mpp}, I_{mpp} and P_{mpp} results from manufacturer and simulated data

	BP5160S		Helios 1500	
STC	Manufacturer	Simulated	Manufacturer	Simulated
V_{mpp} [V]	36.0	35.5	17	16.6
I_{mpp} [A]	4.44	4.40	7.06	6.96
P_{mpp} [W]	160	156	120	115

where V_{mm} is the V_{mpp} of a PV modules and the I_{mm} is the I_{mpp} of a PV module. As can be seen, the values given by the PV module manufacturers agree with the estimations obtained by Equations 3.5 and 3.6. On the simulations of the PV arrays presented in this section we scaled the Equations 3.5 and 3.6 in order to have the I_m and V_m of the entire array. This can be seen in the scripts presented in the annex section. The simulations of Table 3.3 have an error of about 3% as the simulations already done in previous works using the same models [37,48].

3.2.4 Calculation of I_{sc} and V_{oc} (Array)

Considering a PV array composed of Np parallel branches of PV modules, including a number of Ns PV modules in series per branch, Equations 3.3 and 3.4 can be scaled to calculate the V_{oc} and I_{sc} of the entire PV array as follows [9]:

$$Isc = Np\left(\frac{Iscmr}{1000}G + \left(\frac{dIscm}{dT}\right)(Tcell - Tr)\right) \tag{3.7}$$

$$Voc = Ns\left(Vocmr + \left(\frac{dVocm}{dT}\right)(Tcell - Tr) + V_T \ln\left(\frac{Iscm}{Iscmr}\right)\right) \tag{3.8}$$

Then the ratios NRc and NRv defined by Equations 3.1 and 3.2 can be estimated.

3.2.5 Indicators in Fault-Free operation

On the other hand, we defined the ratios NRco and NRvo as the expected values of NRc and NRv, in normal operation of the PV system (fault-free). These indicators are given by:

$$NRco = \frac{I_{mo}}{I_{sc}} \tag{3.9}$$

$$NRvo = \frac{V_{mo}}{V_{oc}} \tag{3.10}$$

where I_{mo} and V_{mo} are the output current and voltage at the maximum power point of the output of the PV array in absence of faults.

The values of I_{mo} and V_{mo} for a PV array of arbitrary series-parallel (Ns x Np) connection of PV modules can be calculated for any condition of G and Tcell by using the following equations that include parameters of the PV modules forming the PV array [9]:

$$\mathrm{Im}\,o = Np\left(\frac{\mathrm{Im}\,mr}{1000}G + \left(\frac{dIscm}{dT}\right)(Tcell - Tr)\right) \tag{3.11}$$

$$Vmo = Ns\left(N_{sc}V_T\ \ln\left(1 + \frac{Iscm - \mathrm{Im}\,m}{Iscm}\left(e^{\frac{Vocm}{N_{sc}V_T}} - 1\right)\right) - \mathrm{Im}\,m\ Rsm\right) \tag{3.12}$$

where a value of n=1 is used for the diode ideality factor, Immr and Tr are the current of the PV module at the maximum power point and the temperature at standard test conditions respectively, N_{sc} is the number of solar cells in series forming the PV module, Rsm is the series resistance of the PV module, I_{scm} and V_{ocm} are the short circuit current and open circuit voltage of the PV module given by Equations 3.3 and 3.4, and I_{mm} is the maximum current of the PV module given by Equation 3.5.

In normal operation of the PV system, fault-free operation, the values of the indicators NRc and NRv should be very similar to the values of NRco and NRvo given by Equations 3.9 and 3.10 and maintain values over specific thresholds.

3.3 Faults on PV systems

Due to the important negative impact of a PV module failure on the final energy production, we developed a method to detect and diagnose faults on PV systems based on the DC side of the inverter. The developed procedure provides us information about when the system is in a constant energy loss. The most common failures of this kind are: String problems, short-circuited modules, total black-out and Soiling.

In the proposed method the main focus of our work is on string problems and short-circuited modules, yet we can detect grid faults and shading effects but these faults on the system need a bigger effort to detect and diagnose and for now could not directly apply the method using the thresholds. Nevertheless, shading effect and grid faults will be also analyzed.

3.3.1 Fault detection

Firstly, the thresholds that confirm a fault-free operation of the system must be fixed depending on the specific characteristics of the PV array, mainly the configuration of series and parallel connection of the PV modules forming part of the array. When one of the values of the indicators, NRc or NRv, is

below the threshold, a fault is detected in the PV system. Table 3.4 shows the most probable faults present in the PV system based on the values of the ratios NRc and NRv.

Table 3.4- Constant Energy Loss Faults in a PV system based on the new indicators

Possible Faults	**NRc**	**NRv**
No Fault	OK	OK
String Fault	Below Threshold	OK
Short-Circuited Modules	OK	Below Threshold
Short-Circuited Modules & String Fault	Below Threshold	Below Threshold

When a fault is detected in the PV system an internal data logger interface of the inverter can be used for the transmission of the measured data and the alarm event to a server or a local network through a standard RS485, an Ethernet connection or optionally with a GSM Modem.

On the other hand, the inverter requires a minimum input voltage (start-up voltage) to start working. A minimum level of irradiance on the PV array is necessary to enable the proper operation of the inverter. Taking into account this fact we considered a minimum level of G= 200 W/m^2 to start the fault detection evaluation procedure in the PV system and to calculate the corresponding current and voltage indicators. Therefore, our study and simulations are based on the time period of the day where we have irradiance values above 200 W/m^2. That period of the day is the same on the three different days, when the data of the three different conditions of work (fault-free, short-circuited modules and string fault) of the PV system were extracted. On the other hand, the period of the day of the extracted data during the conditions of shading and grid-fault were slightly different.

3.3.2 Analysis of the thresholds for indicators of voltage and current

Two of the most common faults in PV systems are due to the appearance of short circuits and open circuits in PV modules forming part of the strings. When an open circuit appears in one string of the PV array the whole string is disconnected and then the output current of the PV array is reduced. On the other hand, when a short-circuit appears in one PV module of a string of the PV array, that PV module is disconnected and the output voltage of the PV array is reduced [43]. The thresholds for current and voltage indicators can be fixed attending to these two situations: A faulty string in the PV array and one PV module short-circuited in a string.

3.3.2.1 Faulty string

A PV array is formed by connection of a number of Np strings of PV modules and having a number of Ns PV modules connected in series per string. In fault-free operation the output current of the PV array at the MPP, I_m, is the product of Np and the maximum output current of one of the PV modules, I_{mm}. So, Equation 3.9 can be rewritten as follows:

$$NRco = \frac{Np\ I_{mm}}{I_{sc}} \tag{3.13}$$

When an open circuit is present in one of the strings, the reduction in the output current of the PV array is equal to the output current of the faulty string, I_{mm}. Then, in case of a faulty string the value of the ratio of current, *NRcfs (new ratio of current for faulty string)*, will be lower than its value in free fault operation mode NRco, and can be calculated as the following equation shows:

$$NRcfs = \frac{(Np-1)\ I_{mm}}{I_{sc}} = \alpha \frac{Np\ I_{mm}}{I_{sc}} \tag{3.14}$$

where α is the relation between the ratios of current in faulty string, NRcfs, and fault-free operation, NRco, given by:

$$\alpha = \frac{NRcfs}{NRco} \tag{3.15}$$

$$\alpha = 1 - \frac{1}{Np} \tag{3.16}$$

Taking into account the above Equations 3.14-3.16, the threshold for the ratio of current in case of fault string, TNRcfs, can be evaluated. When one or more faulty strings are present in the PV system the value of NRc must be below the value indicated by TNRcfs to allow the identification of this kind of fault.

In order to avoid false fault detections we have fixed an offset of a 2% respect the NRco value. Then, the threshold for the ratio of current can be written as follows:

$$TNRcfs = 1.02\ \ \alpha\ \ NRco \tag{3.17}$$

3.3.2.2 Short-Circuited PV module

In fault-free operation the output voltage of the PV array at the MPP, V_m, is the product of Ns and the maximum output voltage of one of the PV modules, V_{mm}. Then, Equation 3.10 can be rewritten as follows:

$$NRvo = \frac{Ns\ V_{mm}}{V_{oc}} \tag{3.18}$$

When a PV module is short-circuited in one of the strings the new value of the voltage ratio, *NRvbm (new ratio of voltage for short-circuited module)*, will be lower than its value in fault-free operation mode, NRvo. The expected value of NRvbm in that situation can be calculated using the following equation:

$$NRvbm = \frac{(Ns-1)\ V_{mm}}{V_{oc}} = \beta \frac{Ns\ V_{mm}}{V_{oc}} \tag{3.19}$$

where β is the relation between the voltage ratios in case of one short-circuited PV module and free fault operation, given by :

$$\beta = \frac{NRvbm}{NRvo} \tag{3.20}$$

$$\beta = 1 - \frac{1}{Ns} \tag{3.21}$$

The threshold for the voltage ratio in case of one short-circuited PV module in a string, TNRvbm, can be evaluated following the same criteria that we used in the previous case of faulty string as follows:

$$TNRvbm = 1.02\ \ \beta\ NRvo \tag{3.22}$$

When one or more PV modules are short-circuited in some of the strings of the PV system, the value of NRvbm will be below the value indicated by TNRvbm given by Equation 3.22, allowing the identification of this kind of fault.

The expressions obtained for α and β in Equations 3.16 and 3.21 respectively, show that both parameters do not depend on the PV module parameters neither on the total power of the PV array. Both parameters depend only on the array configuration, Ns and Np. If the PV array configuration is known, α and β can be evaluated and then the thresholds for the current, TNRcfs, and voltage, TNRvbm, indicators that evidence the presence of faults in the PV system can be fixed by using Equations 3.17 and 3.22.

3.3.2.3 Short-circuited PV Module & String Fault

Both short-circuited PV modules and faulty strings can impact a PV system at the same time. In order to detect both faults at the same time, new indicators were developed using previous ones already developed in this work. This was done with the purpose to have a better and more complete fault detection and diagnosis fault system. The new indicators are: a0, ay, aNp and b0, bx, bNs.

As the indicators a0, ay and aNp are referred to faulty strings, they can be defined by the following Equations:

$$a0 = NRco \tag{3.23}$$

$$ay = TNRcfs - (y-1)(1-\alpha) \tag{3.24}$$

$$aNp = 0 \tag{3.25}$$

where *a0* is always equal to NRco, *ay* is the threshold for *y* number of faulty strings (y>0), and finally *aNp* is always equal to 0 because it's when all strings are in fault. For example, following the Equation 3.24, the thresholds for one faulty string and two faulty strings are calculated by Equations 3.26 and 3.27, respectively:

$$a1 = TNRcfs \tag{3.26}$$

$$a2 = TNRcfs - 1(1 - \alpha) \tag{3.27}$$

As the indicators b0, bx and bNs are referred to short-circuited PV modules, they can be defined by the following Equations:

$$b0 = NRvo \tag{3.28}$$

$$bx = TNRvbm - (x - 1)(1 - \beta) \tag{3.29}$$

$$bNs = 0 \tag{3.30}$$

where *b0* is always equal to NRvo, *bx* is the threshold for *x* number of short-circuited modules (x>0), and finally *bNs* is always equal to 0 because it's when all modules are short-circuited. For example, following the Equation 3.29, the thresholds for one short-circuited module and two short-circuited modules are calculated by Equations 3.31 and 3.32, respectively:

$$b1 = TNRvbm \tag{3.31}$$

$$b2 = TNRvbm - 1(1 - \beta) \tag{3.32}$$

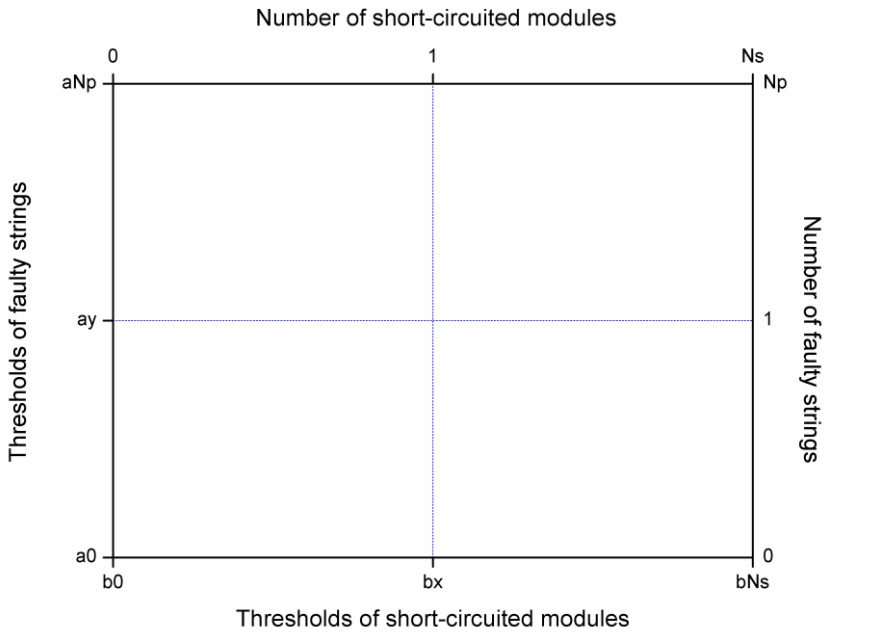

Fig. 3.5- Model for detection of both faults: short-circuited modules and faulty strings

Figure 3.5 shows how we can use these new indicators in order to detect both faults at the same time. The axis of this graph changes with the different system configuration. For example, for a PV system with Ns= 10 and Np= 14, the x axis will start with b0 and then we will have b1, b2, b3, b4, (…), until it ends with bNs. The y axis will start with a0 and then we will have a1, a2, a3, a4, a5, (…), until it ends with aNp. It is important to understand that the value of b0>b1>b2>(…)>bNs and that a0>a1>a2>(…)>aNp, where bNs and aNp are always equal to zero.

Therefore, for example, if:

Case 1:

$$b2 > NRv > b3 \qquad and \qquad a1 > NRc > a2$$

It will be detected *two* short-circuited PV modules and *one* string fault.

Case 2:

$$b0 > NRv > b1 \qquad and \qquad a3 > NRc > a4$$

It will be detected *zero* short-circuited modules and *three* faulty strings in that PV system.

3.4 Simulation Study using the new indicators and thresholds

3.4.1 Introduction

A simulation study was carried out to analyse the potential of the new current and voltage indicators in fault detection as well as the effectiveness of the values estimated in the above section for parameters α , β, TNRvbm and TNRcfs.

The simulation of the PV systems is based in the well-known five parameter model for the solar cell already described in a previous section. The simulation of PV systems using this base model has been implemented in different software environments as: MatLab [4, 44-45], Pspice [30, 43, 46-47] or LabView [48, 49], and experimentally validated. In this study we have selected the MatLab environment for the simulations set. The inputs for the simulation of the PV system are the main parameters of the solar cell model: The cell photocurrent (I_{PH}), the diode saturation current (I_0), the ideality factor of the diode (n), the series resistance (R_s) and the shunt resistance (R_{sh}). Other parameters included as inputs are: The number of solar cells per PV module (N_{sc}, N_{pc}), the configuration of the PV array: Ns and Np and the data corresponding to the irradiance (G) and temperature profiles.

3.4.2 Simulated systems

As seen before, Table 3.1 shows the commercial PV modules selected in this simulation study and their main parameters at STC. The PV modules: Isofoton 106W-12 and Helios 1500 have open circuit voltages around 21 V and short circuit currents over 6 A, while PV modules: BP 5160S and Siemens SP150 have higher open circuit voltages, around 44 V, and lower short circuit currents, around 4.7 A. These differences in open circuit voltage and short circuit current were selected to study the influence of the PV module parameters in the thresholds of the current and voltage indicators when a fault appears in the PV array.

Table 3.5- Systems of study configuration

System of Study	PV module	Ns	Np	P [kWp]
0	Isofoton 106W-12	5	2	1.06
1	Helios 1500	15	2	3.3
2	BP5160S	15	2	4.5
3	Helios 1500	22	2	5.28
4	BP5160S	15	3	7.2
5	Isofoton 106W-12	11	9	10.5
6	SP150	15	6	15
7	Helios 1500	40	4	19.2
8	BP5160S	10	14	21

On the other hand PV arrays with DC output powers ranging from 1 kW up to 21 kW, including different types of the selected PV modules and different configurations of PV modules in series per branch (Ns) and number of parallel branches (Np), were studied to analyse if the size of the PV array affects the values of the thresholds for the current and voltage indicators when a fault appears in the PV array. Table 3.5 describes the different PV arrays included in the simulation study as well as the PV modules forming part of the array and the configuration of the PV array: Ns x Np in each of the case studies.

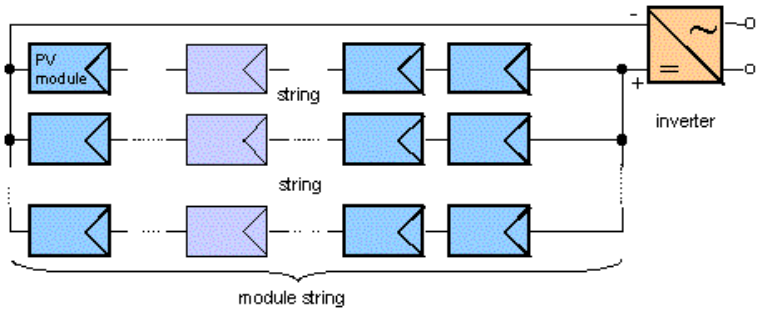

Fig. 3.6- Common scheme of a grid connected PV system

These PV arrays have been simulated, considering a set of real irradiance and temperature profiles in three cases: Normal operation (no faults present in the PV system), faulty string (one string in open circuit) and short-circuited module (one PV module short-circuited in one string). The irradiance and temperature profiles for each of the three cases were taken in three different days.

3.4.3 Indicators values for the simulations of all systems

The evolutions of the indicators: NRco, NRvo, NRcfs and NRvbm have been calculated in each one of the simulations carried out as well as mean values and standard deviations. Table 3.6 shows the average values obtained for those indicators and their standard deviations. The values of the thresholds TNRcfs and TNRvbm calculated by using Equations 3.17 and 3.22 are also given.

As can be seen in Table 3.6, in case of normal operation the values obtained for the voltage ratio, NRvo, vary from 77.89% to 81.05%, while for the ratio of current, NRco, these values vary from 85.20% to 92.23%.

Table 3.6- Results from all the system simulations

System of Study	Normal Operation (No faults)				Faulty String			Short-Circuited PV module		
	NRco (%)	σ NRco	NRvo (%)	σ NRvo	NRcfs (%)	σ NRcfs	TNRcfs	NRvbm (%)	σ NRvbm	TNRvbm
0	90.78	4.70×10^{-3}	81.05	1.12×10^{-2}	45.39	2.31×10^{-3}	46.29	64.80	8.41×10^{-3}	66.13
1	85.20	2.21×10^{-2}	77.95	1.46×10^{-2}	42.60	1.04×10^{-2}	43.45	72.80	1.31×10^{-2}	74.20
2	92.23	2.99×10^{-3}	80.03	1.30×10^{-2}	46.11	1.44×10^{-3}	47.03	74.70	1.30×10^{-2}	76.18
3	85.20	2.05×10^{-2}	77.95	1.47×10^{-2}	42.60	1.03×10^{-2}	43.45	74.40	1.30×10^{-2}	75.89
4	92.23	2.99×10^{-3}	80.03	1.38×10^{-2}	61.48	1.39×10^{-3}	62.71	74.69	1.31×10^{-2}	76.18
5	90.78	4.63×10^{-3}	81.05	1.05×10^{-2}	80.69	4.11×10^{-3}	82.30	73.68	9.56×10^{-3}	75.15
6	92.23	2.93×10^{-3}	79.63	1.45×10^{-2}	76.86	2.43×10^{-3}	78.39	74.76	1.35×10^{-2}	75.80
7	85.46	1.90×10^{-2}	77.89	1.49×10^{-2}	64.09	1.43×10^{-2}	65.37	75.94	1.41×10^{-2}	77.46
8	92.23	2.92×10^{-3}	79.98	1.44×10^{-2}	85.64	2.72×10^{-3}	87.35	71.98	1.30×10^{-2}	73.42

In case of a faulty string in the PV system the values obtained of the ratio of current, NRcfs, are lower than the values of NRco and below the thresholds given by TNRcfs in all cases.

When a PV module is short-circuited in one string the results obtained for the voltage indicator, NRvbm, are also lower than the values obtained for NRvo and below the thresholds, TNRvbm, in all cases.

3.4.4 Obtaining α and β by using both procedures

We have calculated the values of parameters α and β in all cases included in this simulation study. Firstly, the values of both parameters were evaluated using Equations 3.16 and 3.21 using the values of Ns and Np shown in Table 3.5 then we used Equations 3.15 and 3.20 using the results shown in Table 3.6 for: NRco, NRvo, NRvbm and NRcfs. A comparison of the set of values obtained for α and β by using both procedures is shown in Table 3.7.

Table 3.7- Values obtained for α and β

System of Study	α [%]		β [%]	
	1-(1/Np)	NRcfs/NRco	1-(1/Ns)	NRvbm/NRvo
0	50.00	50.00	80.00	79.95
1	50.00	50.00	93.33	93.33
2	50.00	49.99	93.33	93.33
3	50.00	50.00	95.45	95.44
4	66.66	66.66	93.33	92.32
5	88.88	88.89	90.90	90.90
6	83.33	83.34	93.33	93.88
7	75.00	74.99	97.50	97.49
8	92.85	92.85	90.00	89.99

As can be seen in Table 3.7, a good agreement between values obtained from the two procedures for both parameters is achieved. These results are in accordance with the assumption that those parameters depend only on the array configuration, Ns and Np, and can be evaluated by using Equations 3.16 and 3.21.

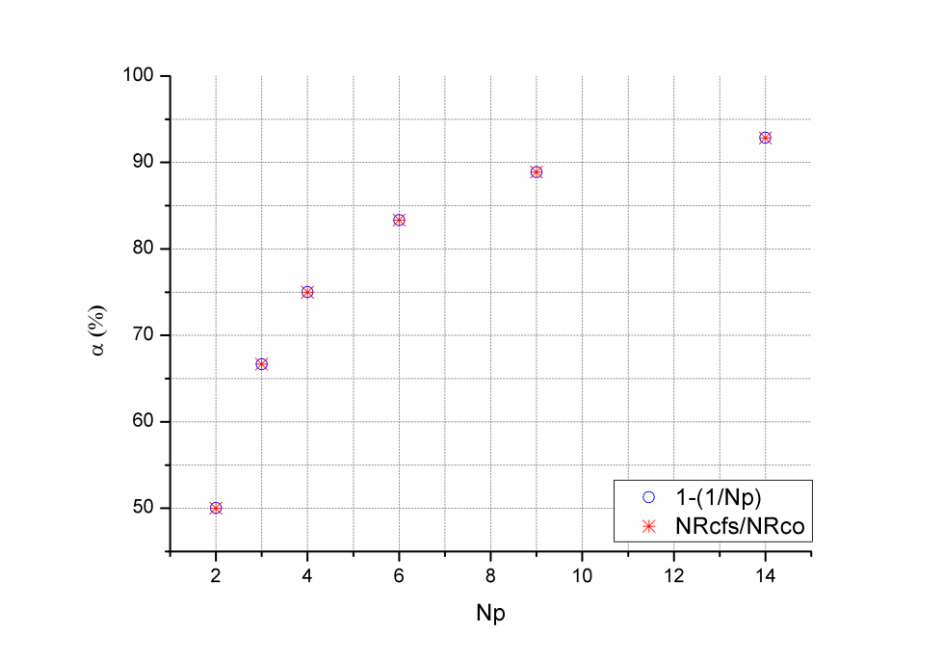

Fig. 3.7- α parameter values as a function of Np

Figure 3.7 shows the values obtained for the parameter α as a function of Np. As can be seen in the figure the values of α vary from 50% in case of a PV array having 2 strings to 92.85% for a PV array formed by 14 strings.

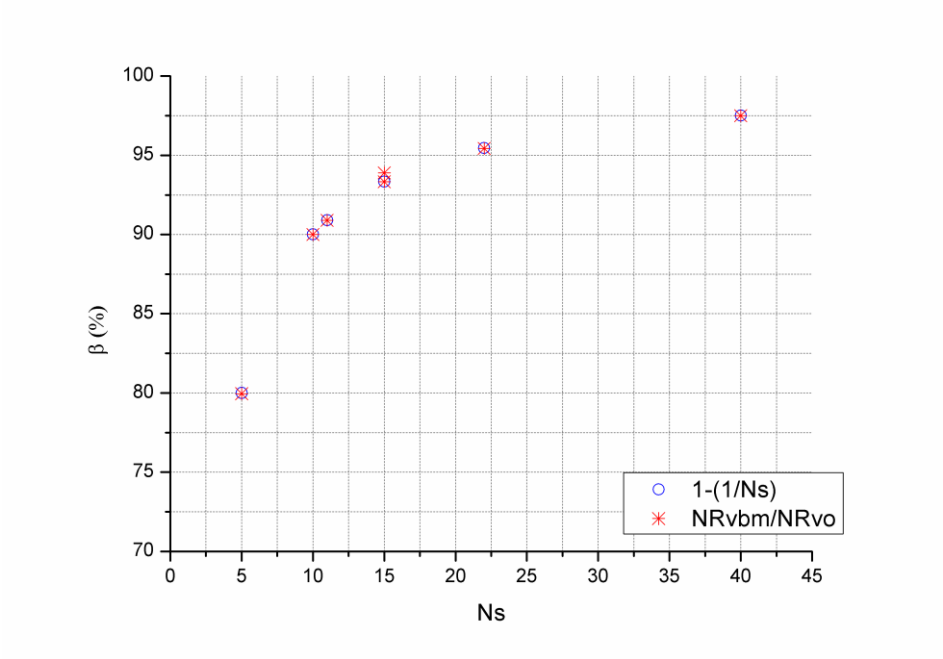

Fig. 3.8- β parameter values as a function of Ns

On the other hand, Figure 3.8 shows the values obtained for the parameter β, the minimum threshold as a function of Ns. The values obtained for β are ranging from 80 % for a PV system formed by strings of 15 PV modules connected in series to 97.5% for a PV system formed by strings containing 40 PV modules in series.

Therefore, with the previous two figures we have the first evidence of the impact of a fault accordingly to the size of the PV system.

3.5 Impacts of string faults and short-circuited modules

3.5.1 Impacts of faulty strings

In this section will be shown how different string faults in a system impact the output Power, Current and Voltage at MPP. Then we will see how the ratios react to these variations. This study of the impact of the faults on the behavior of a PV system was done on every system of the Table 3.5. As a model of a PV system, we chose to show the results of the system of study number 8, as can be seen in Table 3.5, because of the high number of strings presented on the configuration of that system.

This system uses a configuration of Ns=10 and Np=14. The PV module is a BP5160S and the total array power is 21 kWp. The irradiance and temperature used in this simulation are real data.

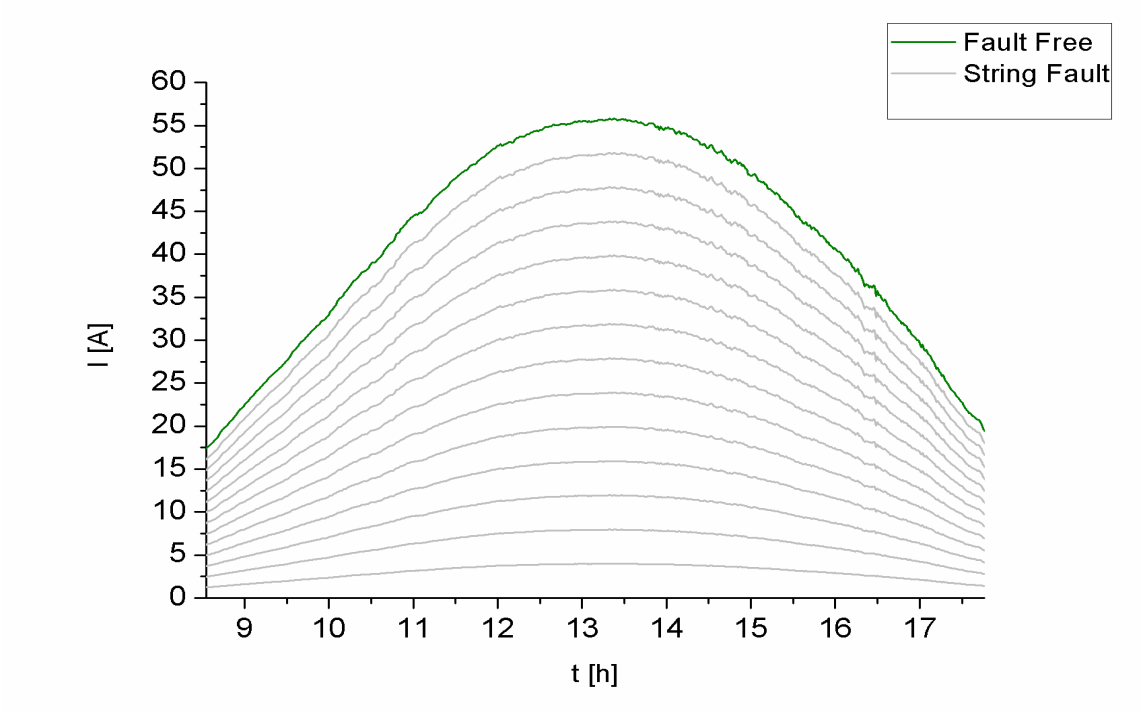

Fig. 3.9- Output Current profile with different number of faulty strings

As can be seen in Fig. 3.9, a fault in a string has a direct impact on the output current of the DC side of the PV system. The green line is related to the maximum output current at DC side, I_m, on free fault operation and the grey lines below are the output current profiles related to the system working with different cases of string faults. The first grey line, the one right below the green one, is the minimum number of strings in fault, 1 string in fault and 13 working strings, and the last grey line represents 13 strings in fault and only 1 working string, making a total of 14 strings that composes de PV system.

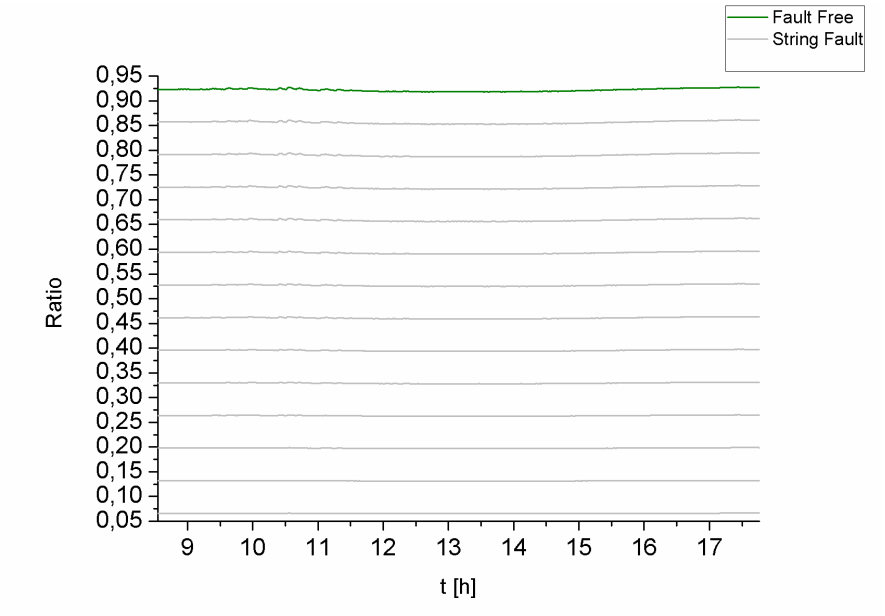

Fig. 3.10- NRc: Current ratio profiles

Figures 3.10 show the evolution of the ratio NRc during the tested period of time for the system number 8. The green line is the NRco. The Figure 3.10 follows the same concept of the Figure 3.9 and NRc have a variation of the same order of the output current. This variation between a line and the other one above (Lc), referring to one less string in fault, can be measured with the Equations 3.33 and 3.34:

$$Lc = 1 - (1 - \left(\frac{1}{Np}\right)) \tag{3.33}$$

$$Lc = 1 - \alpha \tag{3.34}$$

And this difference will be always the same.

The voltage ratio (NRv) in free fault and string fault, with the same data of irradiance and temperature, has the same behavior in both operation conditions.

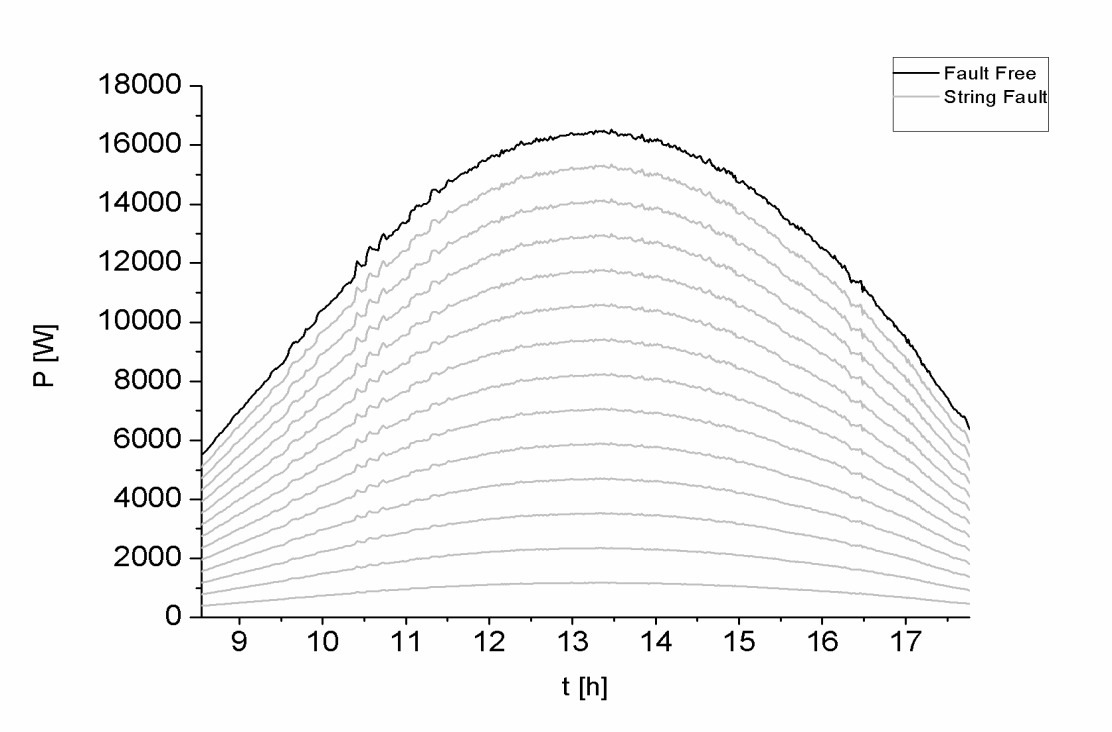

Fig. 3.11- Power profile with different number of faulty strings

With the Figure 3.11 we can see the impact of the different number of faulty strings on the output power of the PV system and this will translate on losses of generated energy.

3.5.2 Impacts of short-circuited PV modules

Now will be shown how different short-circuited modules in a string of a system impact the output power, current and voltage at MPP. As a model of a PV system, we chose again the system of study number 8, as can be seen in Table 3.5, because of the high number of modules connected in series of this system. We could have chosen the system number 7 because of the high number of PV modules connected in series, Ns= 40, but it would take a large amount of time to simulate all the cases of short-circuited modules and yet the system number 8 has the necessary amount of PV modules in series in order to have good results to show.

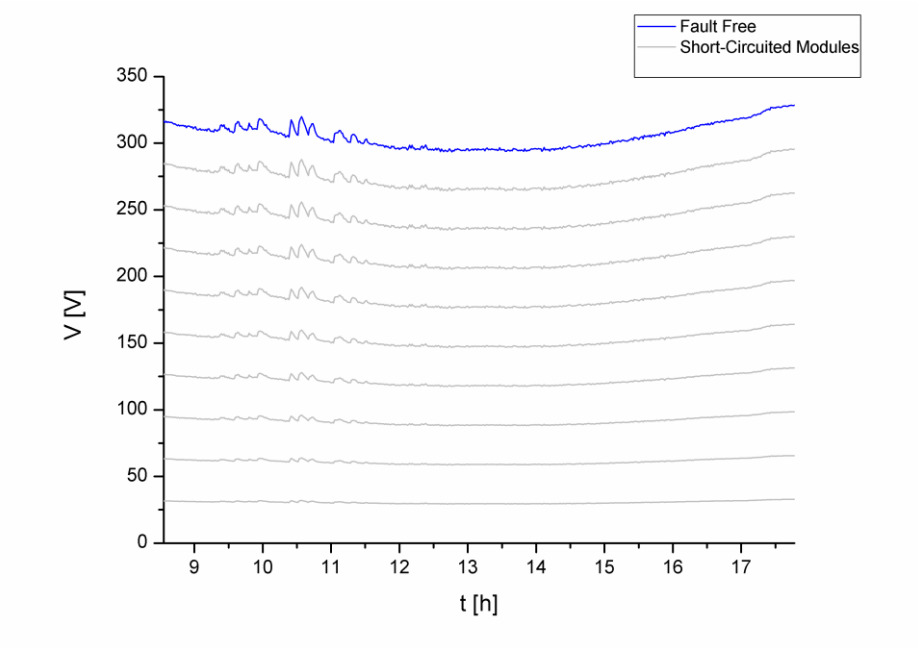

Fig. 3.12 Voltage profile with different number of short-circuited modules

As can be seen in Figure 3.12, a short-circuited module has a direct impact on the voltage of the PV system. The blue line is related to the maximum voltage at DC side, V_m, on free fault operation and the grey lines below are the voltages related to the system working with different numbers of short-circuited modules. The first grey line, the one right below the blue one, is the minimum number of short-circuited modules, 1 short-circuited module and 9 properly working modules, and the last grey line represents 9 short-circuited modules and only 1 properly working module, making a total of 10 PV modules that composes one string of the PV system.

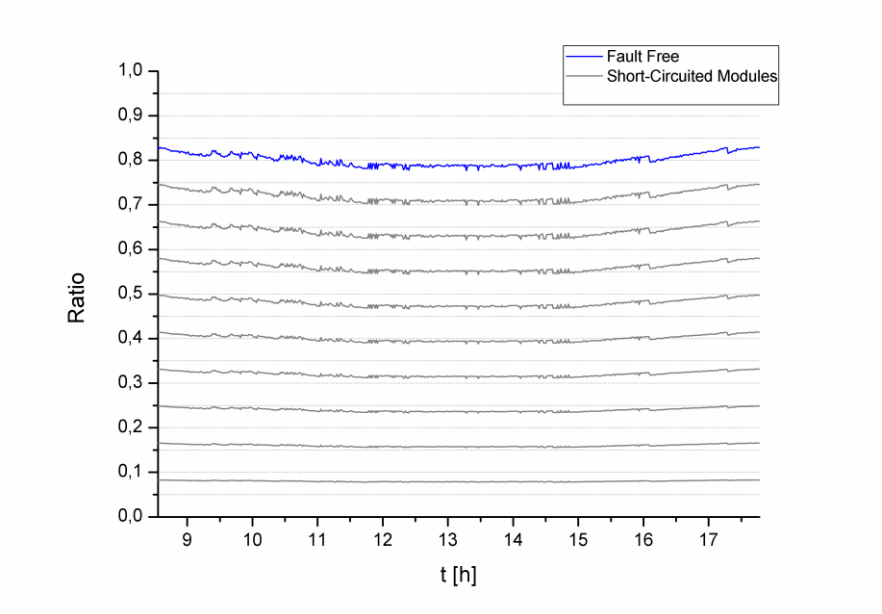

Fig. 3.13- NRv: Voltage ratio profile

Figure 3.13 show the evolution of the ratio, NRv, during the tested period of time for the system number 8. The blue line is the NRvo. The Fig. 3.13 follows the same concept as before and the NRv have a variation of the same order of the voltage. This variation between a line and the other one above (Lv), referring to one less short-circuited module respectively can be measured with the Equations 3.35 and 3.36:

$$Lv = 1 - (1 - \left(\frac{1}{Ns}\right)) \tag{3.35}$$

$$Lv = 1 - \beta \tag{3.36}$$

And this difference will be always the same.

The current ratio in cases of free fault and short-circuited module cases, with the same data of irradiance and temperature, has the same behavior in both operation conditions.

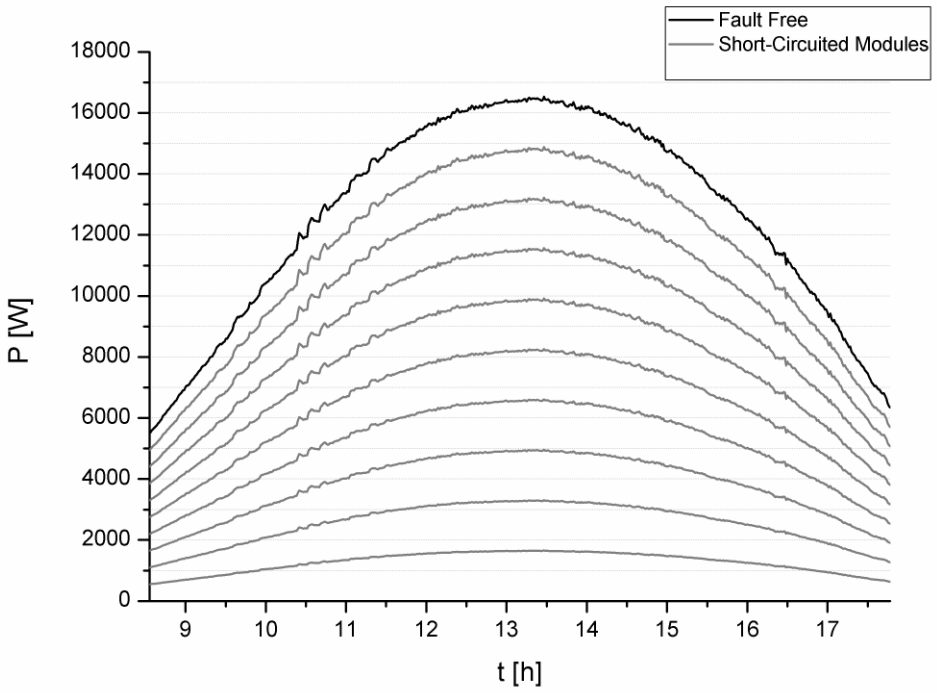

Fig. 3.14- Power profile with different number short-circuited modules

With the Figure 3.14 we can see the impact on the output power of the PV system and this will translate on losses of generated energy.

3.5.3 Impacts on the output Power

This section will focus on PV system number 3 and number 8 in order to analyze and quantify how the previous faults can impact different systems configurations. The configurations, Ns and Np, of these systems are represented in Table 3.5. All these faults will severely impact the output current, voltage and then the output power of the PV system. Following the Equation 3.37, the power losses due to output current or voltage reduction, will impact the output power of the system:

$$P_{max} = I_m \text{ x } V_m \tag{3.37}$$

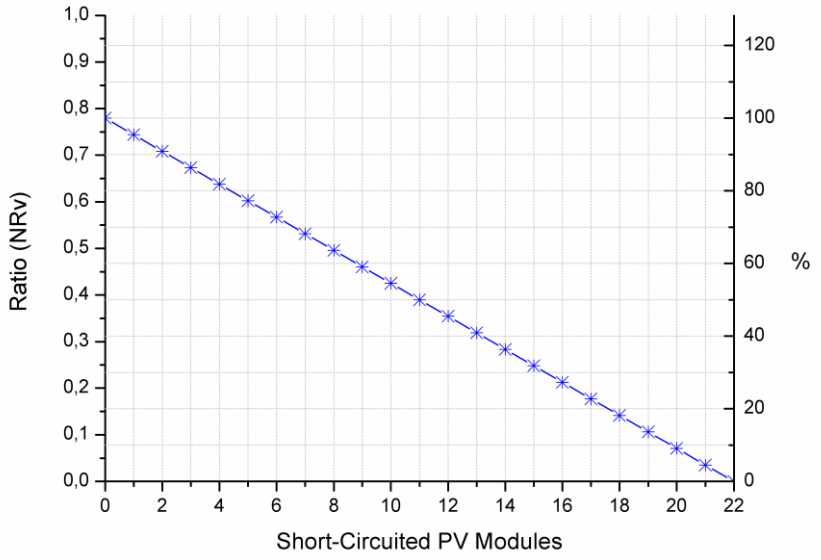

Fig. 3.15- NRv progression – PV system number 3

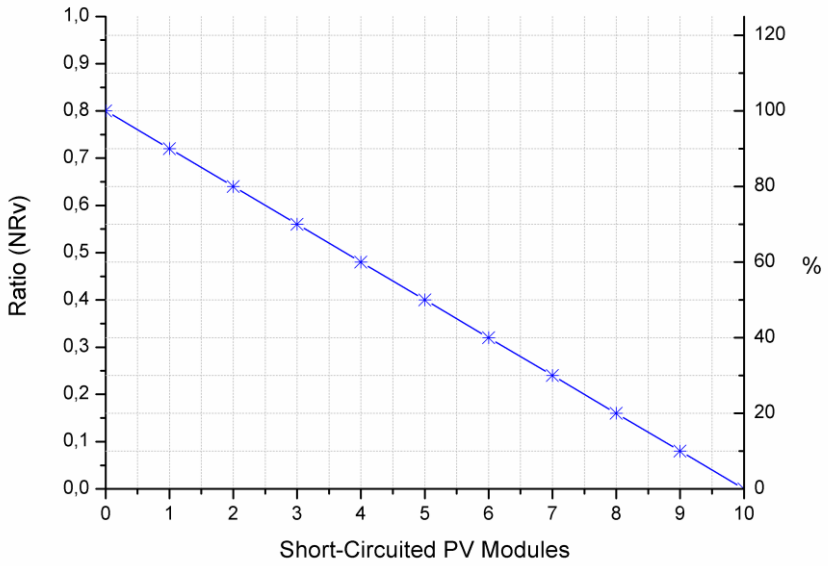

Fig. 3.16- NRv progression – PV system number 8

Figure 3.15 and 3.16 shows the evolution of the ratio, NRv, correspondent to the short-circuited modules for the PV system number 3 and number 8 respectively. With these figures we can have a better view and perception of the variation of ratios when we increase the number of short-circuited modules in a string. The y axis on the right on the graphs shows the percentage correspondent to each ratio. The value of 100% corresponds to the free fault operation of the system and 0% corresponds to a total black-out. The values of the x axis are between the values of 0 and Ns for the short-circuited

modules case, where in these figures, 0 corresponds to fault free operation and Ns corresponds to all modules short-circuited.

$$y = mx + b \tag{3.38}$$

Following the basis Equation of a straight line (3.38), m corresponds to the slope of the line. These graphs were done with OriginPro that is a software very useful when we need to do a lot of modifications on the graphs, but in order to have the equations of the lines we had to use Excel from Microsoft Office. Thus, we obtained the following equations 3.39 and 3.40 for both Figures 3.15 and 3.16, respectively:

$$y = -0.0354x + 0.7795 \tag{3.39}$$

$$y = -0.08x + 0.8003 \tag{3.40}$$

With one short-circuited PV module there is a reduction of about 4,5% and 10% on the output power of the system number 3 and system number 8, respectively. Therefore, with Equation 3.39 and 3.40 we have the slopes of the graphs of Figures 3.17 and 3.18, -0.0354 and -0.08 respectively. Comparing the results, the slope is bigger with a lower value of Ns of a string. Thus, the bigger is the Ns, smaller is the impact of a short-circuited module on the output power of a PV system.

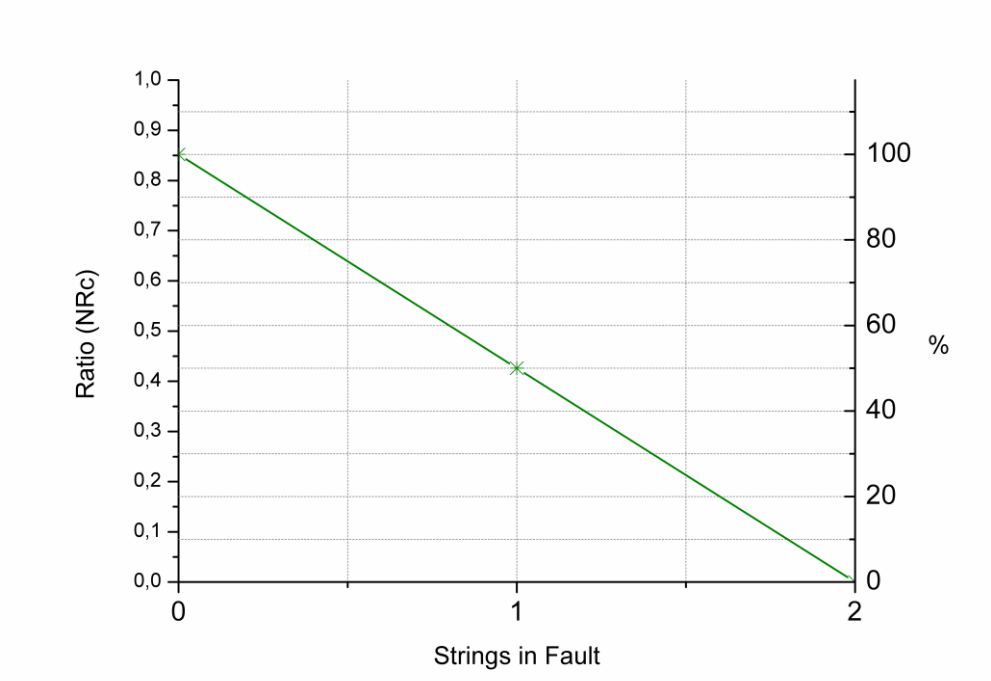

Fig. 3.17- NRc progression – PV system number 3

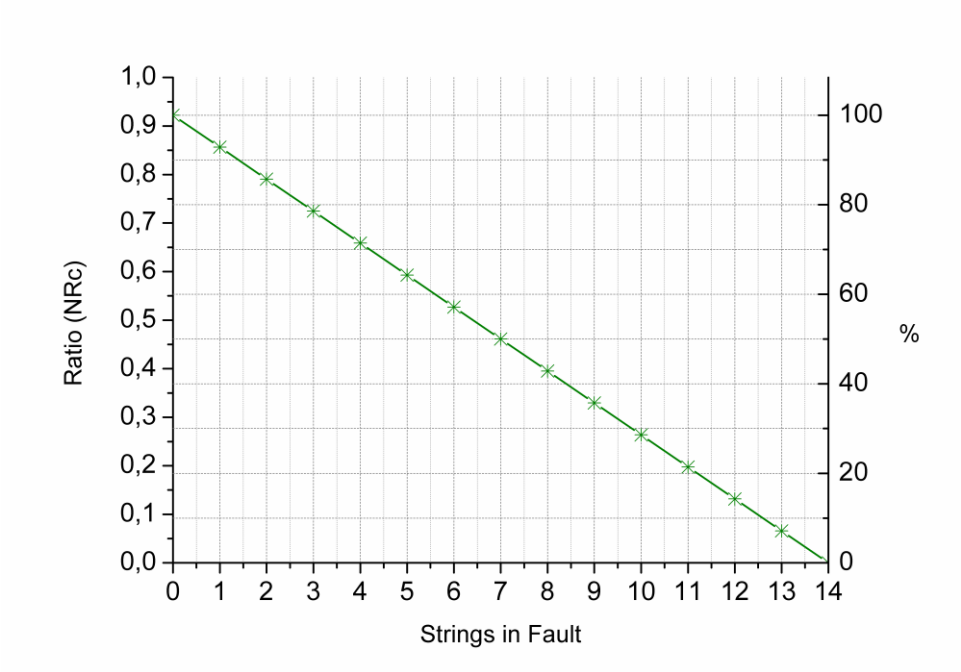

Fig. 3.18- NRc progression – PV system number 8

Figure 3.17 and 3.18 shows the evolution of the ratio, NRc, correspondent to the strings fault for the system number 3 and number 8. As before, the y axis on the right shows the percentage correspondent to each ratio and the value of 100% corresponds to the free fault operation of the system and 0% corresponds to a total black-out. This time, the values of the x axis are between the values of 0 and Np for the strings fault, where in these figures, 0 corresponds to fault free operation and Np corresponds to all strings disconnected.

The following equations 3.41 and 3.42 are for both Figures 3.17 and 3.18, respectively:

$$y = -0.426x + 0.852 \quad (3.41)$$

$$y = -0.0659x + 0.9223 \quad (3.42)$$

With one faulty-string there is a reduction of about 50% and 7% on the output power of the system number 3 and system number 8, respectively. Equations 3.41 and 3.42 show the slopes of both systems, -0.426 and -0.0659 respectively. Comparing the results of Equation 3.41 and 3.42, the slope is bigger with the lower values of Np. Thus, the bigger is the Np, smaller is the impact of a string fault on the output Power of a PV system.

This behavior is the same as in the case of short-circuited modules, thus the bigger the PV system, smaller the impacts of a short-circuited module or a string fault on the output power.

4. Experimental Validation

The procedure of fault detection in grid connected PV systems based on the current and voltage new indicators described in the previous sections was tested in a grid connected PV system located in the Centre de Développement des Energies Renouvelables (CDER), Algeria. This PV system of 9.6 kWp is divided in three sub-arrays of 3.2 kWp each, which are connected to 2.5 kW (IG30 Fronius) single phase inverters. Each sub-array is formed by 30 PV modules (Isofoton 106W-12V) in a configuration of two parallel strings, Np=2, and 15 PV modules in series, Ns=15. The procedure and simulations developed in this work were based on only one sub-array of this PV system.

Nowadays most inverters designed for grid connected PV applications have a wide range of interfaces, in particular sensor inputs and communication interfaces. These sensor inputs can be used to connect irradiance sensors as pyranometers, reference cells and PV module temperature sensors. Therefore these inverters include monitoring capabilities for irradiance and temperature as well as for MPP evolution because of the MPPT (Maximum Power Point Tracker) incorporated in the inverter.

The main advantage of this method of fault detection is that it can be integrated into the inverter without using a complex software simulation avoiding the use of modeling and simulation of PV systems. To accomplish this objective we found two new current, NRc, and voltage NRv. These indicators are used as benchmarks and both relationships can be calculated by the inverter himself.

On this method, the internal inverter hardware and data-loggers are responsible of all needed calculations and the storage of the measured data. The own inverter is able to detect and diagnose the faults in real-time.

The values of parameters α and β for the sub-array calculated using Equations 18 and 22 are 50% and 93.33% respectively.

4.1 System Behavior

We have done specific tests on the system behavior in order to evaluate the capabilities of the developed procedure to detect whether the system has a normal behavior or if there is an abnormality in the output power. The PV system in study was monitored on five different days, each day for a different case of study. The data was monitored within an interval of 1 minute between each measure.

For this purpose, we have tested different faulty cases and a free-fault case. On the following table we remind the possible faults related to the constant behavior of the NRc and NRv respect to their thresholds, already shown in a previous section:

Table 3.4- Constant Energy Loss Faults in a PV system based on the new indicators

Possible Faults	**NRc**	**NRv**
No Fault	OK	OK
String Fault	Below Threshold	OK
Short-circuited modules	OK	Below Threshold
Short-circuited modules and String Fault	Below Threshold	Below Threshold

4.1.1 Case of study 1: Free Fault

A sub-array of the PV system described above was monitored in a day on fault-free operation. Figures 4.1 and 4.2 show respectively the irradiance and cell temperature profiles monitored at the PV installation along that day:

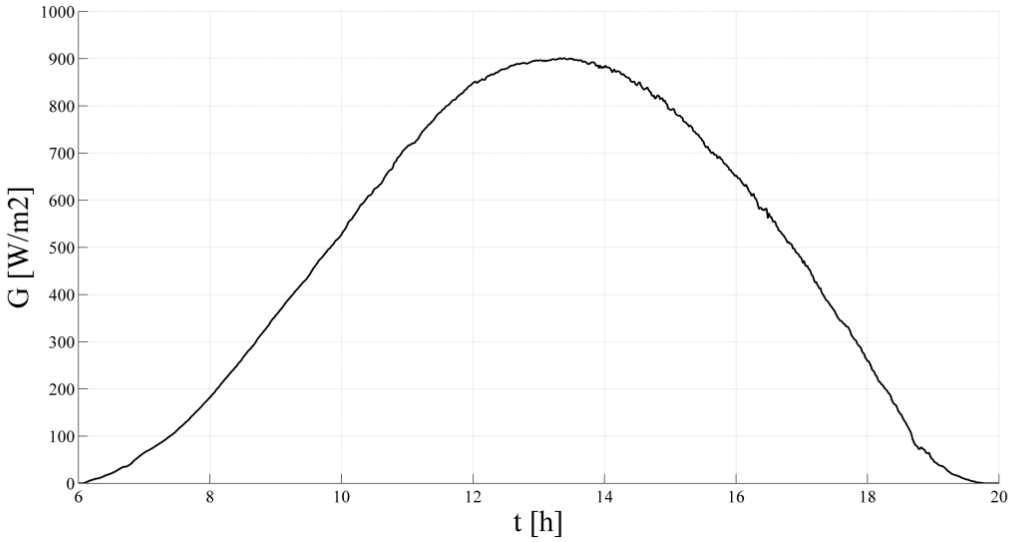

Fig. 4.1- Irradiance profile - Free fault day

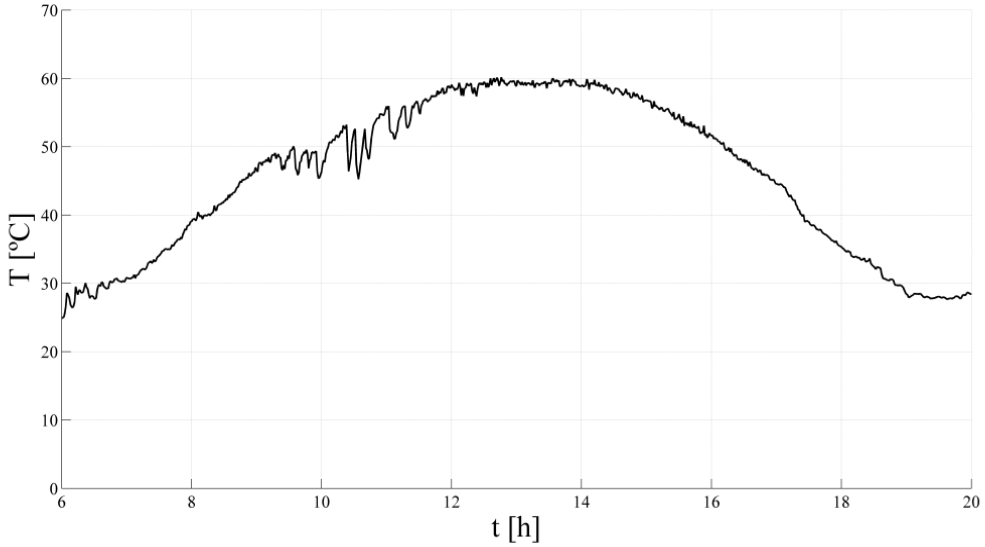

Fig. 4.2- Cell Temperature profile - Free fault day

The evolution of V_{oc} and I_{sc} of this PV array was calculated by using Equations 3.9 and 3.10. Then the current, NRco, and voltage, NRvo, indicators were calculated according to Equations 3.11 and 3.12 and taking into account the monitored profiles of the output voltage and current at the maximum power point (MPP) of the PV sub-array DC output.

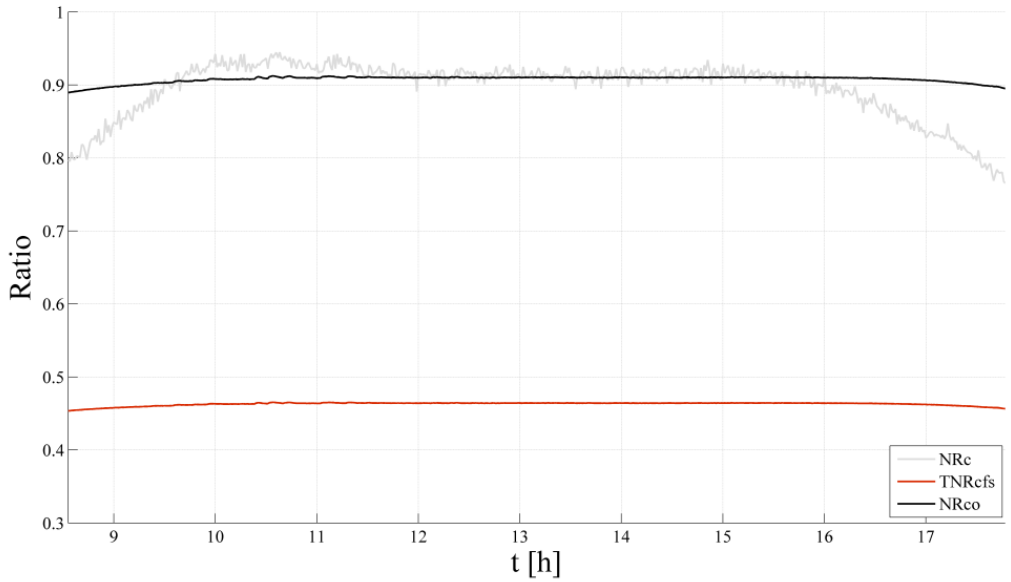

Fig. 4.3- Ratios and threshold for output current – Free fault

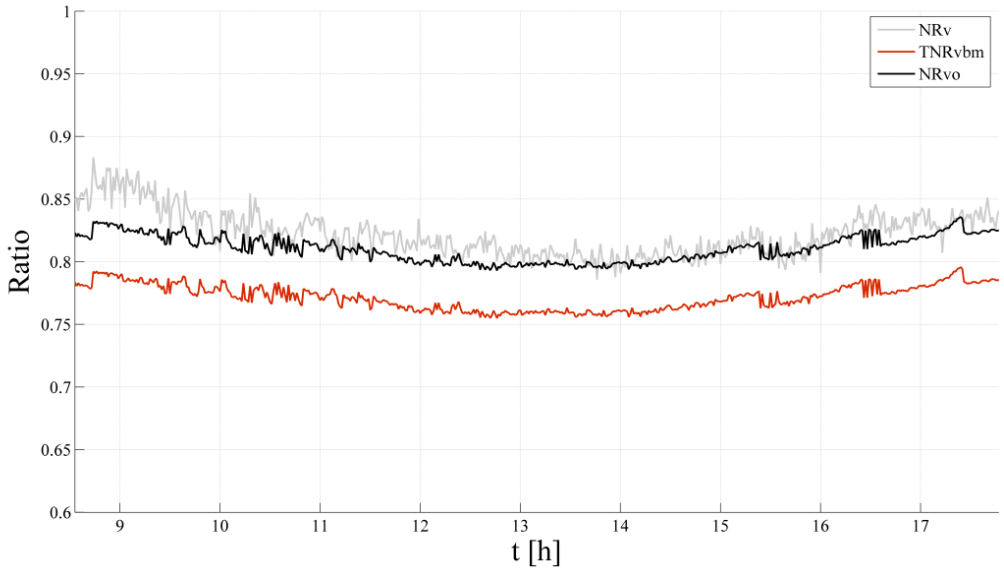

Fig. 4.4- Ratios and threshold for output voltage – Free fault

Figures 4.3 and 4.4 show the evolution of the indicators of current and voltage at DC side, respectively, between 8:33 and 17:47 because of the minimum irradiance of 200W/m^2, as already explained in a previous section. As can be seen in the Figures 4.3 and 4.4, NRc and NRv are over the corresponding thresholds: TNRcfs and TNRvbm, indicating that the PV system is in fault-free operation. NRco and NRvo are the expected values for the ratios of current and voltage, simulated, corresponding to the real irradiance and temperature profiles in this day.

Table 4.1- Ratios and thresholds values – free fault

Ratios	Parameter values (mean)	Standard deviation σ
NRvo (%)	81.05	10.51×10^{-3}
NRv (%)	82.23	17.94×10^{-3}
TNRvbm	78.11	10.20×10^{-3}
NRco (%)	90.77	4.65×10^{-3}
NRc (%)	89.56	39.65×10^{-3}
TNRcfs	46.41	23.74×10^{-3}

Table 4.1 shows the mean (average) values and standard deviations obtained for these parameters in this case of fault-free operation. The mean values of the indicators of current are around 90% and 81% in the case of voltage. As can be seen in Table 4.1, there is a good accordance between expected and real values of NRc, (NRco ~ NRc), and NRv, (NRvo ~ NRv). In both cases the indicators – NRc and NRv - show mean values above the corresponding thresholds, TNRcfs and TNRvbm, respectively.

4.1.2 Case of study 2: String Fault

In this case we are studying the case of a faulty string of a sub-array of the PV system. In order to fully understand how the system and the generated energy of the system reacts to this kind of fault, one of the strings of the sub-array was disconnected from the system and then the evolution of the MPP, the corresponding output voltage and current, was monitored as well as the irradiance and cell temperature. Figures 4.5 and 4.6 show the irradiance and temperature profiles monitored, respectively.

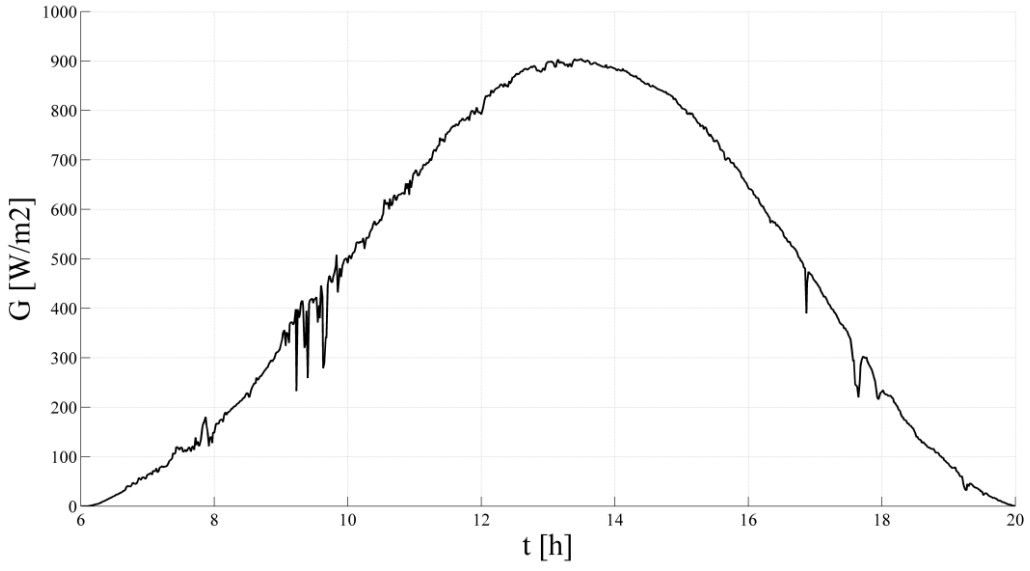

Fig. 4.5- Irradiance profile – string fault day

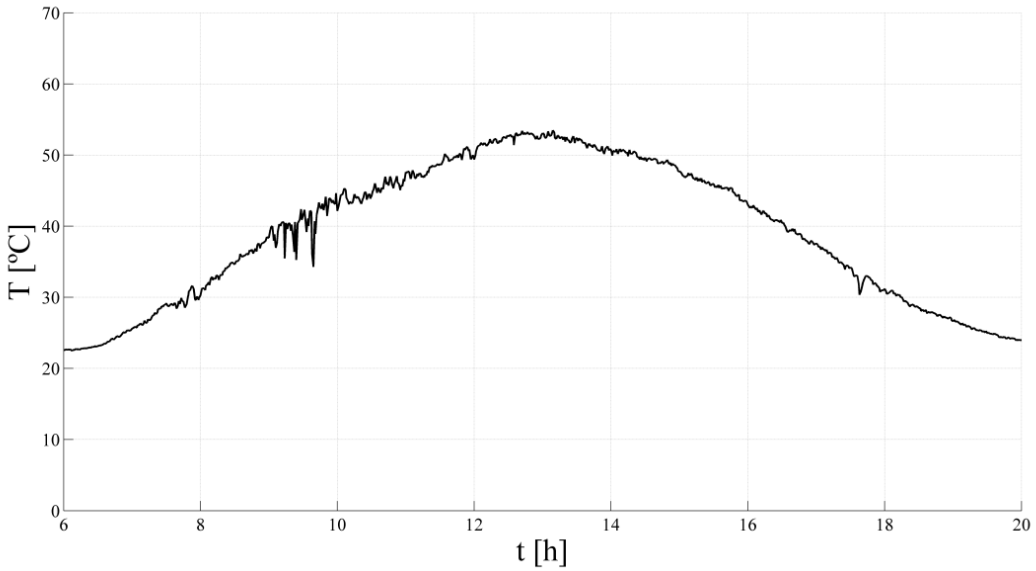

Fig. 4.6- Cell Temperature profile – String fault day

The evolution of the voltage and current indicators was calculated following the same procedure than in the case of fault-free operation described above using monitored data.

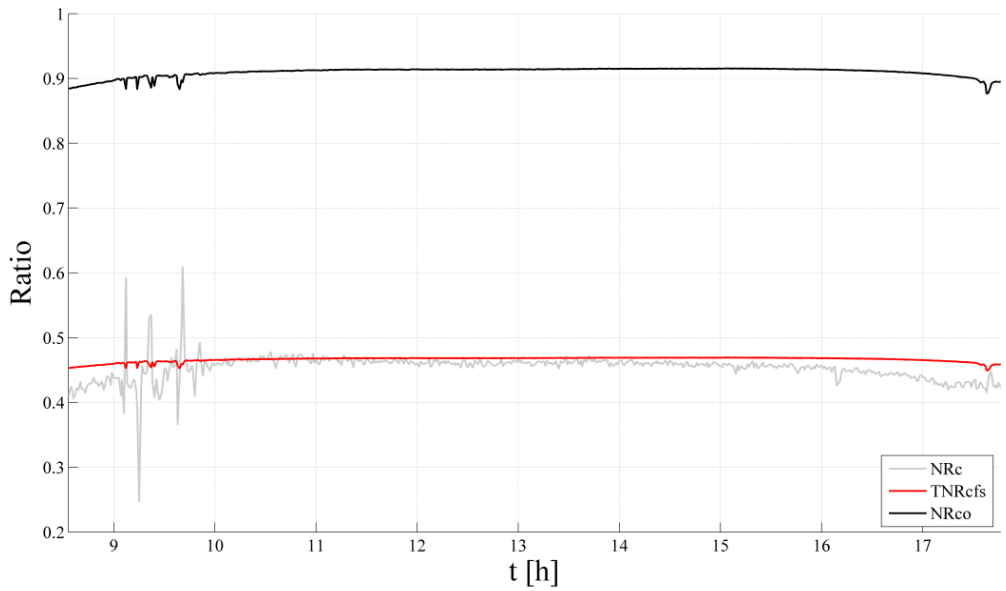

Fig. 4.7- Ratios and threshold for output current – String fault

Figure 4.7 shows the evolution of NRc, NRco as well as the evolution of TNRcfs that was calculated using Equation 3.19. The values for NRco are higher than the values of NRc that is below the threshold given by TNRcfs, as can be seen in figure 4.7 and in Table 4.2.

Following Table 3.4, this situation indicates a fault of one string in the PV array.

Table 4.2- Ratios and thresholds values – String fault

Ratios	Parameter values (mean)	Standard deviation σ
NRvo (%)	81.85	10.52×10^{-3}
NRv (%)	83.59	28.48×10^{-3}
TNRvbm	77.87	10.02×10^{-3}
NRco (%)	90.99	7.43×10^{-3}
NRc (%)	45.34	2.06×10^{-3}
TNRcfs	46.82	3.80×10^{-3}

On the other hand the voltage indicators show a good behavior as can be seen in Figure 4.8. The values of NRv and NRvo are of the same order and the threshold TNRvbm presents a lower value than the voltage ratios. This behavior is similar to the fault-free case. Mean values and standard deviations are given in Table 4.2.

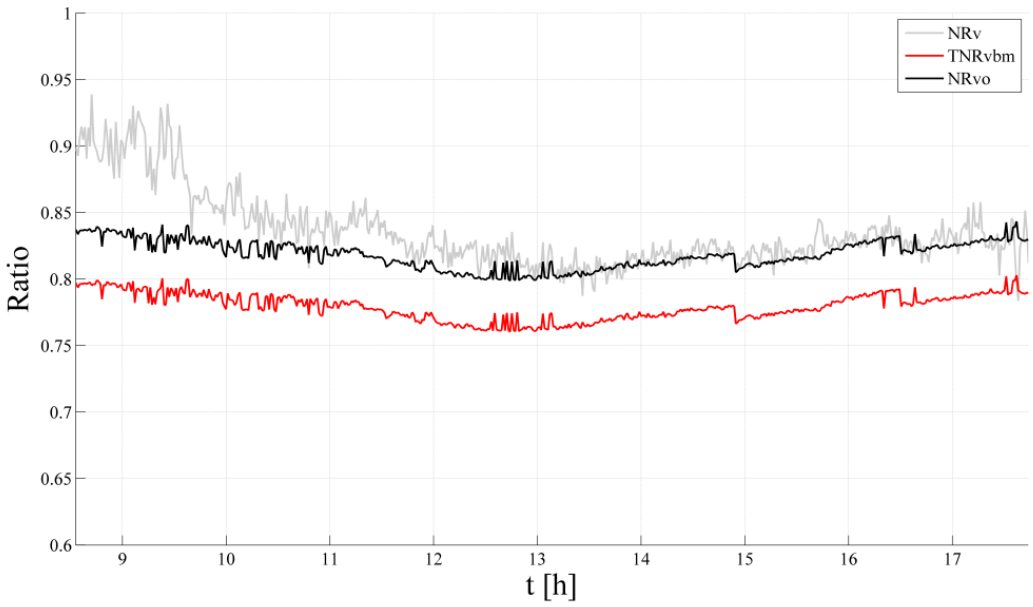

Fig. 4.8- Ratios and threshold for output voltage – String fault

Accordingly to Table 3.4, the results of the current and voltage ratios profiles result in the detection of a faulty string in the PV array.

4.1.3 Case of study 3: Short-circuited PV modules

In this case we are studying the short-circuited PV module of a sub-array of the PV system. In order to fully understand how the output power of the system reacts to this kind of fault, the short-circuited PV module was simulated by manually jumping the PV module with cables. One of the PV modules forming part of a string of the sub-array was short-circuited and then the evolution of the MPP, output voltage and current, was monitored as well as the irradiance and cell temperature along the experiment. Figures 4.9 and 4.10 show the corresponding irradiance and temperature profiles monitored in that day.

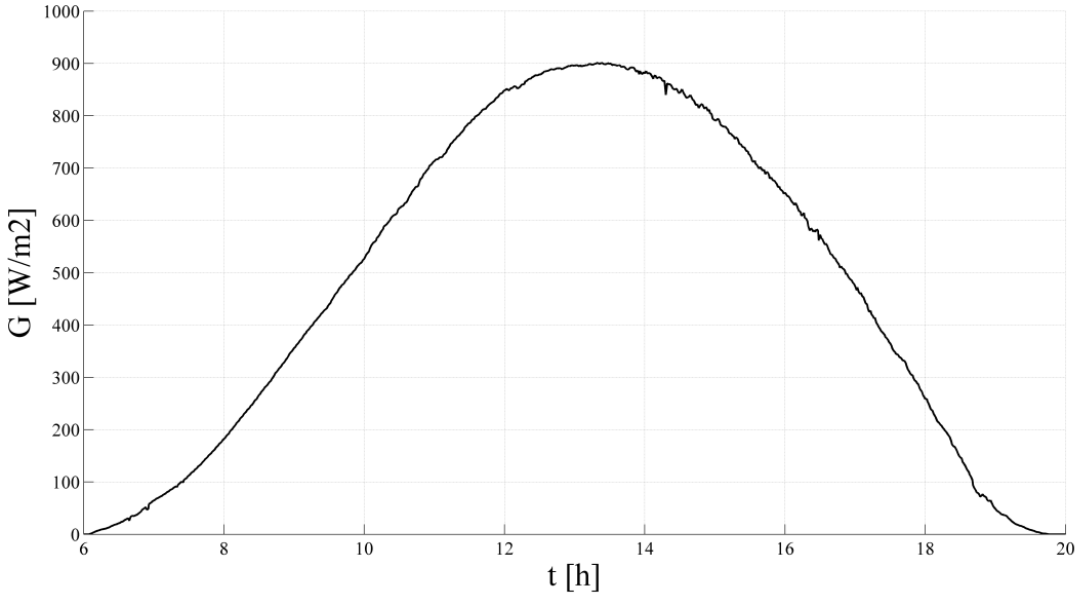

Fig. 4.9- Irradiance profile – Short-circuited module day

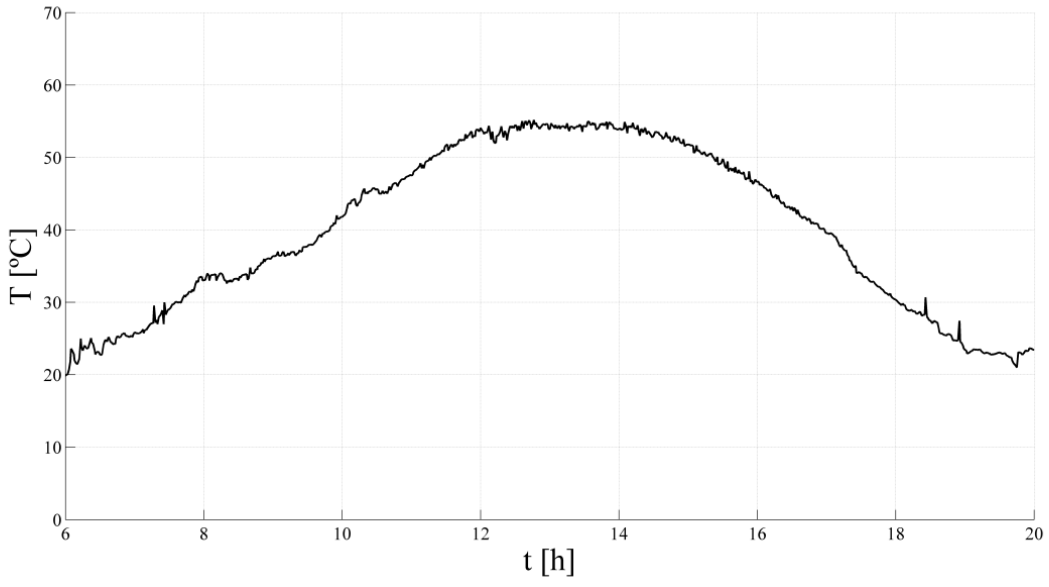

Fig. 4.10- Cell Temperature profile – Short-circuited module day

The evolution of the current and voltage was calculated following the same procedure described in previous sections from the monitored data. Figure 4.11 shows the evolution of NRv as well as the

evolution of NRvo and TNRvbm. The evolution of the ratios of current NRc and NRco as well as the threshold TNRcfs are given in Figure 4.12. Mean values obtained for current and voltage indicators, thresholds, and standard deviations are given in Table 4.3.

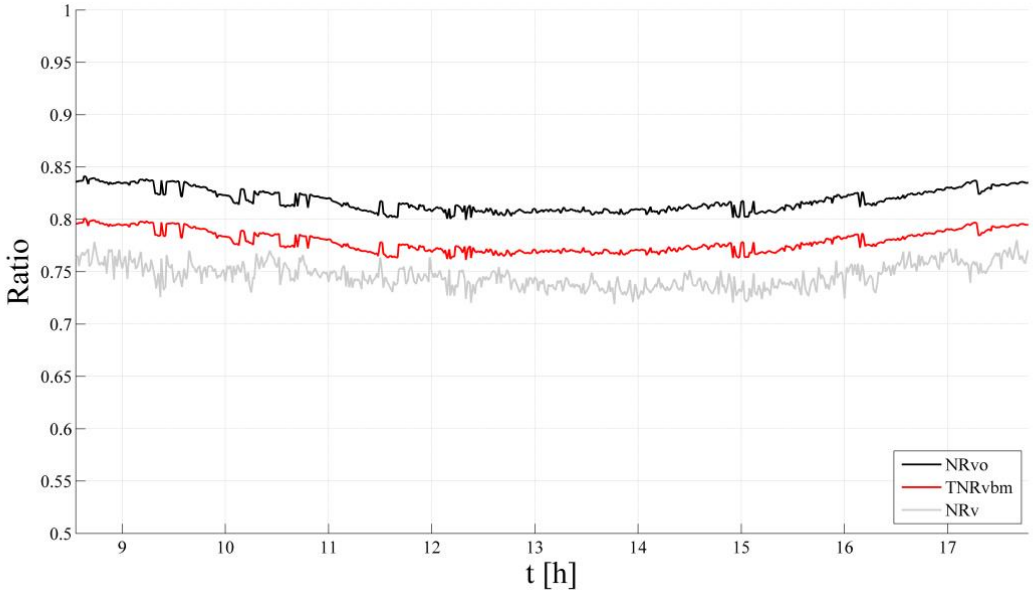

Fig. 4.11- Ratios and threshold for output Voltage – Short-circuited PV module

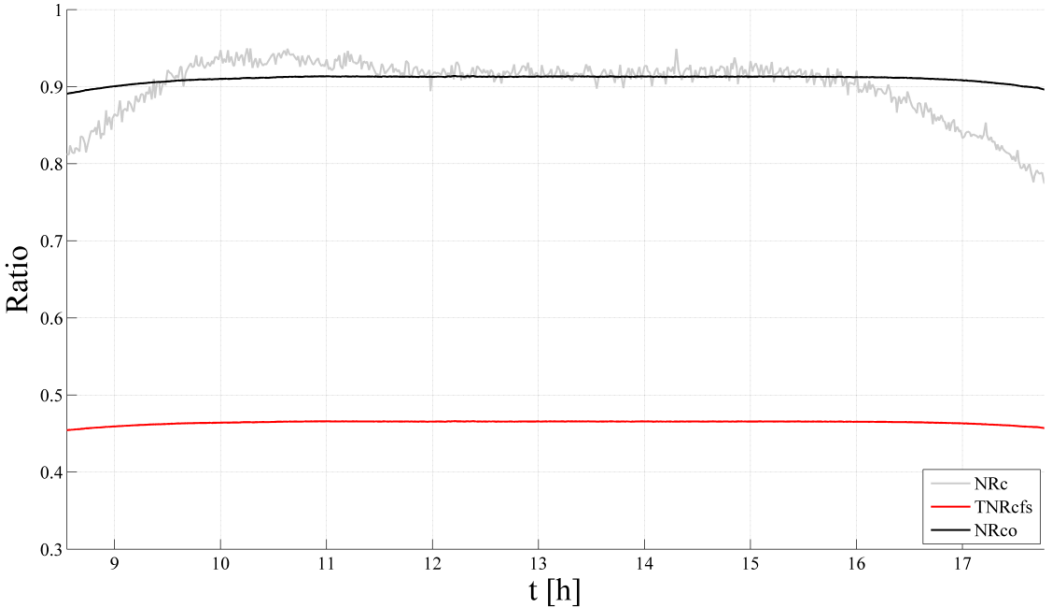

Fig. 4.12- Ratios and threshold for output Current – Short-circuited PV module

As can be seen in Figure 4.11 the values of NRv are below the threshold indicated by TNRvbm showing a fault present in the PV array. The main values obtained for these parameters are shown in Table 4.3.

On the other hand, the evolution of the indicator of current NRc shows a similar behavior to the case of fault-free operation and remains over the threshold TNRcfs. This behavior of NRc is explained because the short-circuited modules of this experimental case is not caused by shading. This means that the irradiance (G) and cell temperature (Tcell) will be similar to the free fault day.

Main values around 91% have been obtained for NRc and NRco while the mean value of TNRcfs is 46.55%, as can be seen in Table 4.3.

Table 4.3- Ratios and thresholds values – one Short-circuited PV module

Ratios	Parameter values (mean)	Standard deviation σ
NRvo (%)	81.81	10.61×10^{-3}
NRv (%)	74.65	12.02×10^{-3}
TNRvbm	77.88	10.1×10^{-3}
NRco (%)	91.28	4.81×10^{-3}
NRc (%)	90.15	37.77×10^{-3}
TNRcfs	46.55	2.45×10^{-3}

From the results obtained for NRc and NRv the fault detected in this experiment corresponds to one short-circuited module in a string of the sub-array as expected and as Table 3.4 shows.

4.2 Detection and diagnose of changing energy loss type of failures

Using these new current and voltage indicators, NRc and NRv respectively, we are able to detect and diagnosis more kinds of faults, although we cannot use exactly the same method as before. For these new faults the behavior of the temporal evolution of NRc and NRv will be different than in case of string fault and short-circuited PV modules. These faults are: Shading and grid faults.

4.2.1 Partial Shadowing

In this case we are studying the case of shadowing of a sub-array of the PV system. The PV plant under study suffers an irregular shade over both strings in winter season because of a nearby telecommunication's pylon, especially at morning times, from 10:00 until 12:30. Another shade is observed at the end of the day due to nearby trees that also hide the reference cell. The shadows may get some PV modules short-circuited or only partial short-circuited due bypass diodes activation.

Output power, voltage and current at DC side were monitored as well as the irradiance and cell temperature along the experiment. Figs. 4.13 and 4.14 show the corresponding irradiance and temperature profiles monitored.

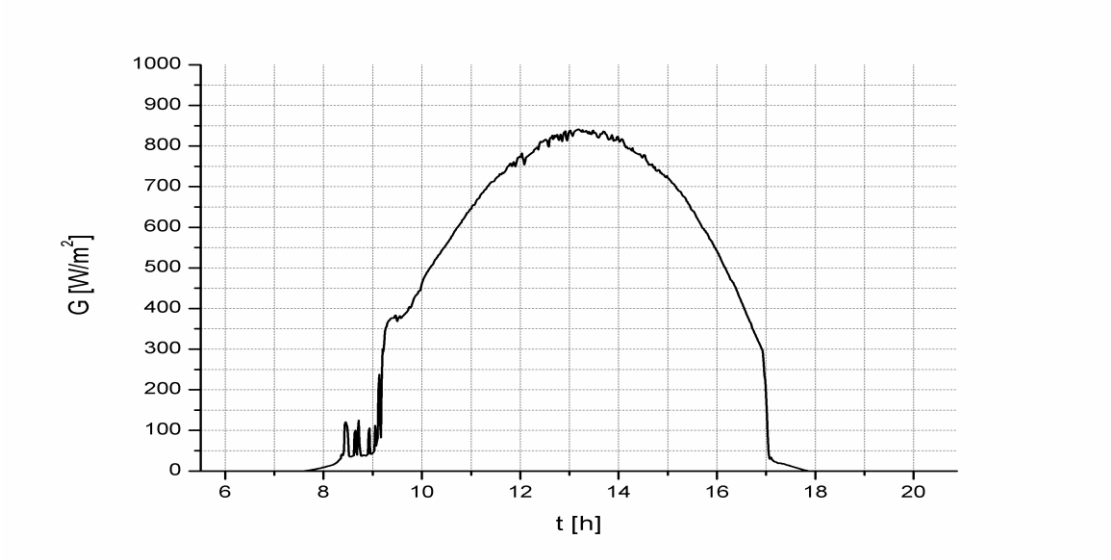

Fig. 4.13- Irradiance profile with Shading

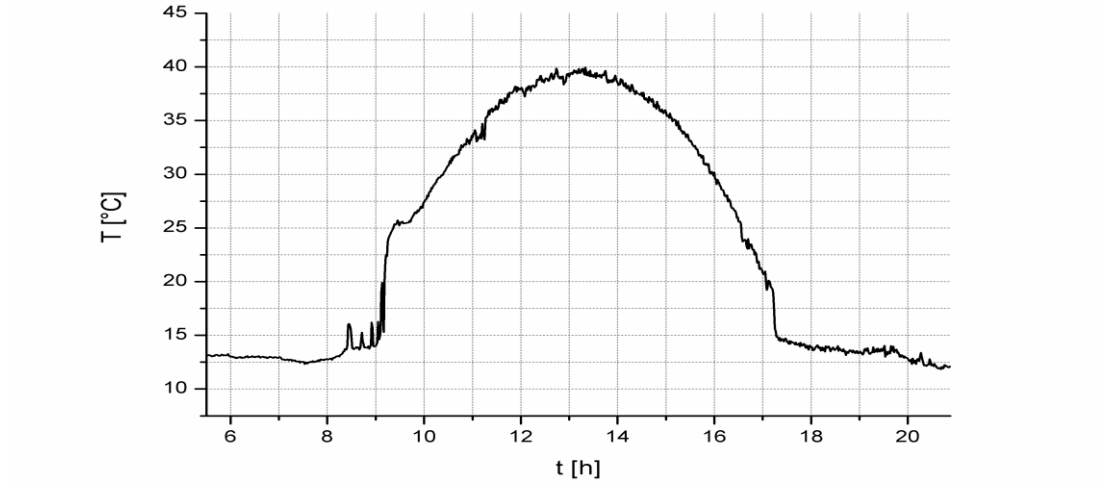

Fig. 4.14- Cell Temperature profile with Shading

Figures 4.13 and 4.14 are data measured by the pyranometer and a thermocouple located at the same place of the PV system. The irradiance profile of the 4.13 is related to the horizontal plane and it shows some shading at the beginning of the day, between 8:30 and 9:30, and at the end of the day, between 17h and 18h. The temperature profile follows the irradiance profile because when the pyranometer is shaded the thermocouple is shaded too, decreasing its temperature.

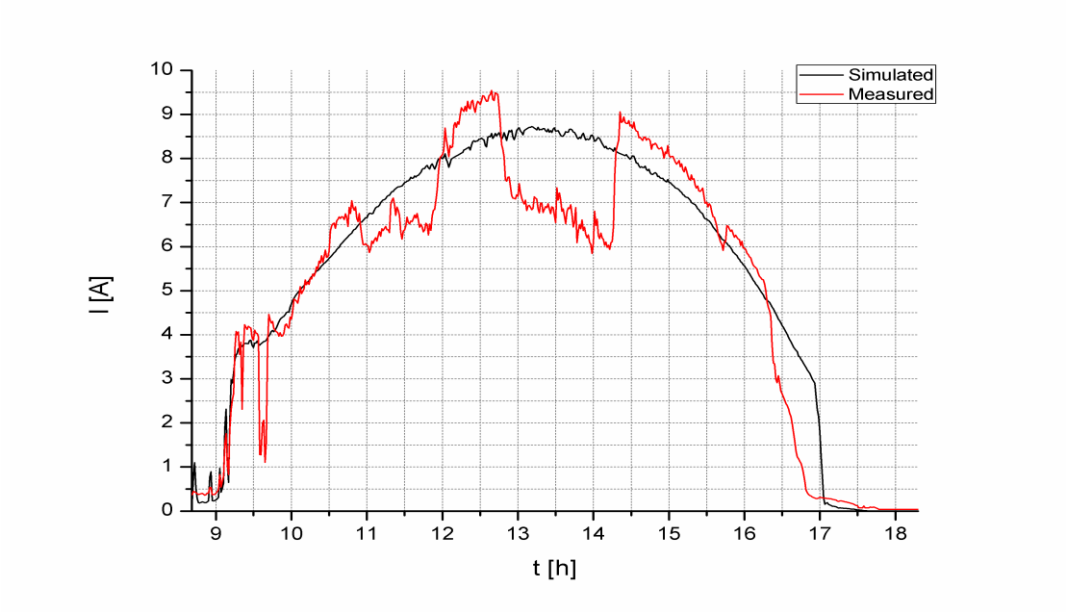

Fig. 4.15- Current profile at DC side of the PV system with Shading

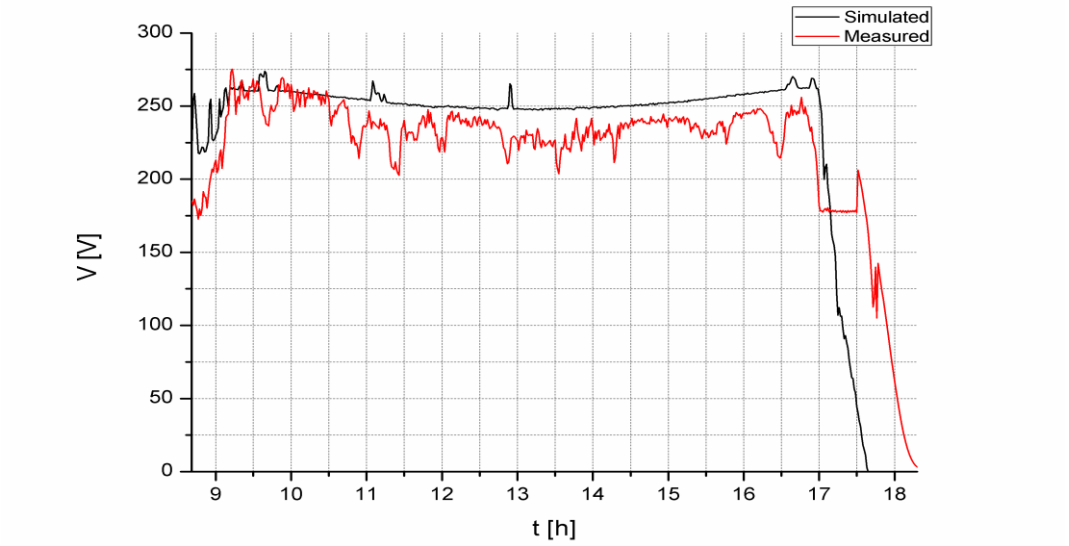

Fig. 4.16- Voltage profile at DC side of the PV system with Shading

The profiles of output voltage, current and power were analyzed between 8:38 and 18:19 because it was the time of the day that the irradiance started to be higher than 200 W/m^2. Figure 4.15 and 4.16 present us the current and voltage profiles at DC side, respectively. As can be seen, the shading has bigger impact on the output current than on output voltage. The measured profile of the output current indicate the presence of partial shadows on the PV array that is not reflected in the irradiance profile because the pyranometer was not shaded in the same way that the whole PV array. Even so, there are a slightly impact on voltage until 17:00. Between 17:00 and 18:00 there is a quick decrease in voltage that make us think that there is a shadow covering almost all the PV system, therefore starting to completely bypass the PV modules some time before the night comes.

Accordingly to Figure 4.13 there should not be shading between 9:30 and 17:15 but seeing Figure 4.15 we see shadow effects between 11:00 and 12:00 and between 12:45 and 14:20. This happens because the irradiance profile was taken by only 1 pyranometer that could not be shaded while there were shadows covering some PV modules away from that pyranometer. This also explains the missing shadow effects on simulated current in Figure 4.15.

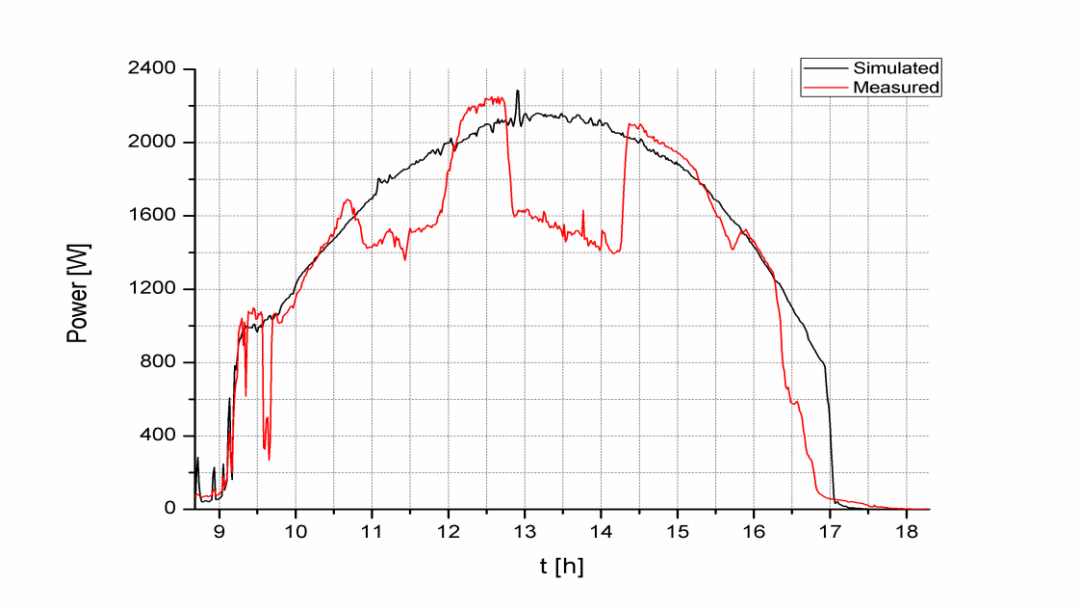

Fig. 4.17- Power profile at the DC side with Shading

Figure 4.17 show that there is a big impact on the output power of the system when it is covered by partial shadows.

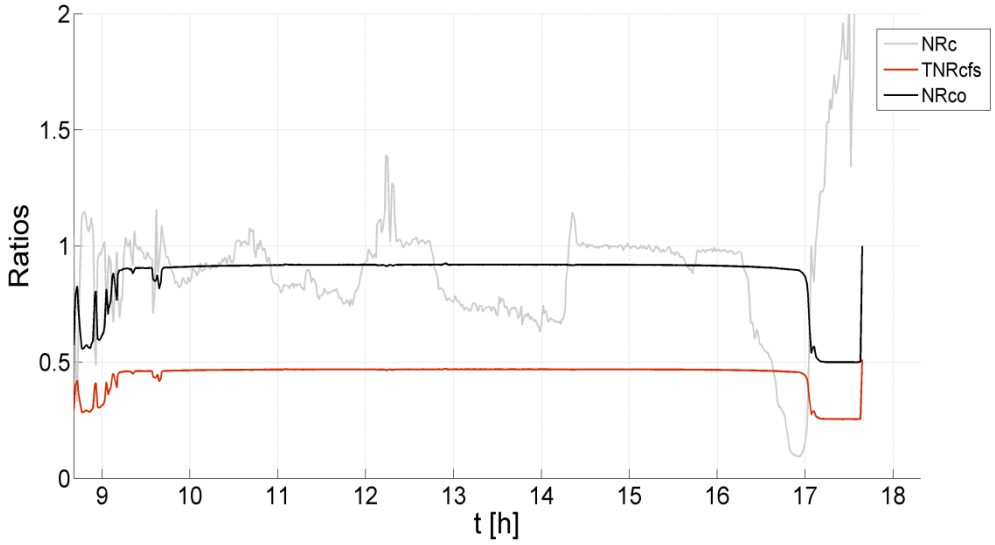

Fig. 4.18- NRc profile with Shading

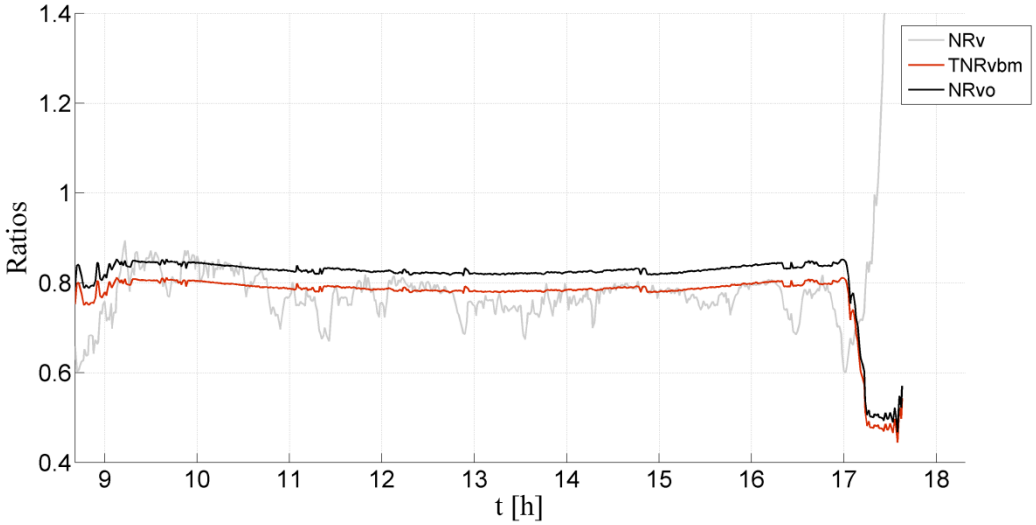

Fig. 4.19- NRv profile with Shading

Figure 4.18 shows that there is a decrease in current at the DC side when some PV modules are shadowed. Between 16:30 and 17:00 there is a decrease in the current output of the PV system because of high shading effects in that period of time. After 17:00 the NRc starts to increase towards infinite because still exists some output current when no irradiance is available which means that at this time I_{sc}=0. The NRc does not have big variations enough to decrease to a value below the threshold TNRcfs and then to automatically detect shadow effects but nevertheless seeing and analyzing the temporal profile of NRc we are able to detect them. The reason because NRc remains over the threshold TNRcfs most of the time is because of the PV system configuration. The PV system is formed by just two parallel strings, so the value of TNRcfs is about 50%. In case of PV systems containing more strings in parallel connection the effect of the shadows will make the NRc indicator go below the threshold.

On the other hand, Figure 4.19 shows some variations on the voltage at DC side and after 17:00 the NRv starts to increase towards infinite values because there is no irradiance resulting in V_{oc}=0. With figure 4.19 we can conclude that with the fault detection method presented in this thesis we can automatically detect shading effects because when shadows cover parts of the array the NRv goes below the threshold TNRvbm during that period of time.

Therefore, we are able to detect shading effects with this method but instead of a constant behavior of the indicators, NRc and NRv, below the thresholds during all day as in case of string faults and short-circuited PV modules, we have a changing behavior of the indicators during certain periods of time.

4.2.2 Grid Fault

In this case we are studying the case of grid fault impact for a sub-array of the PV system. In order to get this data it was needed to wait for a day with high grid inconsistency and then the monitored data was saved [2]. That same day was very cloudy and that is why there are shadows over the PV system in the first half of the monitored day. Output power, voltage and current were monitored as well as the irradiance and cell temperature along the experiment. Figs. 4.20 and 4.21 show the corresponding irradiance and cell temperature profiles monitored.

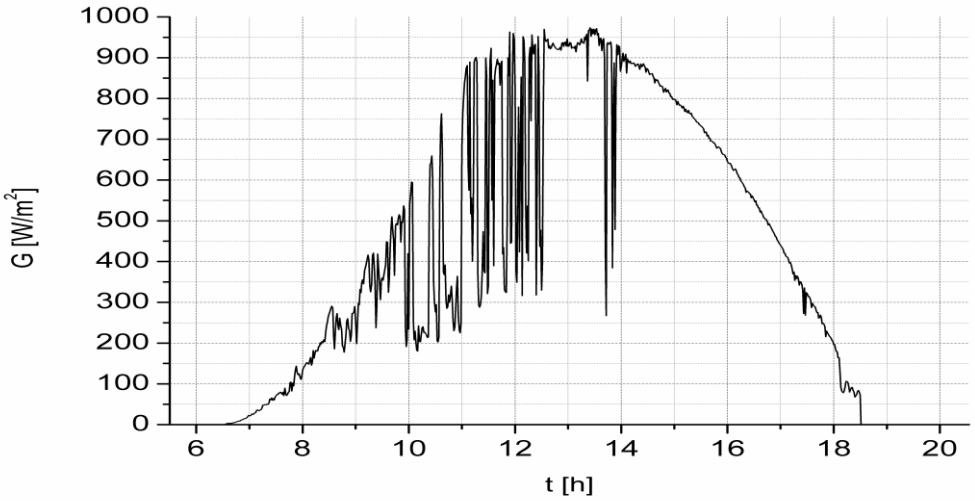

Fig. 4.20- Irradiance profile with Shading

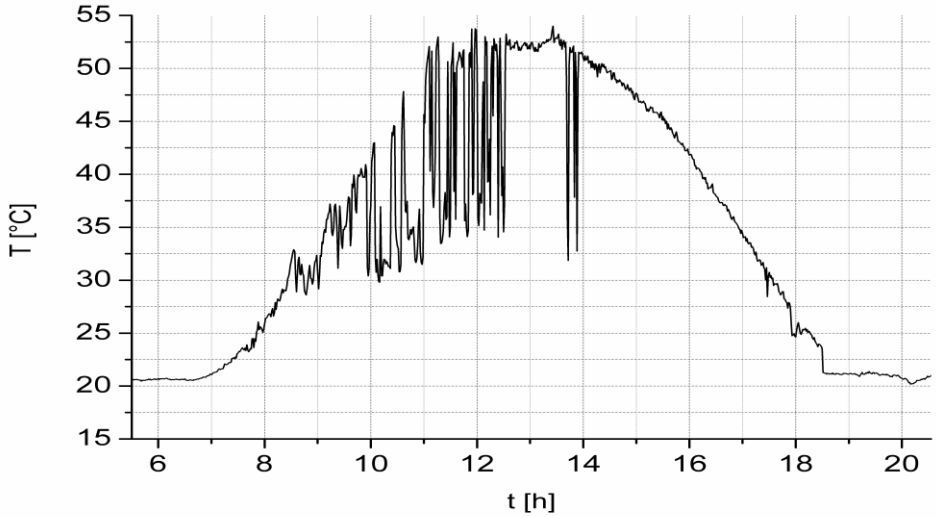

Fig. 4.21- Cell Temperature profile with Shading

Figures 4.20 and 4.21 are data measured by the pyranometer and a thermocouple located at the same place of the PV system. As we can see, the variations on the irradiance, due to the weather conditions, greatly impact the cell temperature.

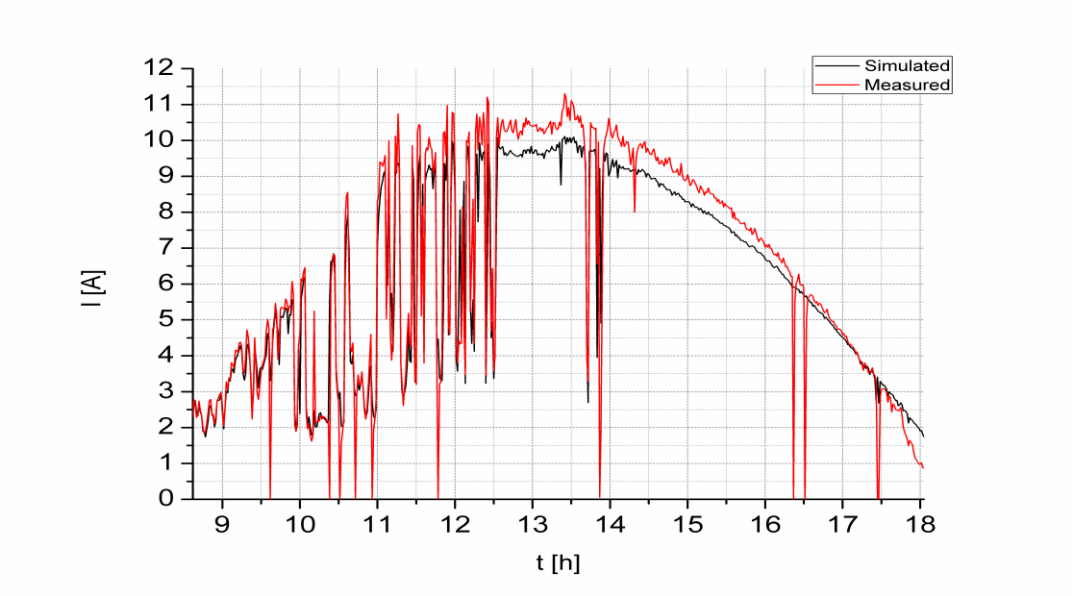

Fig. 4.22- Current profile at DC side of the PV system with Shading and Grid faults

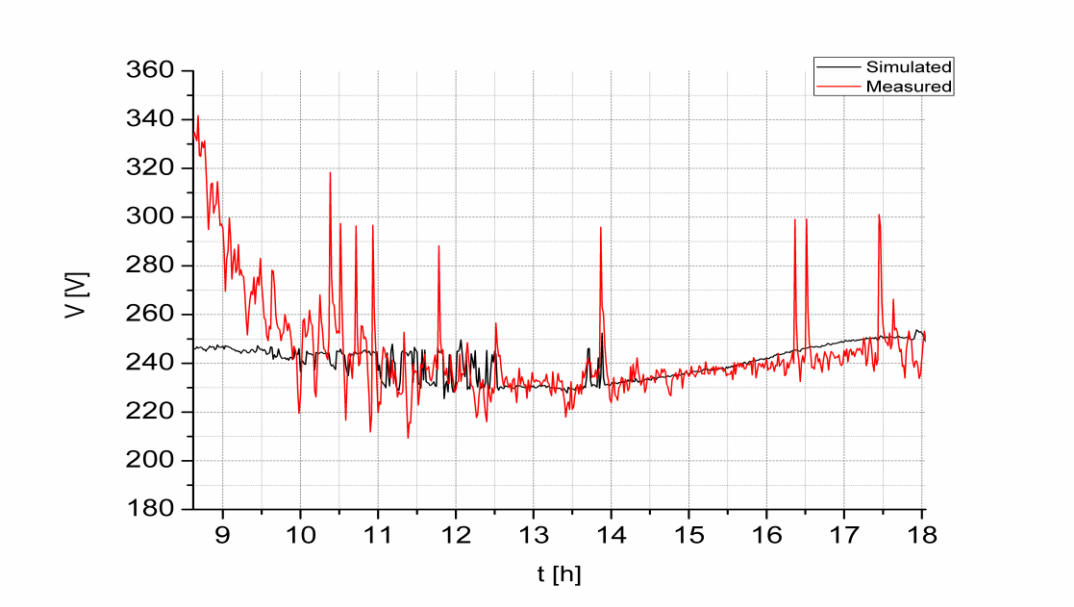

Fig. 4.23- Voltage profile at DC side of the PV system with Shading and Grid Faults

The profiles of output voltage, current and power were analyzed between 8:37 and 18:03 because it was the time of the day that the irradiance started to be higher than 200 W/m^2. Figure 4.22 and 4.23 present us the current and voltage profiles at DC side, respectively. As can be seen, the grid faults and shading effects have bigger impact on the output current than on output voltage. When shading is present, there is a somehow constant decrease in current at the DC side but the voltage at the same side of the inverter, is somehow stable.

When blackouts or a similar fault occur on the grid at AC side, there are some changes on the behavior of the output current and voltage profile of the PV system at DC side. What happens on the output current profile is that at the moment when a grid fault occurs, the current at DC side instantly drops to zero because the inverter switches off as a safety measure to prevent islanding. That can be seen in Figure 4.22 when there appear some spikes of current going to zero values. On the other hand, analyzing Figure 4.23, the voltage profile at DC side, we may see similar effects at the same time of

the day when grid fault occur. When those grid faults occur there are some "positive" spikes on the voltage profile at DC side that mean that for an instant the voltage greatly increases due to a response of the inverter.

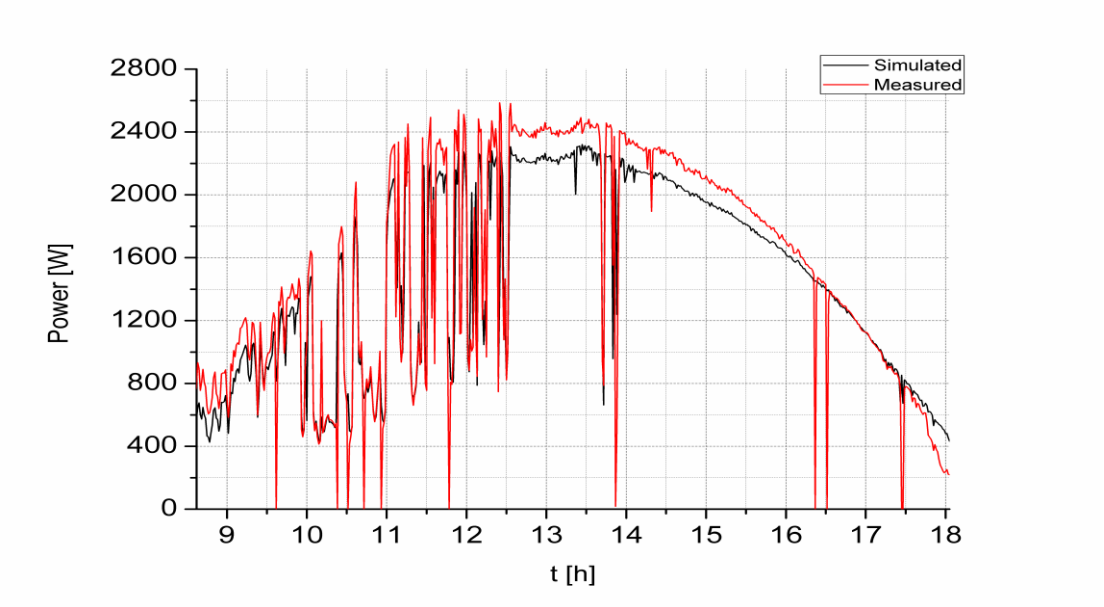

Fig. 4.24- Power profile at DC side of the PV system with Shading and Grid Faults

Figure 4.24 shows a big impact on the output power of the system even when it is covered by partial shadows. It also shows that when faults occur on the grid and the inverter switches off, there is no output power.

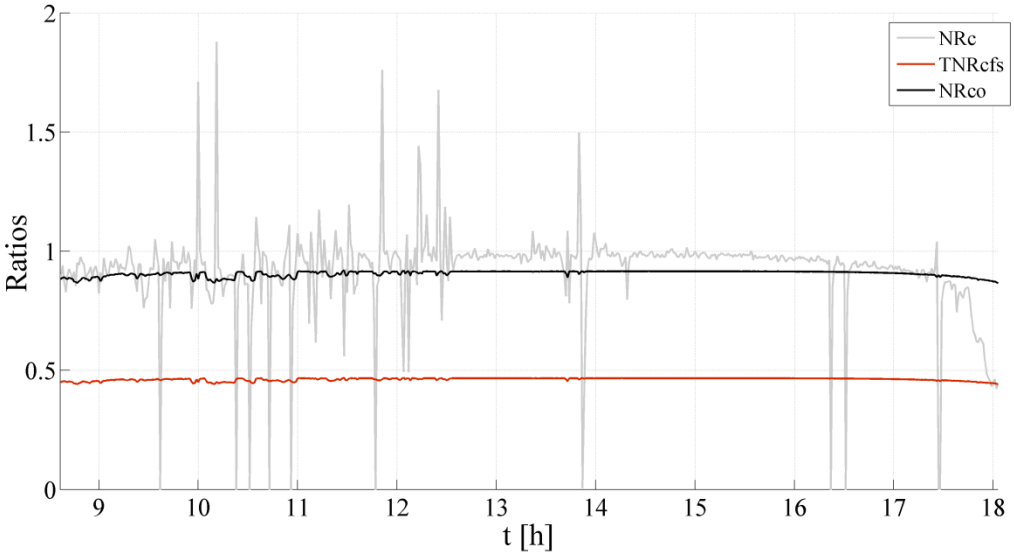

Fig. 4.25- NRc profile with Shading and Grid Faults

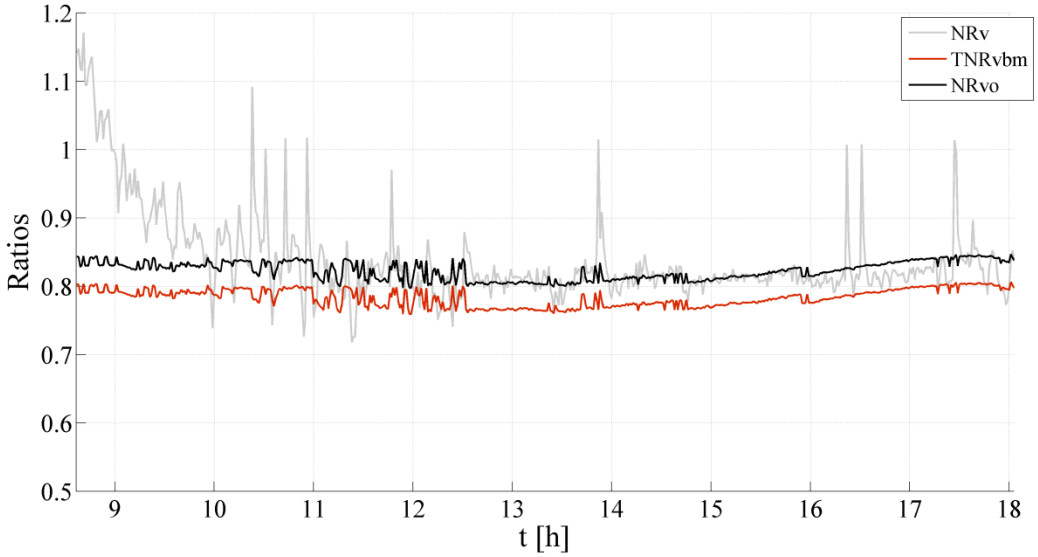

Fig. 4.26- NRv profile with Shading and Grid Faults

Figure 4.25 and 4.26 show the new ratios behavior for current and voltage, NRc and NRv respectively. The explanation for the spikes on the ratios profiles is the same as before on the output current and voltage profiles in Figures 4.22 and 4.23, respectively. Accordingly to figure 4.25, when there is a grid fault we can automatically detect it because the NRc goes to zero for an instant of time and thus below the threshold TNRcfs.

With figure 4.26, NRv profile, we cannot automatically detect grid faults but if we analyze its temporal profile we may be able to detect grid faults because we can see that with a grid fault not only the output current goes to zero but when the inverter switches on and the system start to properly work again, there is a great increase on the output current, a spike on the graph, just after that happens. Therefore, we are able to detect grid faults with this method but instead of a constant behavior of the indicators, NRc and NRv, below the thresholds during all day as in case of string faults and short-circuited PV modules, we have a changing behavior of the indicators during very shorts periods of time. In this case the PV system configuration is not a limitation for the detection; despite we have just two parallel strings, as in the previous section related to shadowing effects. This fact is easy to be understood taking into account that in case of grid failure the input current of the inverter is zero.

5. Conclusions

In this work we have presented a new procedure for automatic detection and diagnosis of main faults in PV systems. The method is based on the evaluation of current and voltage indicators and in the definition of thresholds for both parameters that can help to identify the system faults. The definition of the thresholds is determined by the number of PV modules forming the PV array and its configuration in parallel and series connection.

Firstly, the simulations of the I-V curves, Power curves and MPP using the MatLab matched very well the measured values provided by the manufacturers and then we were able to continue the actual work of fault detection. These simulations also covered output current, voltage and power at DC side.

Afterwards, an intense simulation study was done to verify the definition of the current, NRc, and voltage, NRv, indicators as well as the definition of the corresponding thresholds for short-circuited PV modules and faulty strings. With this study we were able to diagnose the operation conditions of the PV system accordingly to the results of these previous simulations. The thresholds are dependent of the free-fault operation expected ratio values, NRco, NRvo and two new variables, α and β. Initially for the thresholds definition in Equations 3.17 and 3.22, we were going to use the standard deviation of the NRco and NRvo but these deviations were too small and the fault detection method would not properly work as we expected. Thus, we chose to use the 2% value instead of the standard deviations. As explained in a previous section, for the definition of α and β, there are two ways to define them, one using simulations and the other only using the connection configuration of the PV system. It was concluded that we only need the PV system connection configuration in order to define them, thus not needing any kind simulation results to achieve them.

Therefore, this means that the presented method for diagnosis and fault detection does not need extensive simulations. With these simulations we also concluded that the bigger the PV system, the lower is the impact of a fault on the output power of the PV system. Moreover the analysis of the values of both indicators, NRc and NRv, can be useful to identify the number of short-circuited modules and faulty strings present in a PV array as well as its effect on the total output power.

Finally we have verified the fault detection procedure experimentally in real conditions of work of the grid connected PV system at CDER, Algeria. For the cases of one short-circuited module and one faulty string, the results were the expected and the ratios and thresholds worked properly. Sadly, we were not able to experimentally validate a case when both short-circuited module and faulty string would occur at the same time because we did not have the actual data of that fault situation.

Afterwards, we have verified the fault detection of the shading effects and grid faults of the same PV system. We are able to detect grid faults and shading effects with this method but instead of a constant behavior of the indicators, NRc and NRv, below the thresholds during all day as in case of string faults and short-circuited PV modules, we have a changing behavior of the indicators during certain periods of time.

The definition of thresholds for voltage and current indicators must be adapted to the specific PV system to supervise and a training period is recommended to ensure a correct diagnosis and reduce the probability of false faults detected. Therefore, the proposed method is simple but effective detecting the main faults of a PV system.

The results obtained in this work have been the base for a manuscript sent to the journal: Energy conversion & management (Elsevier) to be considered for publication that is now in the review process.

6. Annex

In annex will be shown some examples of the code used on the many simulations done in this work and then the manufacturer sheets of the PV modules used in this work.

The script examples shown are from the validation process where the system simulated is the PV system, Ns=15 and Np=2, using PV module Isofoton 106/12, installed at (CDER), Algeria.

Isofoton 106/12, cell definition*: (esfp_c00.m)*

```
% Constantes físicas
 K       = 1.38E-23;   % Constante de Boltzmann            [J/K]
 q       = 1.6E-19;    % Carga fundamental doelectao   [C]

% Parametros da celula solar
 Areao      = 121.78;   % Area da celula solar    [cm2]
 Rs         = 7.78E-3;     % Resistencia serie       [Ohms]
 Rp         = 11.0556;     % Resistencia paralela   [Ohms]
 n          = 1.14;       % Factor de idealidade do diodo   []
 Ego        = 1.16;       % Energia do GAP a 0ºC          [eV]
 agap    = 7E-14;       % 1º Parametro que relaciona Eg e Ego   [eV/K]
 bgap    = 1100;        % 2º Parametro que relaciona Eg e Ego   [K]
 Jsco       = 0.0229;  % Densidade de corrente de curto-circuito [A/cm2]
 Coef_Jsc = 1.47808E-5; % Coeficiente de temperatura por Jsc [A/Kcm2]
 Voco     = 0.6;        % Tensao em circuito aberto     [V]

% Parametres de precisió dels mètodes numèrics
 Iinc     = 0.0001;     % Precisió dels càlculs de corrent  [A]
 Vinc     = 0.0001;     % Precisió dels càlculs de tensió   [V]
```

***Complement script to define the PV module*: (esfp_g00.m)**

```
% Paràmetres de les associacions sèrie-paral·lel

%   Total Cells= 72
 Nsg  = 36;     % --Número de cèl·lules solars en sèrie           []
 Npg  = 2;      % --Número de cèl·lules solars en paal·lel      []
 Pmod = 1.472;  % --Potència màxima dissipable en una cèl·lula  [W]
% Paràmetres de precisió dels mètodes numèrics
 Iinc = 0.0001;         % Precisió dels càlculs de corrent      [A]
 Vinc = 0.0001;         % Precisió dels càlculs de tensió       [V]
```

I-V and MPP curves: G=1000 W/m^2 & T=25°C script:

```
close all;clear all;clc;

esfparam;% Define as variaveis do sistema
esfp_c00;% Carrega os parametros da celula solar
esfp_g00;% Carrega os parametros do modulo solar

%%%%%%%%%%%%%%%%%%%%%%%%%%%%%%%%%%%%%%%%%%%%%%%%%%%%%%%%%%%%%%%%%%%%%%%%%%
% Curva I-V (figura 1)
% G=1000, T=25

% Dades d'entrada
[G]=1000;
[T]=25;
[Voc]=esfgvoc (G,T);
[Isc]=esfgisc (G,T);
[Vpmp,Ipmp,Ppmp]=esfgpmp (G,T);% Função para obtenção de Vmpp, Impp, Pmpp
[V]=[0:Voc/100:Voc];
[G]=G*ones(1,length(V));
[T]=T*ones(1,length(V));

% Calcula I
[I]=esfgvai (G,T,V);

% Calcula Pmpp
Power=I.*V;

%%%%%%%%%%%%%%%%   Gráficos   %%%%%%%%%%%%%%%%%%

figure (1);%plot de I-V     %%%%%%%%%%%%%%%%%%%%%%%%%%%%%%
eixos =[0 22 0 6];
plot (V,I);
title ('G = 1000 [W/m2], T = 25 [ºC]’);
axis (eixos);
xlabel('V');
ylabel('I');
grid on;

figure (2); %plot max power point   %%%%%%%%%%%%%%%%%%%%%
axis ([0 Voc*1.01 0 +100]);
plot(V,Power,'r');
title ('Curva do Pmpp');
xlabel('V');
ylabel('Power [W]');
grid on;


%%% Obter MPP values
fprintf('Vmpp a 25ºC = %d V \n',Vpmp);
fprintf('Impp a 25ºC = %d A \n',Ipmp);
fprintf('Pmpp a 25ºC = %d W \n',Ppmp);
```

[V(t)] with 1 Short-circuited Module: Validation script:

```
%%
clear all;close all;clc;

esfparam;% Define as variaveis do sistema
esfp_c00;% Carrega os parametros da celula solar
esfp_g00;% Carrega os parametros do modulo solar

%%%%%%%%%%%%%%%%%%%%%%%%%%%%%%%%%%%%%%%%%%%%%%%%%%%%%%%%%%%%%%%%%%%%%%%%%%%%%%%

% Dados de entrada

tempo_irrad_freefault_e_bypass1 = 'tempo_irrad_freefault_e_bypass1.xlsx';
X= xlsread(tempo_irrad_freefault_e_bypass1,'A184:A738');% hora (h)
G= xlsread(tempo_irrad_freefault_e_bypass1,'B184:B738');% G (W/m2)
T= xlsread(tempo_irrad_freefault_e_bypass1,'J184:J738');%Tcell [ºC] ao longo do dia
Vdc= xlsread(tempo_irrad_freefault_e_bypass1,'K184:K738');%Vdc_meas (V) ao longo do dia
fprintf('%d \n', Vdc);

%%
%gráficos
figure (1);
hold on;
axis ([5 20 0 250]);
xlabel('t [h]');
ylabel('V [V]');
grid on;


i=1;
for i=1:length(G)

%     tic
   %output para uma celula
   [Vpmp,Ipmp,Ppmp]=esfcpmp(G(i),T(i));

   % valores de 1 modulo (72 celulas)
   Vpmp_g=Vpmp*36; %36 celulas em serie
%    Ipmp_g=Ipmp*2; %2 celulas em paralelo

   % valores de 1 array (30 modulos)
   Vmpp_array =Vpmp_g*14; %15 modulos em serie
%    Impp_array =Ipmp_g*2; %2 modulos em paralelo
%    Pmpp_array =Impp_array.*Vmpp_array;

   t=X(i);%experiencia
   plot (t,Vmpp_array,'b');

%    fprintf('Iter %d \n', i);%para testar o tempo
%    toc

%    fprintf('Vmpp do array em i=%d = %d V \n',i,Vmpp_array);
%    fprintf('Impp do array em i=%d = %d A \n',i,Impp_array);
%    fprintf('Pmpp do array em i=%d = %d W \n',i,Pmpp_array);
   fprintf('%d \n',Vmpp_array);
end

hold on
plot (X,Vdc,'r');
```

[I(t)] with 1 String Fault: Validation script:

```
%%
clear all;close all;clc;

esfparam;% Define as variaveis do sistema
esfp_c00;% Carrega os parametros da celula solar
esfp_g00;% Carrega os parametros do modulo solar

%%%%%%%%%%%%%%%%%%%%%%%%%%%%%%%%%%%%%%%%%%%%%%%%%%%%%%%%%%%%%%%%%%%%%%%%%%%%%%%

% Dados de entrada

tempo_irrad_stringfault = 'tempo_irrad_stringfault.xlsx';
X= xlsread(tempo_irrad_stringfault,'A184:A738');% hora (h)
G= xlsread(tempo_irrad_stringfault,'B184:B738');% G (W/m2)
T= xlsread(tempo_irrad_stringfault,'J184:J738');%Tcell [ºC] ao longo do dia
Idc= xlsread(tempo_irrad_stringfault,'H184:H738');%Idc_meas (A) ao longo do dia

fprintf('%d \n', Idc);
%%
%gráficos
figure (1);
title (' I[A] - 5am to 8pm: blue (simulated) , red (measured) :: S0St');
hold on;
axis ([5 20 0 10]);
xlabel('t [h]');
ylabel('I [A]');
grid on;


%%
i=1;
for i=1:length(G)

%     tic
   %output para uma celula
   [Vpmp,Ipmp,Ppmp]=esfcpmp(G(i),T(i));

   % valores de 1 modulo (72 celulas)
%     Vpmp_g=Vpmp*36; %36 celulas em serie
   Ipmp_g=Ipmp*2; %2 celulas em paralelo

   % valores de 1 array (30 modulos)
%     Vmpp_array =Vpmp_g*15; %15 modulos em serie
   Impp_array =Ipmp_g*1; %2 modulos em paralelo
%     Pmpp_array =Impp_array.*Vmpp_array;

   t=X(i);%experiencia
   plot (t,Impp_array,'b');

%     fprintf('Iter %d \n', i);%para testar o tempo
%     toc
%
%     fprintf('Vmpp do array em i=%d = %d V \n',i,Vmpp_array);
%     fprintf('Impp do array em i=%d = %d A \n',i,Impp_array);
%     fprintf('Pmpp do array em i=%d = %d W \n',i,Pmpp_array);
     fprintf('%d \n', Impp_array);
end

hold on
plot (X,Idc,'r');
```

[P(t)] Free Fault: Validation script:

```
%%
clear all;close all;clc;

esfparam;% Define as variaveis do sistema
esfp_c00;% Carrega os parametros da celula solar
esfp_g00;% Carrega os parametros do modulo solar

%%%%%%%%%%%%%%%%%%%%%%%%%%%%%%%%%%%%%%%%%%%%%%%%%%%%%%%%%%%%%%%%%%%%%%%%%%%%%%%

% Dados de entrada

tempo_irrad_freefault = 'tempo_irrad_freefault.xlsx';
X= xlsread(tempo_irrad_freefault,'A184:A738');% hora (h)
G= xlsread(tempo_irrad_freefault,'B184:B738');% G (W/m2)
T= xlsread(tempo_irrad_freefault,'J184:J738');%Tcell [ºC] ao longo do dia
F= xlsread(tempo_irrad_freefault,'D184:D738');% P_meas (W) ao longo do dia

%fprintf('%d \n', F);

%%
%gráficos
figure (1);
hold on;
axis ([8.55 17.783 0 2800]);
xlabel('t [h]');
ylabel('P [W]');
grid on;


i=1;
for i=1:length(G)

%     tic
    %output para uma celula
    [Vpmp,Ipmp,Ppmp]=esfcpmp(G(i),T(i));

    % valores de 1 modulo (72 celulas)
    Vpmp_g=Vpmp*36; %36 celulas em serie
    Ipmp_g=Ipmp*2; %2 celulas em paralelo

    % valores de 1 array (30 modulos)
    Vmpp_array =Vpmp_g*15; %15 modulos em serie
    Impp_array =Ipmp_g*2; %2 modulos em paralelo
    Pmpp_array =Impp_array.*Vmpp_array;

    t=X(i);%experiencia
    plot (t,Pmpp_array,'b');

%     fprintf('Iter %d \n', i);%para testar o tempo
%     toc
%
%     fprintf('Vmpp do array em i=%d = %d V \n',i,Vmpp_array);
%     fprintf('Impp do array em i=%d = %d A \n',i,Impp_array);
%     fprintf('Pmpp do array em i=%d = %d W \n',i,Pmpp_array);
    fprintf('%d \n', Pmpp_array);
end

hold on
plot (X,F,'r');
```

[NRc]: Validation script:

```
clear all;close all;clc;

esfparam;% Define as variaveis do sistema
esfp_c00;% Carrega os parametros da celula solar
esfp_g00;% Carrega os parametros do modulo solar

%%

% Dados de entrada
tempo_irrad_stringfault = 'tempo_irrad_stringfault.xlsx';
X= xlsread(tempo_irrad_stringfault,'A184:A738');% hora (s)
G= xlsread(tempo_irrad_stringfault,'B184:B738');% G (W/m2)
T= xlsread(tempo_irrad_stringfault,'J184:J738');%Tcell [ºC] ao longo do dia
I_meas= xlsread(tempo_irrad_stringfault,'H184:H738');%Impp: dc side

%gráficos
figure (1);
hold on;
axis ([8.55 17.83 0 1]);
% axis auto;
xlabel('t [h]');
ylabel('Im/Isc');
grid on;

i=1;
for i=1:length(G)
%     [G]=Gx*ones(1,length(Gin));
    [Isc]=(esfgisc (G(i),T(i)))';
    Isc_array=2*Isc; %array contem 30 modulos, Np=2
    Racio(i)=I_meas(i)/Isc_array;
%     fprintf('t=%d,  Im=%d,  Isc_array=%d,  racio=%d \n',X(i),I_meas(i),Isc_array,Racio(i));
    fprintf('%d \n', Racio(i));
end

plot (X,Racio,'r');
```

[NRv]: Validation script:

```
clear all;close all;clc;

esfparam;% Define as variaveis do sistema
esfp_c00;% Carrega os parametros da celula solar
esfp_g00;% Carrega os parametros do modulo solar

%%

% Dados de entrada
tempo_irrad_stringfault = 'tempo_irrad_stringfault.xlsx';
X= xlsread(tempo_irrad_stringfault,'A184:A738');% hora (s)
G= xlsread(tempo_irrad_stringfault,'B184:B738');% G (W/m2)
T= xlsread(tempo_irrad_stringfault,'J184:J738');%Tcell [ºC] ao longo do dia
V_meas= xlsread(tempo_irrad_stringfault,'K184:K738');%Vmpp: dc side

%gráficos
figure (1);
hold on;
% axis auto;
axis ([8.55 17.83 0 1]);
xlabel('t [h]');
ylabel('Vm/Voc');
grid on;

i=1;
for i=1:length(G)

%     [G]=Gx*ones(1,length(Gin));
    [Voc]=(esfgvoc (G(i),T(i)))';
    Voc_array=15*Voc; %array contem 30 modulos. Ns=15, Np=2
    Racio(i)=V_meas(i)/Voc_array;
%     fprintf('t=%d,  Vm=%d,  Voc_array=%d,  racio=%d \n',X(i),V_meas(i),Voc_array,Racio(i));
    fprintf('%d \n', Racio(i));
end

plot (X,Racio,'b');
```

Now the manufacturer sheets of the PV modules studied are presented:

HELIOS TECHNOLOGY

H1500 PHOTOVOLTAIC MODULES

NEW GENERATION PHOTOVOLTAIC MODULE

The **H1500** module represents the state of the art in the PV market and is particularly suitable to grid connection systems. It utilizes 36 HT 165x165 mm high efficiency I-MAX monocrystalline cells, developed by Helios to meet the market need of the new millennium. The high power of the **H1500** modules means that fewer units need to be left, installed and interconnected, comparing to the smaller modules. This is especially relevant to grid connected applications and large systems where low installation costs are desiderable. Thanks to the I-MAX technology developed by Helios for its range of high efficiency modules, the **H1500** performs an increased current output by 10-17% at operating battery voltage when installed in a stand alone system. High power output, compact and light weight design, prouven reliability, make this module to provide power in virtually any climate, under the toughest environmental and operating conditions.
Every single cell and module are tested throughout the manufacturing process to guarantee at least 30 years effective service life.
The **H1500** module is avaiable in two power output versions, to better meet the customer's needs.
Robust construction and heavy duty anodized aluminium frame design make this module suitable to all power applications.
For an easy and quick serial connection the module can be optionally supplied equipped with multicontact connectors.

H1500 / 110W - 120W

Guaranteed power ≥ 80% 25 years
Relative humidity up to 100%
Dimensions 1530 x 690 x 34 mm ± 1 mm
Weight Kg. 14
Tolerance on technical data: ± 5%

CE

ELECTRICAL SPECIFICATIONS (at 100 mW/cm², 25°C, AM 1,5)
MODULE H1500

Peak Power (Wp)	**Watts**	**110**	**Watts**	**120**
Short circuit current (Isc)	Amps	7.22	Amps	7.88
Open circuit voltage (Voc)	Volts	21	Volts	21
Voltage at maximum power (Vmp)	Volts	17	Volts	17
Current at maximum power (Imp)	Amps	6.47	Amps	7.06
Typical Current at battery operating voltage (12-13.8 V)	**Amps**	**6.9**	**Amps**	**7.5**
NOCT (Nominal operating cell temperature)	°C	43±2	°C	43±2
Change of Voc with temperature ß	mv/°C	-90	mv/°C	-90
Wind loading or surface pressure	N/m2 2400 (200 km/h equiv.)		N/m2 2400 (200 km/h equiv.)	
Hailstone Impact Resistance	24 mm at 80 km/h		24 mm at 80 km/h	
Storage and operating temperature	°C from -40 to +95		°C from -40 to +95	
Maximum System Voltage	Volts	1000	Volts	1000

MODULE 110 W

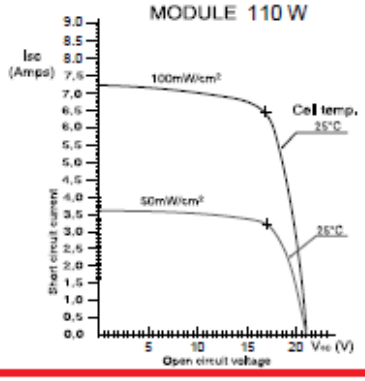

MODULE 120 W

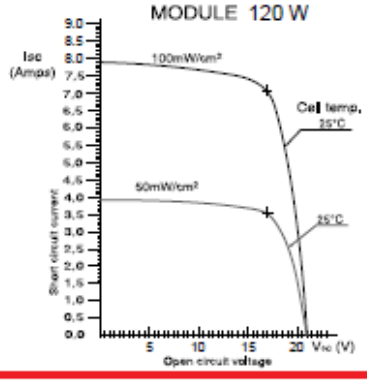

Intelligent module design

- All cells are electrically matched to assure the greatest power output possible.
- Ultra-clear tempered glass provides excellent light transmission and protects from wind, hail, and impact.
- Torsion and corrosion-resistant anodized aluminum module frame ensures dependable performance, even through harsh weather conditions and in marine environments.
- Built-in bypass diodes (24V configuration) help system performance during partial shadowing.

High quality

- Every module is subject to final factory review, inspection, and testing to assure compliance with electrical, mechanical, and visual criteria.
- 72 PowerMax® single-crystalline solar cells deliver excellent performance even in reduced light or poor weather conditions.
- Cell surfaces are treated with the Texture Optimized Pyramidal Surface (TOPS™) process to generate more energy from available light.
- Fault tolerant multi-redundant contacts on the front and back of each cell provide superior reliability.
- Solar cells are laminated between a multi-layered polymer backsheet and layers of ethylene-vinyl acetate (EVA) for environmental protection, moisture resistance and electrical isolation.
- Durable backsheet provides the module underside with protection from scratching, cuts, breakage, and most environmental conditions.
- Laboratory tested for a wide range of operating conditions.
- Ground continuity of less than 1 ohm for all metallic surfaces.
- Manufactured in ISO 9001 certified facilities to exacting Siemens quality standards.

Easy installation

- Standard Sp junction box is designed for trouble-free field wiring and environmental protection.
- Light weight, aluminum frame and pre-drilled mounting holes for easy installation.
- Modules may be wired together in series or parallel to attain required power levels.

Options

- The module is supplied from the factory in a standard 24 volt configuration.
- Modified versions of the solar module are also available, e.g. as frameless laminate. Please contact your Siemens Solar dealer for further information.

Performance warranty

- 25 Year limited warranty on power output.

Further information on solar products, systems, principles, and applications is available in the Siemens Solar product catalog.

Solar module SP150

Electrical parameters		(24 V)
Maximum power rating P_{max}	[W_p][1]	150
Rated current I_{MPP}	[A]	4.4
Rated voltage V_{MPP}	[V]	34.0
Short circuit current I_{SC}	[A]	4.8
Open circuit voltage V_{OC}	[V]	43.4
Thermal parameters		
NOCT[2]	[°C]	45±2
Temp. coefficient of the short-circuit current		2.06 mA / °C
Temp. coefficient of the open-circuit voltage		-.077 V / °C
Qualification test parameters[4]		
Temperature cycling range	[°C]	-40 to +85
Humidity freeze, Damp heat	%RH]	85
Maximum permitted system voltage	[V]	600 V (1000 V per IEC 1215)
Wind Loading	PSF [N/m²]	50 (2400)
Maximum distortion[3]	[°]	1.2
Hailstorm / hailstones	inches [mm]	1.0 (ø 25)
	MPH [m/s]	52 (v = 23)
Weight	Pounds [kg]	32.6 (14.8)

[1] W_p (Watt peak) = Peak power
Air Mass AM= 1.5
Irradiance E= 1000 W/m²
Cell temperature T_C= 25 °C

[2] Normal Operating Cell Temperature at:
Irradiance E = 800 W/m²
Ambient temperature T_a = 20 °C
Wind speed v_W= 1 m/s

[3] Diagonal lifting of the module plane

4) Per IEC 61215 test requirements

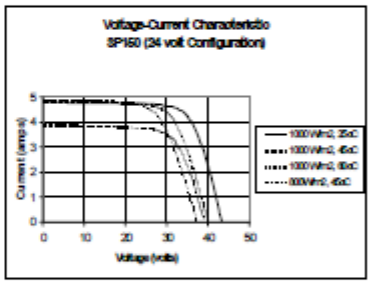

Module dimensions

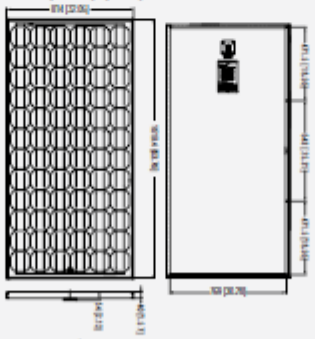

Hole diameter 0.26 inch (6.6 mm)
Hole dimensioning referred to hole center

Sp J box

Maximum cable diameter: 4 mm²
Degree of protection: IP54

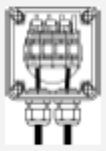

Your address for photovoltaics from Siemens Solar:

Siemens modules are recyclable.

Siemens Solar GmbH
A joint venture of
Siemens AG and E. ON Energie AG
Postfach 46 07 05
D-80915 München
Germany

Siemens Solar Industries
P.O. Box 6032
Camarillo, CA 93011, U.S.A.
Tel: 805-482-6800
Fax: 805-388-6395
Web site: www.siemenssolar.com
E-mail: ssi.sales@solar.siemens.com

Siemens Showa Solar Pte. Ltd.
166 Kallang Way
Singapore 349249
Tel: 65-842-3886
Fax: 65-842-3887
e-mail: ssspv@solar.siemens.com.sg

Printed in U.S.A.

Typical Electrical Characteristics[1]	BP 5160S	BP 5170S
Maximum Power (P_{max})[2]	160W	170W
Voltage at P_{max} (V_{mp})	36.0V	36.0V
Current at P_{max} (I_{mp})	4.44A	4.72A
Warranted minimum P_{max}	150W	160W
Short-circuit current (I_{sc})	4.7A	5.0A
Open-circuit voltage (V_{oc})	44.0V	44.2V
Temperature coefficient of I_{sc}	(0.065±0.015)%/°C	
Temperature coefficient of V_{oc}	–(160±10)mV/°C	
Temperature coefficient of Power	–(0.5±0.05)%/°C	
NOCT[3]	47±2°C	
Maximum System Voltage[2]	600V	

Notes

1. These data represent the performance of typical BP 5160S and BP 5170S modules as measured at their output terminals. The data are based on measurements made in accordance with ASTM E1036-85 corrected to SRC (Standard Reporting Conditions, also known as STC or Standard Test Conditions), which are:
   - illumination of 1 kW/m² (1 sun) at spectral distribution of AM 1.5 (ASTM E892-87 global spectral irradiance);
   - cell temperature of 25°C.
2. U.S. NEC rating.
3. The cells in an illuminated module operate hotter than the ambient temperature. NOCT (Nominal Operating Cell Temperature) is an indicator of this temperature differential, and is the cell temperature under Standard Operating Conditions: ambient temperature of 20°C, solar irradiation of 0.8 kW/m², and wind speed of 1 m/s.
4. During the stabilization process which occurs during the first few months of deployment, module power may decrease approximately 3% from typical P_{max}.

BP 5170S I-V Curves

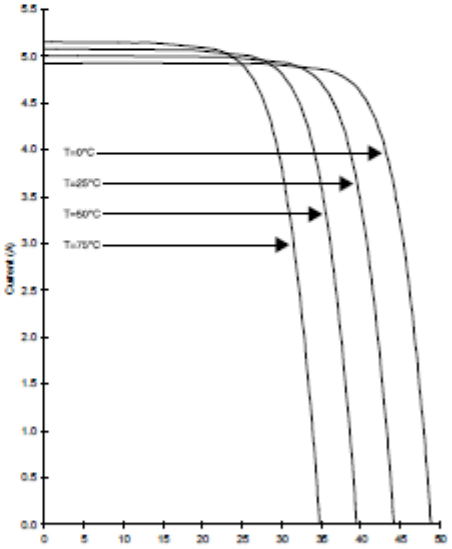

ISOFOTON

Monokristallines Solarmodul
ISOFOTON I - 106/12 und I - 110/12

Das monokristalline Solarmodul **ISOFOTON I - 106/12** und **I - 110/12** bietet Ihnen eine qualitativ hochwertige Komponente für Ihre Photovoltaikanlagen. Die langjährige Erfahrung von **ISOFOTON** auf dem Gebiet der Modulherstellung garantiert ein hervorragendes Preis – Leistungsverhältnis und das bei einem rein europäischen Produkt.

Die Module bestehen aus 72 monokristallinen quadratischen Solarzellen, die in zwei Lagen EVA eingebettet sind. Die Frontseite aus Solarsicherheitsglas mit höchster Lichtdurchlässigkeit sowie die Solarzellen mit reflexionsarmer Oberfläche garantieren einen hohen Wirkungsgrad bei unterschiedlichsten Strahlungsbedingungen. Die Rückseite der Module ist mit weißem Tedlar ausgeführt (auf Anfrage sind andere Farben möglich). Ein stabiler Rahmen aus eloxiertem Aluminium bietet neben der hohen mechanischen Stabilität auch eine einfache Montagemöglichkeit.

Die Solarzellen des Moduls sind 2 x 36 Zellen in Reihe verschaltet (*Nennspannung 17,4V*). Zwei getrennte Anschlußdosen mit integrierten Bypassdioden ermöglichen einen einfachen Anschluss.

Qualitätsmerkmale

ISOFOTON Standard-Garantie

- 25 Jahre Leistungsgarantie
- 10 Jahre Produktgarantie
- Jedes Modul wird einer 100 %igen Endkontrolle unterzogen
- Das **ISOFOTON** Solarmodul **I - 106/12** und **I - 110/12** übertrifft die international festgelegten Normwerte und erfüllt: Schutzklasse II und ISPRA - Zertifikat IEC 1215

Technische Daten	I - 106/12	I - 110/12
Nennleistung P_{MPP}, (Leistungsabweichung)	106 W, (5%)	/ 110 W, (10%)
Kurzschluss-Strom I_{SC}	6,54 A	/ 6,76 A
Leerlaufspannung U_{OC}	21,6 V	/ 21,6 V
Strom bei Nennleistung I_{STC}	6,10 A	/ 6,32 A
Spannung bei Nennleistung U_{STC}	17,4 V	/ 17,4 V
Zellenoberfläche	103,6 cm²	
NOCT (80 mW/cm², AM 1.5, 20°C)	47 °C	
		als Laminat
Länge	1310 mm	1305 mm
Breite	652 mm	647 mm
Höhe (Rahmen)	34 mm	3,4 mm
Höhe (mit Anschlussdose)	57 mm	57 mm
Gewicht	11 kg	10,5 kg
Montagebohrungen Ø	7 mm	–

Elektrische Werte unter Standard Testbedingungen: 1000 W/m², Zellentemperatur 25 °C, Spektrum AM 1.5
Technische Änderungen, die dem Fortschritt dienen, behalten wir uns vor.

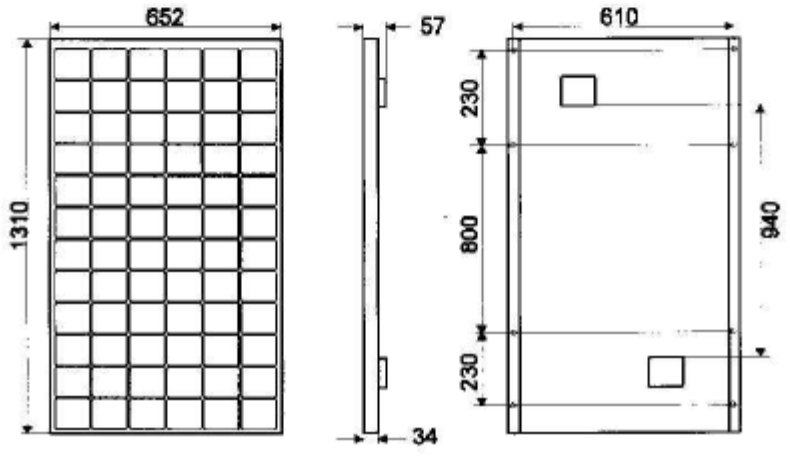

7. References

[1] Murillo, D.G., 2003. Modelado y análisis de sistemas fotovoltaicos, PhD thesis, Universitat Politècnica de Catalunya.

[2] Chouder, A., 2010. Analysis, Diagnosis and Fault Detection in Photovoltaic Systems, PhD thesis, Universitat Politècnica de Catalunya.

[3] Capogna, V., 2012. Development of monitoring and automatic fault detection solutions for grid-connected photovoltaic systems, MSc SELECT thesis, Universitat Politècnica de Catalunya.

[4] Chouder, A. and Silvestre, S., 2010. Automatic supervision and fault detection of PV systems based on power losses analysis. Energy Conversion and Management. 51: 1929-1937.

[5] Gokmen, N., Karatepe E., Celik, B. and Silvestre, S., 2012. Simple diagnostic approach for determining of faulted PV modules in string based PV arrays. Solar Energy. 86: 3364-3377.

[6] Silvestre, S., Chouder, A., Karatepe, E., 2013. Automatic fault detection in grid connected PV systems. Solar Energy. 94: 119-127.

[7] J.A.Duffie, W. B., 2006. Solar Engineering of Thermal Process. Hoboken, NJ: Wiley.

[8] C.Barreiro, P. A., 2011. PV by-pass diode performance in landscape and portrait modalities. Photovoltaic Specialists Conference (PVSC) (pp. 003097 - 003102). Dept. of Electr. & Comput.

[9] Castañer, L., Silvestre, S., 2002. Modelling Photovoltaic systems using PSpice. John Wiley & Sons, LTD, 47.

[10] http://pveducation.org/pvcdrom, Março, 2014.

[11] Sonnenenergie, D. G., 2008. Planning and installing photovoltaic systems: a guide for installers, architects and engineers, Earthscan, London, UK.

[12] Lahcene, D. and Eddine, Z.D., 2013. Automatic monitoring and Fault detection of grid connected PV systems.

[13] Castañer, L., Silvestre, S., 2002. Modelling Photovoltaic systems using PSpice. John Wiley & Sons, LTD, 179.

[14] Castañer, L., Silvestre, S., 2002. Modelling Photovoltaic systems using PSpice. John Wiley & Sons, LTD, 216-217.

[15] Luque, A. and Hegedus, S., 2002. Handbook of photovoltaiv science and engineering, Wiley, 788.

[16] http://www.solar-electric.com/mppt-solar-charge-controllers.html, Março, 2014.

[17] http://www.energydepot.com/RPUres/library/PhotovoltaicSystems.asp, Fevereiro, 2014.

[18] https://www.ema.gov.sg/media/files/books/pv_handbook/20080509114101_9803_PV_Handbook_25apr08.pdf, Março, 2014.

[19] http://www.homepower.com/articles/solar-electricity/design-installation/potential-pv-problems, Fevereiro, 2014.

[20] http://electricalconnection.com.au/article/10014841/avoiding-common-solar-panel-installation-mistakes, Janeiro, 2014.

[21] L. M. Moore, H. N., 2008. Five Years of Operating Experience at a Large, Utility-scale Photovoltaic Generating Plant. PROGRESS IN PHOTOVOLTAICS: RESEARCH AND APPLICATIONS, 249 – 259.

[22] Enbar, N., 2010. PV O&M Practices, NREL.

[23] McEvoy, A., Markvart, T. And Castañer, L., 2012. Practical Handbook of Photovoltaics Fundamentals and Applications, AP, 1073-1075.

[24] Y. Yagi, H. K., 2003. Diagnostic technology and an expert system for photovoltaic systems using the learning method. Solar Energy Material & Solar Cells, 655-663.

[25] A. Drews, A. d., 2007. Monitoring and remote failure detection of grid-connected pv systems based on satellite observations. Solar Energy, 548–564.

[26] S. Stettler, P. T., 2006. Spyce: satellite photovoltaic yield control and evaluation. Proceedings of the 21st European photovoltaic solar energy conference ,2613–2616.

[27] M. Muselli, G. N., 1998. Utilization of meteosat satellite-derived radiation data for integration of autonomous photovoltaic solar energy systems in remote areas. Energy conversion and Management, 1–19.

[28] Chao, K.H., Hob,S.H. and. Wang, M.H., 2008. Modeling and fault diagnosis of a photovoltaic system. Electric Power Systems Research. 78: 97-105.

[29] K. H. Chao, C. T., 2010. A novel fault diagnosis method based-on modified neural networks for photovoltaic systems in Advances in Swarm Intelligence. Eds. Springer Berlin/Heidelberg.

[30] Chine, W., Mellit, A., Pavan, A.M., Kalogirou, S.A., 2014. Fault detection method for grid-connected photovoltaic plants. Renewable Energy, 66: 99-110.

[31] Ducange, P.,Fazzolari, M.,Lazzerini, B. and. Marcelloni. F., 2011. An Intelligent system for detecting faults in photovoltaic fields. In: Proc. of the 11th International conference on Intelligent Systems Design and Applications (ISDA), pp. 1341-6.

[32] Mellit, A. and Kalogirou, S.A., 2011. ANFIS-based modelling for photovoltaic power supply system: A case study. Renewable Energy, 36: 250-258.

[33] Syafaruddin, Karatepe, E. and Hiyama, T., 2011. Controlling of artificial neural network for fault diagnosis of photovoltaic array. In: IEEE 16th International Conference on Intelligent System Application to Power Systems, pp. 1-6.

[34] Vergura, S., Acciani, G., Amoruso, V., Patrono, G.E. and Vacca F., 2009. Descriptive and Inferential Statistics for Supervising and Monitoring the Operation of PV Plants. IEEE Trans. On Industrial Electronics, 56: 4456-4463.

[35] S. Vergura, G. A., 2009. Descriptive and inferential statistics for supervising and monitoring the operation of pv plants. IEEE Transactions on Industrial Electronics, 4456–4464.

[36] Mellit, A., 2006. Development of an expert configuration of standalone power pv system based on adaptive neuro-fuzzy inference system (anfis). IEEE Mediterranean Electrotechnical Conference (pp. 893-869).

[37] Chouder A, Silvestre S., 2009. Analysis model of mismatch power losses in PV systems. J Sol Energy Eng;131(2):24504-1-5.

[38] Mayor JC, Durisch W., 2000. Application of a Generalized model for the electrical characterisation of a commercial solar cell. In: Proceedings of the VI World renewable energy congress, WREC, Brighton, UK.

[39] Durisch W, Mayor JC., 2003. Application of a generalized current voltage model for solar cells to outdoor measurements on siemens SM 110 module. In: Proceedings of the 3rd world conference on photovoltaic energy conversion, Japan.

[40] B. Marion et al, 2005. Performance Parameters for Gid-Connected PV systems, Proc, 31st IEEE PVSC.

[41] Häberlin H, Beutler Ch., 1995. Normalized representation of energy and power for analysis of performance and on-line error detection in PV systems. In: 13th EU PV conference on photovoltaic solar energy conversion, Nice, France; p. 934–7.

[42] Liu Benjamin YH, Jordan Richard C., 1961. Daily insolation on surfaces tilted toward the equator. ASHRAE; 3(10):53–9.

[43] Silvestre, S., Boronat, A. and Chouder, A., 2009. Study of bypass diodes configuration on PV modules. Applied Energy, 86: 1632-1640

[44] Tsai, H.L., 2010. Insolation-oriented model of photovoltaic module using MatLab/Simulink. Solar Energy; 84: 13181326.

[45] Chouder, A., Silvestre, S., Sadaoui, N. and Rahmani, L., 2012. Modeling and simulation of a grid connected PV system based on the evaluation of main PV module parameters. Simulation Modelling Practice and Theory; 20: 46-58.

[46] Moreno, A., Julve, J., Silvestre, S. and Castañer, L., 2000. Spice macromodelling of photovoltaic systems. Prog. Photovolt: Res. Appl. 8: 293306.

[47] Di Vincenzo, M.C. and Infield, D., 2013. Detailed PV array model for non-uniform irradiance and its validation against experimental data. Solar Energy; 97: 314 -331.

[48] Chouder, A., Silvestre, S., Taghezouit, B., Karatepe, E., 2013. Monitoring, modeling and simulation of PV systems using LabVIEW. Solar Energy.

[49] Yu, T. C., Lin, Y. B. and Chang, F. S., 2013. Establishment of the Photovoltaic Simulation System Using Mixed Programming with LabVIEW and Simulink. In: Intelligent Technologies and Engineering Systems (pp. 383-394).Springer.

[50] Carrero C., Amador J., and Arnaltes S., 2007. A single procedure for helping PV designers to select silicon PV modules and evaluate the loss resistances.